DESIGN OF NITRIC OXIDE-RELEASING MACROMOLECULARS SCAFFOLDS FOR ANTIMICROBIAL APPLICATIONS

Yuan Lu

A dissertation submitted to the faculty of the University of North Carolina at Chapel Hill in partial fulfillment of the requirements for the degree of Doctor of Philosophy in the Department of Chemistry.

Chapel Hill
2013

Approved by

Mark H. Schoenfisch

Royce W. Murray

Valerie S. Ashby

James F. Cahoon

Alexander J. M. Miller

ABSTRACT

YUAN LU: Design of Nitric Oxide-Releasing Macromolecular Scaffolds for Antimicrobial Applications
(Under the direction of Professor Mark H. Schoenfisch)

Nitric oxide (NO)-releasing materials have attracted much attention for antimicrobial applications due to the physiological roles of NO in immune defense. Prior study showed enhanced bactericidal efficacy of NO-releasing silica particles compared to small molecule NO donors, attributable to the efficient NO delivery into the interior of the bacteria. Unfortunately, these silica particles elicited significant toxicity towards mammalian cells at the concentrations for biofilm eradication. To address this limitation, my research has focused on the design of NO-releasing macromolecular scaffolds with enhanced bactericidal efficacy and reduced toxicity against mammalian cells. Herein, the synthesis of NO-releasing silica particles, dendrimers, and chitosan oligosaccharides with tunable NO-release kinetics, chemical structures (exterior hyrophobicity, ionic characteristics) and physical properties (size, morphology, molecular weight) were presented. The bactericidal efficacy of these NO-releasing scaffolds was evaluated against both planktonic bacteria and biofilms. Nitric oxide-releasing dendrimers with intermediate hydrophobicity and NO-releasing chitosan oligosaccharides exhibited enhanced antibacterial activities and proved effective at eradicating biofilms at the concentrations eliciting no toxicity against mammalian cells.

ACKNOWLEDGEMENT

I am extremely grateful for all of the support that I received throughout my graduate study at the University of North Carolina at Chapel Hill. I would like to thank Dr. Schoenfisch for giving me the opportunity to work on these exciting projects and all the group members for their contributions to my research, especially Dr. Chenghong Li, Danielle Slomberg, Dr. Bin Sun, Angela Broadnax, and Anand shad. I also want to express my gratitude to Dr. Amar S. Kumbhar and Dr. Neal Kramarcy for their assistance with the training and operation of scanning electron microscopy and confocal microscopy. At last, thanks for National Institute of Health for the financial support.

TABLE OF CONTENTS

LIST OF SCHEMES

LIST OF TABLES

LIST OF FIGURES

LIST OF ABBREVIATIONS AND SYMBOLS

^{o}C	degree(s) Celsius
%	percentage(s)
±	statistical margin of error or tolerance
[…]	concentration
µL	microliter(s)
µm	micrometer)s)
µmol	micromole(s)
aq	aqueous
Ar	argon gas
atm	atmosphere
BSA	bovine serum albumin
CFU	colony forming unit
CH_3	methyl
Cl^-	chlorine ion
cm	centimeter(s)
CO_2	carbon dioxide
Cu^{2+}	copper ion
d	day(s)
DMF	dimethylformamide
EDTA	ethylenediamine-tetraacetic acid
e.g.	for example

et al.	and others
etc.	and so forth
EtOH	ethanol
g	gram(s)
G	generation
h	hour(s)
H^+	hydrogen ion
H_2O	water
H_2O_2	hydrogen peroxide
HCl	hydrogen chloride
HNO	nitroxyl
i.e.	that is
K	kelvin
L	liters
M	molar concentration
MeOH	methanol
mg	milligrams
min	minute(s)
mL	milliliter(s)
mM	millimolar concentration
mmol	millimole(s)
N-	nitrogen bound
N_2	nitrogen gas

N_2O_3	dinitrogen trioxide
Na^+	sodium ion
NaCl	sodium chloride
nm	nanometer
NMR	nuclear magnetic resonance
NO	nitric oxide
O_2	oxygen
ONOO	peroxynitrite
PAMAM	polyamidoamine
PBS	phosphate buffered saline
PEG	poly(ethylene glycol)
pH	-log of proton concentration
PI	propidium iodide
ppb	parts per billion
ppm	parts per million
PPI	polypropylenimine
s	second(s)
t	time
TEOS	tetraethyl orthosilicate
THF	tetrahydrofuran
TSB	tryptic soy broth
UV	ultraviolet

v:v	volume/volume
vs.	versus
wt	weight

Chapter 1

Macromolecular Nitric Oxide Delivery Systems

1.1 Introduction

Nitric oxide (NO) is a diatomic free radical produced endogenously by various nitric oxide synthase (NOS) enzymes that catalyze the conversion of L-arginine to L-citrulline and NO.[1-2] Several bioregulatory processes are mediated by NO including vasodilation, angiogenesis, neurotransmission, macrophage destruction of foreign pathogens, gastrointestinal motility, muscle contractility, etc.[3-12] Due to NO's integral role in human physiology, deficiencies in NO biosynthesis or the overproduction of NO have been linked to a number of diseases including Parkinson's disease and cancer.[13-15] As such, the development of NO-based therapies have become a major target in drug discovery.

Small molecule NO donors have been widely implemented to unravel some of the mysteries of NO in physiology, and proposed as potential therapeutics for diseases requiring NO therapy.[16-25] Numerous reports have demonstrated the therapeutic role of NO in anti-cancer, antimicrobial, cardioprotective and anti-thrombotic applications.[16-25] Despite the promising therapeutic potential of small molecule NO donors, low NO payloads and the lack of targeted NO release to a specific site have hindered the clinical development of NO-releasing therapeutics. In response, macromolecular NO-releasing scaffolds have been designed to target NO delivery and enhance therapeutic utility (e.g.,

antimicrobial efficacy).[26-27] In this introduction chapter, I will set the stage for my thesis research by reviewing recent developments in the design and applications of NO-releasing macromolecular scaffolds. In particular I will focus on the bactericidal efficacy of macromolecular NO-releasing scaffolds as a function of NO-release kinetics, chemical structures and scaffold sizes.

1.2 *N*-Diazeniumdiolate Functionalized Macromolecules

1.2.1 N-Diazeniumdiolate Formation and Nitric Oxide Release Characteristics

Perhaps the most widely studied NO donor class, are *N*-diazeniumdiolates formed via the reaction of amines with high pressures of NO (5 atm).[28] As shown in Scheme 1.1, a nucleophilic amine substrate attacks the electrophilic nitrogen atom of NO. In the subsequent step, the resulting radical species reacts rapidly with an additional molecule of NO forming a zwitterionic intermediate. Upon addition of a strong base (e.g., sodium methoxide), the intermediate is deprotonated and results in the formation of a stable *N*-diazeniumdiolate. Efficient formation of *N*-diazeniumdiolate NO donors requires both appropriate precursor structures (e.g., secondary amines) and the presence of a base (e.g., sodium methoxide). Although primary and secondary amine adducts both can be used to form *N*-diazeniumdiolates formation, secondary amine adducts are typically characterized by a greater diazeniumdiolate conversion efficiency due to the increased basicity.[29-30] Moreover, the nitrosamine byproduct formed on primary amine-modified scaffolds upon NO liberation may be problematic for biomedical applications due to its carcinogenic nature.[31]

N-diazeniumdiolate structures are particularly attractive for biomedical applications because they decompose spontaneously in physiological milieu to yield two moles of NO per mole of amine precursor.[30] For small molecule alkyl secondary amine species, the proton-initiated decomposition of the diazeniumdiolate follows first-order decay kinetics with rates governed by the pH of the solution.[30] More rapid *N*-diazeniumdiolate decomposition is often observed at low pH. Another factor that influences NO-release kinetics is the chemical structure of the amine precursor.[30] For example, hydrophobic polyamines often have extended NO release due to slower hydration. *N*-diazeniumdiolates may also be stabilized by free primary amines whereby a cyclic ring is formed, resulting in slower decomposition of the NO donor due to the enhanced stability.[32] Compared to small molecule *N*-diazeniumdiolate NO donors, macromolecular scaffolds generally exhibit more controllable NO-release kinetics as both the hydrophobicity and local pH within the scaffold may be tuned. As such, a number of macromolecular scaffolds have been developed to store and release NO.[27, 29, 33-36]

1.2.2 N-Diazeniumdiolate-Modified Polymers

Although the majority of NO-releasing materials reported in the literature have been utilized as coatings for medical devices, my thesis is uniquely focused on the study of water soluble polymers and nanomaterials as NO-delivery vehicles. Such scaffolds may prove useful for a number of administration routes including topical, pulmonary, oral, ocular, and injection delivery.[26, 35, 37-38] Zhou et al. reported the first water soluble macromolecular NO-releasing scaffolds. Water soluble *N*-diazeniumdiolate-functionalized poly(ethylenimine) (PEI) was synthesized.[37] The PEI scaffolds exhibited a large NO storage capacity (i.e., ~3.84 μmol/mg) and slow NO-release kinetics

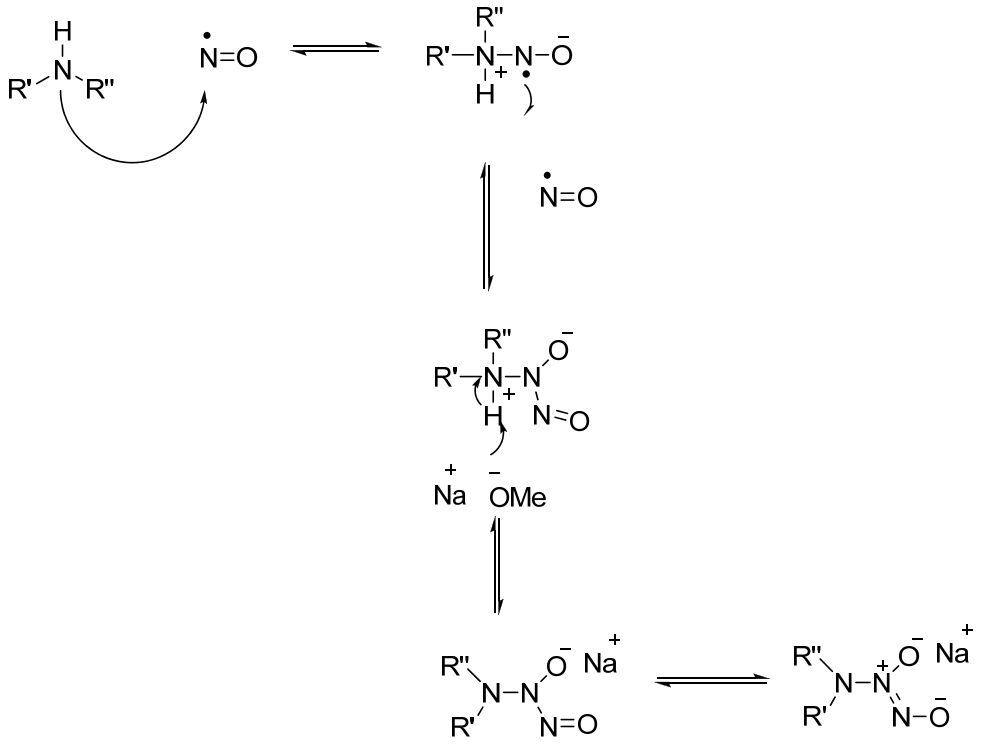

Scheme 1.1 Formation of *N*-diazeniumdiolate in the presence of NaOMe.

(i.e., half-life ~192 min) due to the inherently large precursor content and basic local pH, respectively.

To achieve more rapid NO release, carboxylated PEI and Proline-incorporated PEI were synthesized.[37] As expected, the carboxylic groups on the PEI scaffolds accelerated the decomposition of *N*-diazeniumdiolates (half life ~59 min) by lowering the local pH near the *N*-diazeniumdiolate species. The proline-incorporated PEI also exhibited faster NO release (~24 min) due to the rapid decomposition kinetics of PROLI/NO.[37] Despite the large NO storage and tunable NO release, the PEI scaffold was inherently toxic raising safety concerns for biomedical application of these materials. To synthesize scaffolds with reduced toxicity, West et al. reported the synthesis of amino-acid lysine-poly(ethylene glycol) (PEG) dendrimers for NO storage by conjugating NO on the lysine residues.[35] Briefly, dendrimers are synthetic, highly branched macromolecules of nanometer dimensions, for which bonds radiate out from a central core in a regular branching pattern.[39] With respect to their application as NO-releasing scaffolds, the multivalency of the dendrimers allows for facile modification with NO to allow large NO payloads. However, the PEG-lysine dendrimers were characterized by low NO storage due to the low diazeniumdiolate conversion efficiency characteristic of primary amines on lysine residues. In addition, the lack of control over the NO-release kinetics limited the application of the lysine-PEG dendrimers. To increase the total NO storage, the Schoenfisch lab has synthesized secondary amine-functionalized polypropylenimine (PPI) dendrimers with significantly enhanced NO storage capacity (up to 5.6 μmol NO/mg).[29] Varied NO-release kinetics was furthered by tuning the exterior hydrophobicity of the dendrimer. Compared to dendrimers with short hydrocarbon chains (C1) on their exterior

(i.e., half-life ~28 min), the long hydrocarbon chains (C7)-modified dendrimers exhibited extended NO release (i.e., half life of 86 min) as a result of the delayed water uptake/hydration. The multivalent exterior of dendritic NO-releasing scaffolds also enables the combination of NO donors with other functionalities, including those necessary for imaging and targeting.[29] To fully explore the effects of size and exterior modifications on NO release properties and antibacterial activity, more structural diverse NO-releasing dendrimers must first be synthesized.

1.2.3 N-Diazeniundiolate-Functionalized Micro- and Nanoparticles

Micro- and nanoparticles have been widely employed for drug delivery due to their potential to elicit controlled release of an active compound at a desired site.[40] Many methods exist for preparing such materials. For an example related to NO, Pulfer et al. synthesized epoxide-crosslinked polyethyleneimine microspheres using a water-in-oil emulsion method.[41] Conversion of interior amines to NO-releasing diazeniumdiolates resulted in particles with long NO-release half-lives due to the basicity of the local NO donor environment ($t_{1/2}$ = 66 h). These particles were doped into the pores of Gore-tex vascular grafts with a yield of 10 nmol NO/mg graft materials.[41] Analogous to water soluble PEIs, however, the crosslinked PEI particles present toxicity risks inherent to the PEI scaffolds. To fabricate biocompaticle NO-releasing micro-particles, Jeh et al. reported the encapsulation of *N*-diazeniumdiolate-modified proline (PROLI/NO) within biodegradable polyethylene oxide-co-lactic acid (PELA) or poly-lactic-co-glycolic acid (PLGA) microparticles by a double emulsion method.[42] Both particles were capable of releasing ~120 nmol NO/mg with a half life of ~4.0 min.

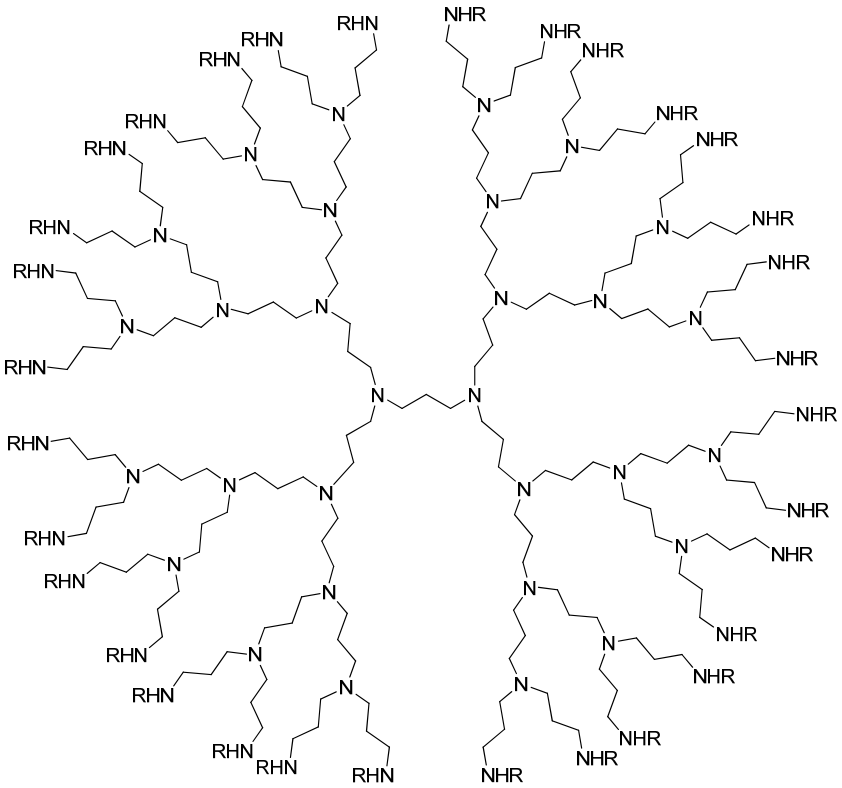

Figure 1.1 Secondary-amine functionalized polyethylenimine (PPI) dendrimers.

The size of the PELA particles (~2 μm) may allow for subsequent inhalation therapy whereas the much larger PLGA particle (23.5 μm) are less useful as stand-alone therapeutics.[43] Although these biodegradable NO-releasing particles are anticipated to show reduced toxicity (this was not studied), their low NO storage and inability to control NO release have limited their use as therapeutics.

Over recent years, a number of *N*-diazeniumdiolate NO donor-modified nanoscaffolds have been created to make use of the drug delivery advantages of nanomaterials and better harness the power of NO. For example, NO-releasing gold nanoparticles were synthesized by conjugating polyamine ligands onto the surface of gold nanoparticles and then functionalization with NO.[34] These materials exhibited a NO storage capacity of 0.386 μmol/mg with durations exceeding 16 h.[34] Although the particles exhibited desirable properties (e.g., water solubility and multivalency) for pharmacological applications,[34] the cost of the gold and necessary solvents greatly hindered their further development as NO-based therapeutics (primarily due to scale up concerns). To prepare low cost NO-releasing nanoparticles, silica-based materials have been extensively studied. Zhang et al. reported the synthesis of *N*-diazeniumdiolate NO donor-modified fumed silica particles (200 to 300 nm) by grafting aminosilanes onto the particle surface and then functionalizing the secondary amines with NO.[44] The NO donor-grafted particles released ~0.56 μmol NO/mg with a half-life of 43 min under physiological conditions.[44] The low NO storage was a result of the limited number of silanol groups on the particle surface to modify with aminosilanes. To enhance NO storage, Shin et al. has synthesized aminosilane/tetraethoxysilane (TEOS) hybrid

particles by co-condensation of aminosilanes with TEOS.[45] In contrast to surface grafted particles, the hybrid particles contained amines (aminosilanes) throughout the silica scaffold, resulting in significantly larger NO storage (~1.8 μmol/mg). Furthermore, the total NO storage (i.e., 0.056–1.8 μmol/mg) and kinetics (i.e., half life 0.5–12 h) proved tunable by varying the amount and types of aminosilanes, respectively.[45] To further control the size of NO-releasing silica particles, a reverse microemulsion technique was used to synthesize NO-releasing silica particles with distinct sizes (i.e., 50, 100, 200 nm) by controlling the organic solvents and reaction time.[27] In a reverse microemulsion strategy, smaller organic solvent molecules can penetrate deeper into the surfactant layer, decreasing the overall size of the water droplet and ensuing particles.[27] As such, high molecular weight organic solvents (i.e., heptanes) were used to yield 100 and 200 nm sized particles in 3 and 18 h reactions, respectively. In contrast, low molecular weight organic solvent (i.e., pentane) resulted in smaller particles (i.e., 50 nm).[27] Collectively, NO-releasing silica particles have shown varied NO-release kinetics and sizes, facilitating studies on the influence of NO-release kinetics and scaffold size on biological effects (i.e., biocidal activity). To date, particle shape has been neglected despite its role in drug delivery efficiency.[46-47]

1.3 *S*-Nitrosothiol Functionalized Macromolecules

1.3.1 S-Nitrosothiol Formation and NO-Release Characteristics

In contrast to *N*-diazeniumdiolate NO donors, *S*-nitrosothiols (RSNO) are the endogenous transporters of NO in the body and form the basis of a number of NO signaling cascades.[48] For example, *S*-nitrosoglutathione (GSNO) is an endogenous *S*-nitrosothiol (SNO) that plays a critical role in NO signaling.[48] *S*-nitrosothiols are formed

either via the reaction of thiols (e.g., glutathione) with dinitrogen trioxide or through a host of redox mechanisms involving metabolites of NO and transition metal centers.[49] Nitric oxide stored in this way also regulates several biological processes including vasodilation, platelet activation, neurotransmission, and tissue inflammation.[49] Nitrosated cysteine on albumin and other serum proteins account for a large portion of the ~1.8 μM nitrosothiol concentration in blood.[50] In the lab, nitrosothiols can be synthesized by the reaction of free thiols in acidified sodium nitrite solution.[51] Small molecule RSNOs (e.g., GSNO, *S*-nitroso-*N*-acetyl-D,L-penicillamine (SNAP)) synthesized via this method have been employed as NO sources to better understand the many roles of NO in regulatory biology.[52]

Compared to *N*-diazeniumdiolate NO donors, *S*-nitrosothiols decompose through a multitude of pathways.[53-54] Photo and thermal irradiation of RSNOs result in homolytic cleavage of the S-N bond, yielding NO and the thiyl radical. The thiyl radical may subsequently react with an RSNO to generate a disulfide and an additional equivalent of NO.[53-54] Dicks et al. have shown that Cu(I), resulting from the reduction of Cu(II) via trace thiolate ions, is active in a catalytic RSNO decomposition mechanism.[55] Transnitrosation between a thiol and an RSNO may also occur, resulting in the transfer of the nitroso functionality and the formation of a new RSNO species that may decompose via the aforementioned pathways.[53-54] As opposed to the proton-induced *N*-diazeniumdiolate NO donors breakdown, the multiple decomposition pathways of *S*-nitrosothiols, especially light irradiation, represents an alternative trigger for spatial and temporal control over NO release.[51] Although small molecule *S*-nitrosothiols have demonstrated great antiplatelet, antimicrobial, and vasodilatory activities,

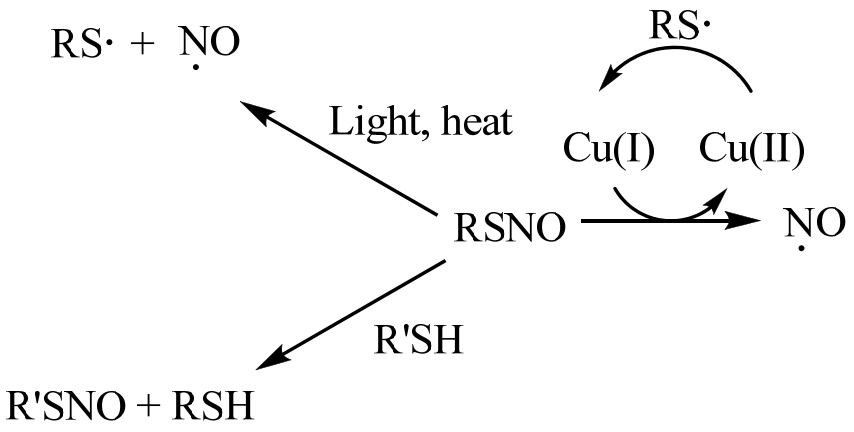

Scheme 1.2 Decomposition pathways of *S*-nitrosothiol.

both the inability to target the NO to a specific site and the rapid systemic clearance in vivo have hindered their clinical development.[56] As such, recent research has focused on the synthesis of macromolecular NO-releasing vehicles via *S*-nitrosothiol NO donors.

1.3.2 S-Nitrosothiol Silica Particles

Analogous to the *N*-diazeniumdiolate-grafted fumed silica mentioned previously, Frost et al. reported the synthesis of surface grafted *S*-nitrosothiol-modified silica particles by anchoring *S*-nitrosothols onto the particle surface.[57] In a typical synthesis, thiolated silanes were tethered to the surface of fumed silica particles, and then converted to the corresponding *S*-nitrosothiol form by reaction with *tert*-butylnitrite. The NO storage for the *S*-nitrosothiol-modified silica particles was roughly 0.138 μmol NO/mg with release of NO readily controlled by the duration and intensity of heat or light to initiate NO release. The low NO storage of these particles was attributed to the limited surface area for the grafting of *S*-nitrosothiols. To increase NO storage capacity, Riccio et al. synthesized thiol-modified silica particles by co-condensation of a thiolated silane and tetraethoxysilane. Enhanced NO storage was anticipated due to the incorporation of thiolated silanes throughout the particles. The nitrosation of the thiol-modified particles resulted in significantly increased NO storage (up to ~4.40 μmol NO/mg) and tunable sizes (241-718 nm).[58] However, the duration of NO release in PBS shielded from light at 37 ^{o}C was only ~24 h due to the instability of primary *S*-nitrosothiols.[58] More extended NO release is desired to enable better understanding of the effects of larger NO exposure to bacteria, cells, and tissue.

1.3.3 S-Nitrosothiol Poly(amidoamine) (PAMAM) Dendrimers

The size of a drug delivery scaffold greatly influences the delivery efficiency and related therapeutic performance.[27] While NO-releasing silica particles range in size from ~50 to 1000 nm, dendrimers can be synthesized at sizes less than 10 nm.[45, 58-59] While maintaining high drug payloads per unit of drug carrier.[60] Indeed, previous work on *N*-diazeniumdiolate-modified polypropylenimine dendrimers revealed a greater NO storage capacity (~5.6 μmol/mg) compared to other types of macromolecular scaffolds.[29] The multivalent exterior of dendrimers also enables the attachment of additional functionalities on a single scaffold, making them extremely useful for drug targeting to a specific tissue type.[39] Stasko et al. synthesized *S*-nitrosothiol PAMAM dendrimers by modifying the exterior primary amines with either *N*-acetyl-D,L-penicillamine (NAP) or *N*-acetyl-L-cysteine (NACys), followed by the nitrosation of the dendritic thiols.[59] Chemiluminescent NO detection was used to demonstrate that the dendrimers stored ~2 μmol NO/mg.[59] The kinetics of NO release was found to be highly dependent on the structure of the nitrosothiol (i.e., tertiary vs. primary). Primary nitrosothiol-functionalized dendrimers exhibited slower NO-release kinetics due to the "cage effect", causing recombination of NO and thiyl radical, resulting in *S*-nitrosothiol reformation. Despite the greater NO storage of these dendrimers, the NO release in PBS at 37 ^{o}C was negligible for both primary and tertiary *S*-nitrosothiol-modified dendrimers when shielded from light, hindering the utility of these materials in applications where light triggered NO release is not feasible. *S*-nitrosothiol-modfied dendrimers capable of releasing large amounts of NO under physiological conditions (dark, 37 ^{o}C) remains an important opportunity for study.

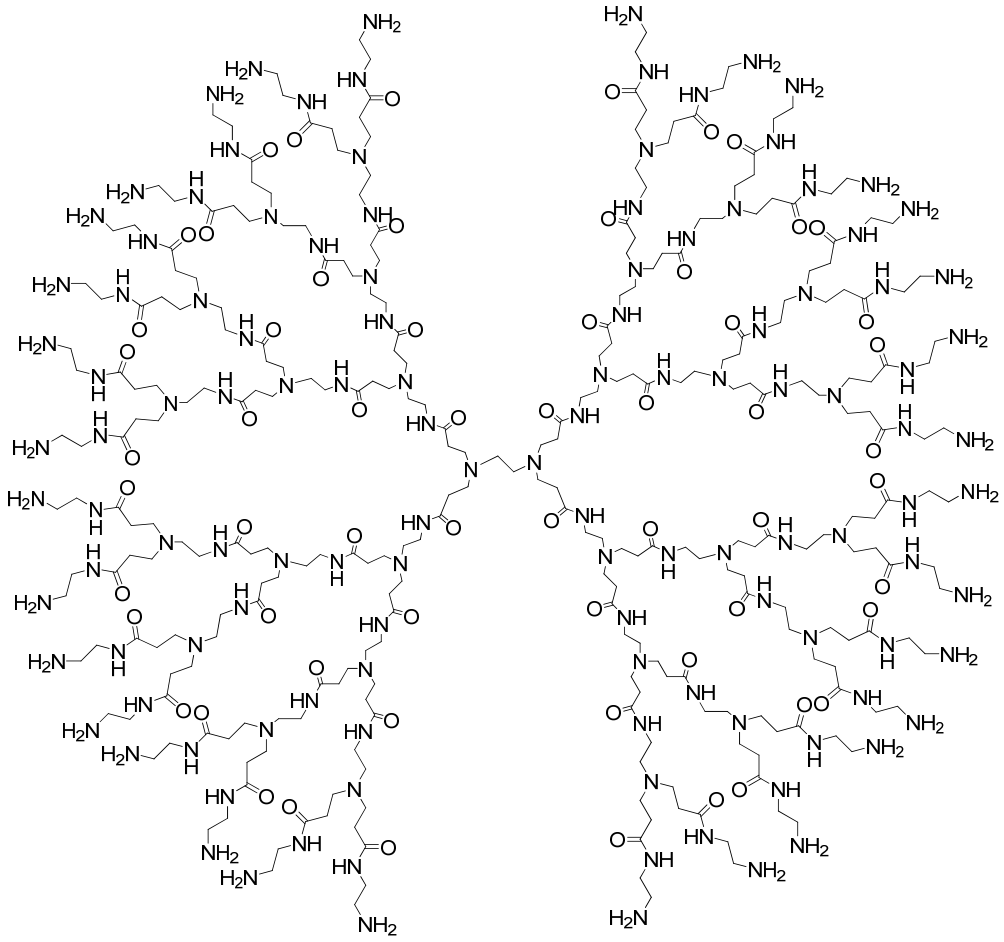

Figure 1.2 Chemical structure of generation 3 poly(amidoamine) (PAMAM) dendrimers.

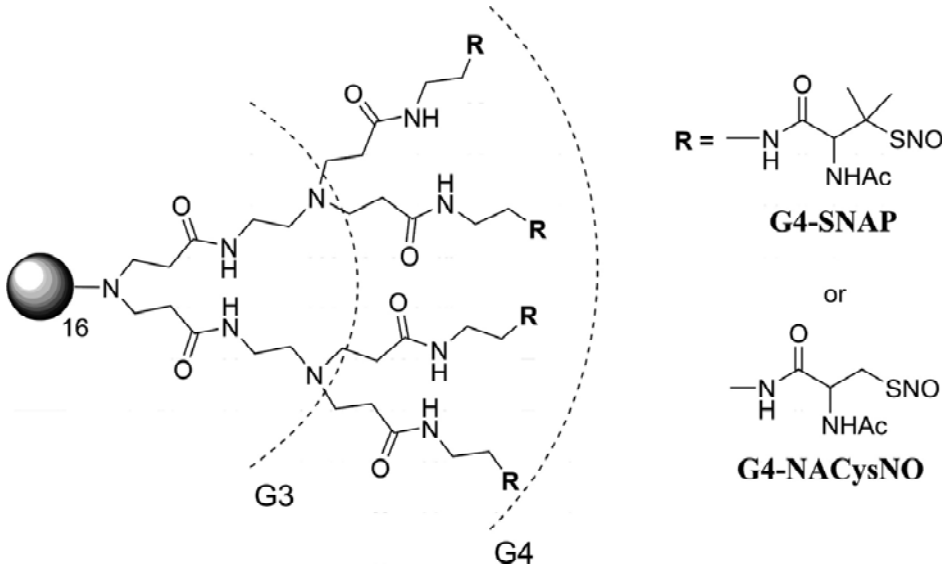

Figure 1.3 Generation 4 PAMAM dendrimers with a completely modified exterior (64 thiols) of *S*-nitroso-*N*-acetyl-D,L-penicillamine (G4-SNAP) or *S*-nitroso-*N*-acetylcysteine (G4-NACysNO).

1.4 Antibacterial properties of Nitric Oxide

Bacteria in nature exist in two states – free-floating planktonic bacteria and bacterial biofilms.[61] Medically relevant infections such as those associated with medical implants, diabetes mellitus, and cystic fibrosis are often caused by bacterial biofilms.[61-63] Biofilms are communities of microorganisms adhered to a surface and embedded within a self-produced exopolysaccharides (EPS) matrix, which anchors and protects the encapsulated bacteria from immune cells and antibiotics.[64] Along with protective EPS inhibiting the penetration of antibiotics, biofilms exhibited other defense mechanisms such as overexpression of stress-responsive genes, oxygen gradients within the biofilm matrix, and differentiation of a subpopulation of biofilm bacteria into resistant dormant species.[65-68] Collectively, this results in greater resistance to antimicrobial action of agents/drugs compared to planktonic bacteria. As such, antimicrobial agents capable of eradicating biofilms are urgently needed.[69-77]

Fortunately, NO plays a key role in the natural immune response to pathogens.[1, 78] Both NO and its reactive byproducts (e.g., peroxynitrite and dinitrogen trioxide) exert significant oxidative and nitrosative stress on bacteria to facilitate killing. Nitrosative stress occurs when thiols on proteins and DNA are nitrosated, impairing normal function. Oxidative stress is mostly observed through lipid peroxidation that readily destroys the bacterial membrane integrity.[1, 78] As such, gaseous NO and NO-releasing scaffolds have been used as antimicrobial agents against planktonic bacteria and biofilms. In this section, recent development of NO gas, small molecule NO donors, and NO-releasing macromolecular scaffolds as antibacterial agents are reviewed.

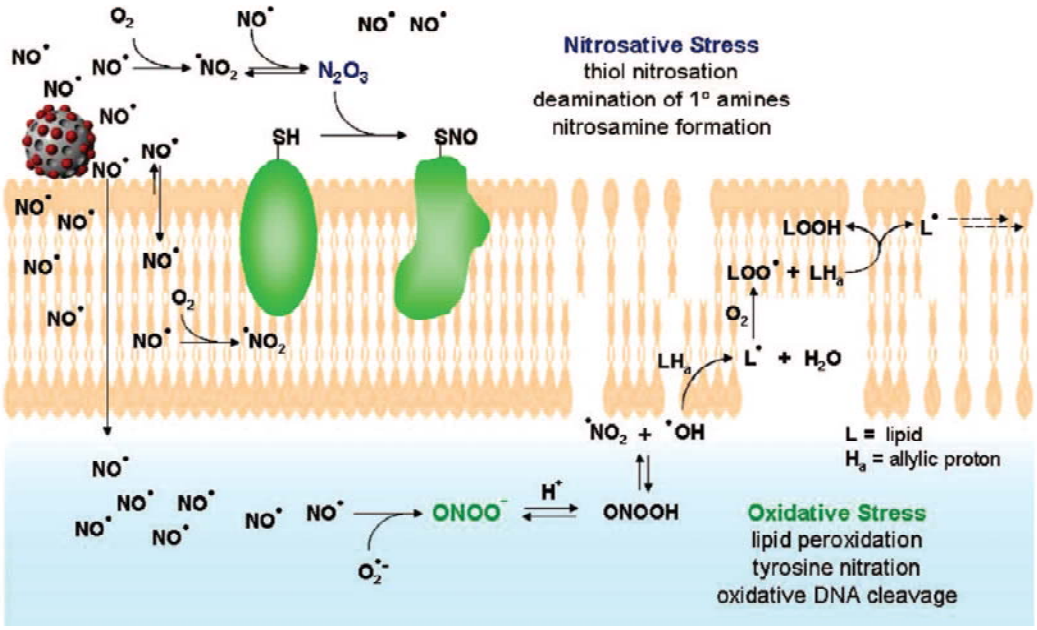

Figure 1.4 Proposed mechanisms by which NO acts as an antibacterial agent[26]

1.4.1 Gaseous NO (gNO)

Gaseous NO (gNO) is an FDA-approved therapy and has been clinically used in the U.S. to treat pulmonary hypertension.[79] Due to the established protocol of administration, gaseous NO has also been studied as a strategy to treat bacterial infection. Gahaffari et al. reported on the use of gaseous NO (gNO) to eradicate clinical isolates of *Staphylococcus aureus*, methicillin-resistant *S. aureus* (MRSA), *Escherichia coli*, Group B *Streptococcus*, *Pseudomonas aeruginosa*, and *Candida albicans*.[80] Medical grade gNO was delivered to bacteria cultures using a horizontal-flow delivery system. Exposure to gNO at 200 ppm for ~4.1 h completely inhibited bacterial growth. Additionally, the authors reported that the NO exposure did not elicit cytotoxicity against human fibroblast cells for up to 48 h. Despite the bactericidal efficacy and low cytotoxicity of gNO, the cumbersome delivery system and safety concerns of possible nitrogen dioxide formation by the oxidation of gNO warranted more efficient NO-delivery systems.[81]

1.4.2 Small Molecule Nitric Oxide Donors as Antibacterial Agents

N-diazeniumdiolate and *S*-nitrosothiol NO donors enable nearly instantaneous release of NO under physiological conditions, allowing for a wide range of biomedical applications including as antimicrobial agents. Indeed, small molecule NO donors have been used to demonstrate antibacterial action.[82-84] Examples of readily available small molecule NO donors include 1-[2-(carboxylato)pyrrolidin-1-yl]diazen-1-ium-1,2-diolate (PROLI/NO), *N*- diazeniumdiolated diethyltriamine (DETA/NO), *S*-nitroso-*N*-acetylcysteine (SNAC), and S-nitrosoglutathione (GSNO) (Scheme 1.3). In some of the earliest work, Dukelow et al. reported the utility of *N*-diazeniumdiolated diethyltriamine (DETA/NO) for the treatment of acute *Pseudomonas aeruginosa* (*P. aerguginosa*)

pneumonia in a mouse model.[82] Pneumonia was induced by intratracheal instillation of *P. aeruginosa* (3×10^7 CFU/mL). Mice were treated with nebulized DETA/NO (12.5 or 125 μmol) at 4 and 12 h or continuous gaseous NO (10 or 40 ppm) before being sacrificed. Nebulized DETA/NO was shown to decrease the pulmonary bacterial load in mice with pneumonia by ~65% whereas inhaled NO gas had no significant effect on bacterial viability. Despite the enhanced bactericidal efficacy of DETA/NO, its use as an NO therapy is hindered due to the substantial toxicity observed.[82] In contrast, *S*-nitrosothiol NO donors such as GSNO and SNAC are endogenous transporters of NO.[48] The NO-mediated antimicrobial activity of GSNO and SNAC has been studied using several pathogens associated with infectious eye diseases.[84-86] For example, Cariello et al. evaluated the antimicrobial activity of GSNO and SNAC against clinical isolates *Pseudononas aeruginosa*, *Staphylococus aureus*, *Serratia marcescenes*, *Enterobacter aerogenes* from patients with infectious keratitis.[84] Both NO-release scaffolds proved effective at inhibiting and killing all bacterial strains. SNAC showed greater antimicrobial activity than GSNO against all bacteria, with Gram-positive bacteria being more susceptible to the NO-releasing *S*-nitrosothiols.[84]

Although the NO-mediated antimicrobial activity of small molecule NO donors demonstrates the potential of NO-releasing scaffolds as antimicrobial agents, the low NO payloads and inability to target the NO delivery limits their therapeutic usefulness. A recent review has highlighted the benefits of macromolecular scaffolds for drug delivery over small molecule NO-releasing systems.[87]

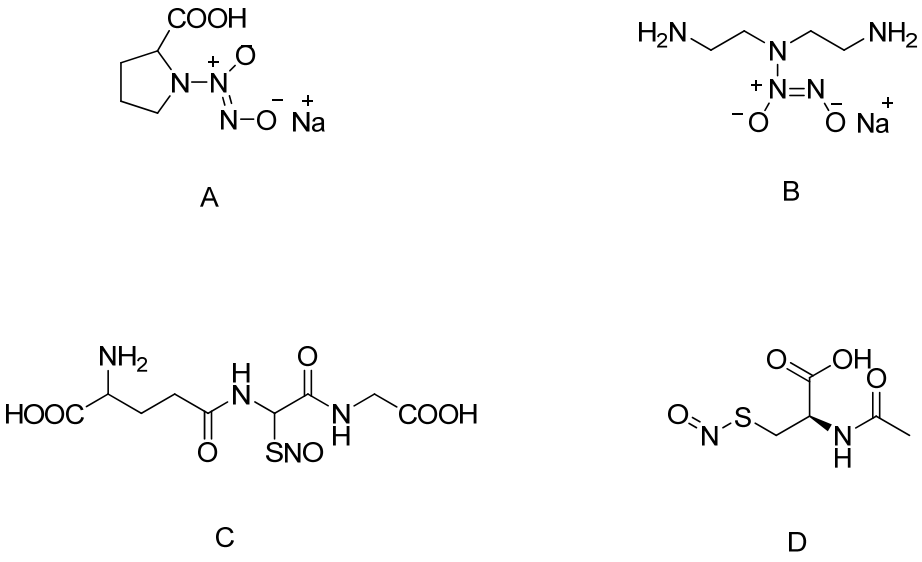

Scheme 1.3 Structure of small molecule NO donors. A) 1-[2-(carboxylato)pyrrolidin-1-yl]diazen-1-ium-1,2-diolate (PROLI/NO); B) *N*- diazeniumdiolated diethyltriamine (DETA/NO); C) *S*-nitroso-*N*-acetylcysteine (SNAC); D) S-nitrosoglutathione (GSNO).

Indeed, work by former group members in the Schoenfisch lab has shown enhanced bacterial killing and reduced cytotoxicity of NO-releasing silica particles compared to small molecule NO donors.[26] A wide range of NO-releasing macromolecular scaffolds have been synthesized to date including particle and dendrimer scaffolds modified with nitrite, *N*-diazeniumdiolates, and *S*-nitrosothiols. In contrast to *S*-nitrosothiol-modified macromolecular scaffolds, nitrite-containing and *N*-diazeniumdiolate-modified materials have exhibited larger NO payloads under physiological conditions (dark, 37 ^{o}C), and thus represent more suitable systems as antibacterial therapeutics.

1.4.3 Nitrite-Containing NO-releasing Macromolecular Scaffolds

When exposed to low pH or reducing agent, nitrites are able to generate exogenous NO and have been used to treat skin infections.[88] Nitrite has also been incorporated into macromolecular scaffolds for NO release. For example, Friedman et al. reported the synthesis of nitrite-containing hydrogel/glass nanoparticles by lyophilizing a gel formed from the mixture of tetramethyl orthosilicate, polyethylene glycol, chitosan, glucose, and sodium nitrite in a 0.5 mM sodium phosphate buffer.[89] The encapsulated sodium nitrite was reduced to NO within the matrix with thermally generated electrons from glucose. The NO-release profile at 37 ^{o}C of the resulting particles showed an initial burst of NO at 20 pmol NO/mg particle followed by a steady state of NO at 8 pmol NO/mg particle. To evaluate the susceptibility of clinical MRSA strains to these NO-releasing hydrogel/glass nanoparticles, 10^7 colony forming unit (CFU)/mL MRSA suspensions were incubated with the particles at concentrations ranging from 313 to 5000 μg/mL.[90] The minimum inhibitory concentration (MIC) for the NO-releasing hydrogel/glass nanoparticle against 11 clinical isolated MRSA ranged from 313 to 2500 μg/mL.[90] Additionally, the efficacy

of the hydrogel/glass nanoparticle in killing MRSA was studied in mice.[90] Full thickness excision wounds of 5 mm diameter were infected by inoculation using 10^7 CFU MRSA in phosphate buffered saline (PBS). The wounds were then treated with 5 mg NO-releasing hydrogel/glass particles at 1 and 72 h. On day 7, MRSA growth was inhibited by 5-logs for mice treated with NO-releasing hydrogel/glass nanoparticles compared to untreated wounds.[90]

Although the nitrite-containing nanoparticles exhibited an inhibitory effect on bacterial growth, their ability to kill bacteria was not evaluated. The poor control over NO release and particle morphologies along with the carcigenic risk of nitrite clearly limit their application as antimicrobial therapeutics.[91] To prepare less toxic NO-releasing scaffolds, recent research has focused on the development of *N*-diazeniumdiolate NO donor-modified macromolecular scaffolds as antimicrobial agents.

1.4.4 N-Diazeniumdiolate-Functionalized Silica Nanoparticles

Silica nanoparticles have been studied extensively as scaffolds for drug delivery due to their relatively low toxicity and tunable size.[92] Most recently, the ability to store NO onto silica scaffolds have has also been demonstrated.[27, 45] For example, Hetrick et al. reported the synthesis of aminosilane/tetraethoxysilane (TEOS) hybrid particles with tunable NO-release kinetics and sizes, allowing for study of how size and NO-release kinetics affect antibacterial activity. Among the particles synthesized, the utility of TEOS/*N*-(6- Aminohexyl)aminopropyltrimethoxysilane (AHAP3) hybrid silica particles as novel antibacterial agents was demonstrated against *Pseudomonas aeruginosa*.[26] Comparison of the bactericidal efficacy of the NO-releasing nanoparticles to small molecule 1-[2-(carboxylato)pyrrolidin-1-yl]diazen-1-ium-1,2-diolate (PROLI/NO)

demonstrated enhanced bactericidal efficacy for the particles-derived NO due to particle-bacteria association and more efficient NO delivery.[93] The bactericidal NO dose from the NO-releasing silica particles (i.e., 0.6 μmol/mL) was also much lower than that required from small molecule NO donors PROLI/NO (i.e., 4.5 μmol/mL). The NO-releasing silica particles also elicited less toxicity to mammalian cells at the minimum bactericidal concentration (MBC) compared to small molecule NO donors PROLI/NO, indicating the improved therapeutic potential of these macromolecular scaffolds.[26] To study how scaffold size affects bactericidal efficacy, NO-releasing AHAP/TEOS hybrid silica particles of three distinct sizes (e.g., 50, 100, 200 nm) were synthesized by reverse microemulsion.[27] The similar NO storage (~1 μmol/mg) and NO-release kinetics (t_m=0.6 min) allowed for a study of size-dependent bacterial killing against *P. aeruginosa*. Briefly, the bactericidal efficacy of the NO-releasing nanoparticles against *P. aeruginosa* increased with decreasing particle size as a result of improved particle-bacteria association.[27]

The ability of nitric oxide (NO)-releasing silica nanoparticles to kill biofilm bacteria was reported by Hetrick et al.[38] Replicative viability experiments revealed that > 99% of bacteria from *Pseudomonas aeruginosa*, *Escherichia coli*, *Staphylococcus aureus*, *Staphylococcus epidermidis*, and *Candida albicans* biofilms were killed via NO release, with the greatest efficacy (>99.999% killing) against Gram-negative *P. aeruginosa* and *E. coli* biofilms.[38] Unfortunately, the NO-releasing silica particles exhibited significant toxicity to mammalian cells (~80% cell viability reduction) at concentrations required to eradicate biofilms, necessitating the design of NO-releasing silica particles with enhanced biocidal activity and reduced toxicity to mammalian cells.

1.4.5 N-Diazeniumdiolate-NO donors-Modified Dendrimers

Based on the silica size study, the use of dendrimers as NO-delivery vehicles were expected to exhibit more enhanced antibacterial activity. Sun et al. evaluated the antibacterial activity of a series of NO-releasing poly(propylene imine) (PPI) dendrimers against both Gram-positive and Gram-negative planktonic bacteria, including methicillin-resistant *Staphylococcus aureus*.[94] The bactericidal efficacy of the NO-releasing dendrimers was highly dependent on their exterior functionality with hydrophobic functionalization exhibiting enhanced bactericidal efficacy due to facilitating greater association with bacteria and allowing for more efficient intracellular NO delivery. In contrast to the control dendrimers (non-NO-releasing), the NO-releasing dendrimers also showed less cytotoxicity to L929 mouse fibroblast cells due to the lower dose of material required.[94] However, dendrimers with hydrophobic exteriors proved toxic (>80% viability reduction) at 2x minimum bactericidal concentrations (~30 μg/mL), a potential concern when used to eradicate biofilms where larger doses of material are required. As such, dendrimers with tunable exterior hydrophobicity should be evaluated to study the impact of such functionalization on the bactericidal efficacy and cytotoxicity to mammalian cells.

1.5 Impact of Particle Morphologies on Drug Delivery Efficiency

Recent work on particle design for drug delivery to mammalian cells indicates the importance of particle shape on particle-cell adhesion strength, internalization rate, biodistribution, cytotoxicity, phagocytosis and circulation time.[95-109] In particular, rod-like nanoparticles have been shown to influence mammalian cell internalization and circulation time compared to their spherical or cubic counterparts.[101-105] For example,

rod-like PEG hydrogel, mesoporous silica and needle-shaped poly(lactide-co-glycotide) (PLGA) particles with high aspect ratios (e.g., aspect ratio of 3) were found to be internalized in a faster rate compared to their spherical or cubic counterparts. [47, 99, 102-103] PLGA needles also exhibited substantially larger cytoplasmic delivery of drug.[47] In contrast, gold nanorods with high aspect ratio were less internalized by human breast adenocarcinoma cell line (MCF-7),[110] indicating that the interaction between particles and cells depends on both particle properties (e.g., morphology, surface chemistry) and cell type. Likewise, particle shape may play an important role in particle phagocytosis and circulation time in the blood stream.[46] Filomicelles with high aspect ratios were reported to exhibit reduced rates of phagocytosis and long circulation half-lives (e.g., ~5 days) in comparison to spherical micelles.[108] Although the influence of particle shape on particle interactions with mammalian cells and macrophages has been noted in prior reports, the effect of particle shape on antibacterial efficacy has not been evaluated carefully to date.

1.6 Mesoporous Silica Particles for Drug Delivery

Mesoporous silica materials were first developed by Mobil Oil Corporation using surfactant molecules as templates for silicate polymerization.[111] To date, both acidic[112-113] and alkaline[111, 114-115] synthetic strategies have been used to prepare mesoporous silica materials.[116-120] According to a mechanism proposed by Stucky and coworkers,[112-113, 121] mesophase formation arises from the multidentate binding of silicate species to surfactant micelle interfaces *via* electrostatic interactions. The resulting liquid crystal phases self-assemble by charge density matching across the interface, and continuously grow end-to-end or side-to-side through accretion into well-formed particles.[122] Mesoporous particles

with unique porous structures have been widely used as drug delivery systems for tissue engineering[123], diabetes, [124]inflammation,[125] and cancer[92] due to their tailorable pore structure, high specific surface area, and large pore volume, allowing for the encapsulation of therapeutic agents. The size and morphology of the resulting particles are easily tuned in a scalable, cost-effective, and controllable manner.[126] Control over the aspect ratio of micron-sized mesoporous silica rods under acidic condition was reported by Naik et al by adjusting silane concentration and pH.[122] As shown in Figure 1.5, the large surface area of mesoporous silica particles may result in larger NO storage by anchoring larger amount of aminosilanes on the particle surface.

1.7 Chitosans for Nitric Oxide Release

Although silica particles and dendrimers with controlled NO release and size can be synthesized, certain applications may require scaffolds capable of degradation after the NO release expires. For example, NO-induced eradication of the biofilms in the lungs of cystic fibrosis might benefit more from NO-releasing scaffolds that degrade over time. Chitosan, the second most abundant natural biopolymer, has been widely used for a number of applications including tissue engineering, drug delivery, and antimicrobial agents, due to its biocompatibility, biodegradability and cationic composition.[127-130] The development of chitosan derivatives as NO-releasing scaffolds has also been explored due to the high concentration of amine precursors necessary for *N*-diazeniumdiolate NO donor formation.[131-133]

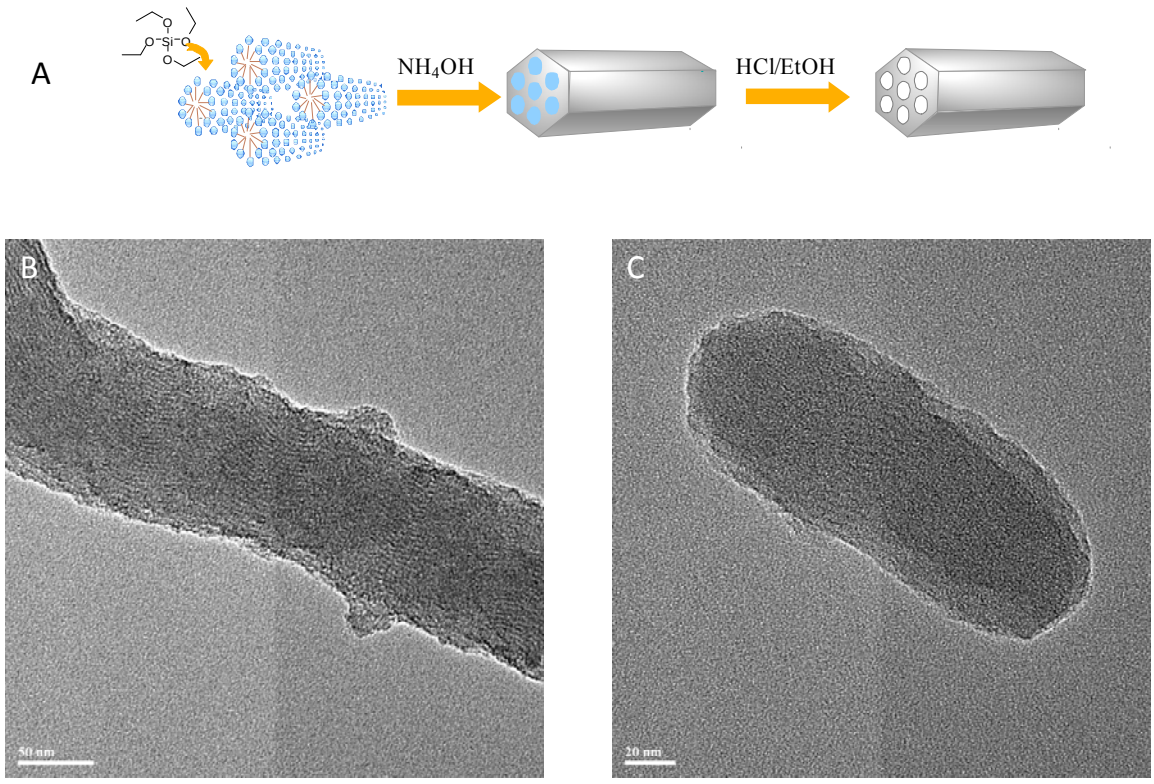

Figure 1.5 Synthesis of mesoporous silica particles by A) surfactant-templated routes and representative transmission electron microscopy images of particles with different morphologies. B) particles with high aspect ratio; C) particles with low aspect ratio.

To date, the *N*-diazeniumdiolate NO donor-functionalized chitosan polysaccharides (~60 to 220 kD) have been characterized by low *N*-diazeniumdiolate conversion efficiency and NO storage (~0.2 μmol/mg), likely the result of chitosan's insolubility under the basic conditions required for *N*-diazeniumdiolate formation (Scheme 1.4).[131-133] The potential bactericidal efficacy of such scaffolds would clearly be limited due to their insolubility under physiological conditions and low NO payloads.[134,135] In this regard, chitosan oligosaccharides (< 20 kD) may prove more useful as NO-releasing scaffolds due to their solubility under basic conditions. Multiple strategies have been reported for degrading chitosan into oligomer derivatives, including direct oxidative and enzymatic degradation.[136-137] Compared to enzymatic degradation where enzymes (e.g., chitosanase) are required, oxidative degradation by hydrogen peroxide represents a more facile and economic approach. The molecular weight (M_w) of the product can be controlled by varying the oxidation conditions (e.g., concentration of hydrogen peroxide and temperature) and determined by the classic Mark-Houwink equation.[138]

1.8 Impact of NO-Release Kinetics

Although NO has been shown to be an important mediator of wound healing, the foreign body response and bactericidal efficacy, the exact effects of NO-release kinetics remains unclear.[139] Nichols et al. designed NO-releasing polyurethane-coated wires that were implanted into porcine subcutaneous tissue to evaluate the foreign body response as a function of NO release. The NO-release kinetics of the polyurethane coating were controlled by the type of NO-releasing silica particle dopants (e.g., *N*-diazeniumdiolate- and *S*-nitrosothiol-modified silica particles) and polyurethane.

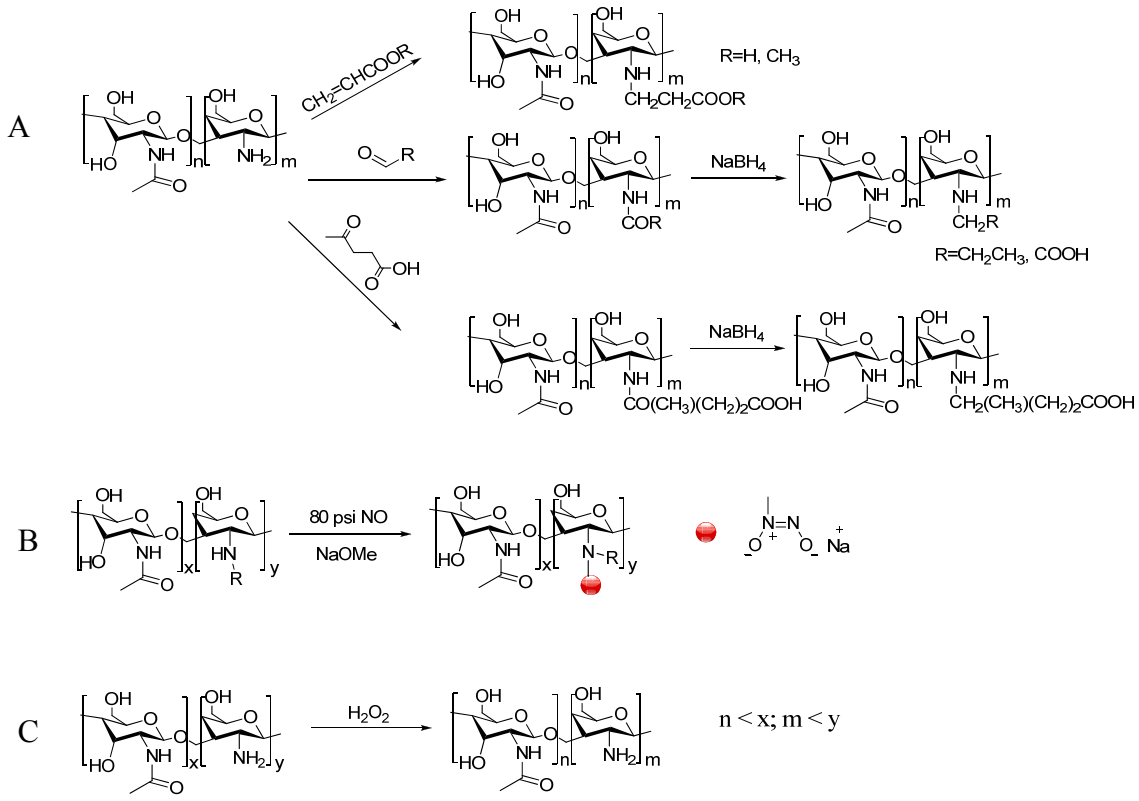

Scheme 1.4 Synthesis of A) secondary amine-; and B) *N*-diazeniumdiolate-modified chitosan polysaccharides; and, C) oxidative degradation of chitosan polysaccharides. R=$CH(CH_3)CH_2CH_2COO^-Na^+$, $CH_2CH_2COO^-Na^+$, $CH_2CH_2COOCH_3$, $CH_2COO^-Na^+$, $CH_2CH_2CH_3$.

The most prolonged NO release was achieved using *S*-nitrosothiol silica particle-doped polyurethane, with a duration of 14 d. Histological analysis revealed that materials with longer release durations (i.e., 14 d) and greater NO payloads more significantly reduced the collagen encapsulation at 3 and 6 weeks relative to faster, more finite NO-releasing coatings.[139] Analogously, the bactericidal efficacy of NO-releasing materials may also depend on the amount of NO released and the NO-release kinetics. Prior work by Hetrick et al. demonstrated that the rapid NO release (e.g., half life ~18 min) from *N*-Methylaminopropyltrimethoxysilane (MAP3)/TEOS hybrid NO-releasing silica particles exhibited 1000-fold improvement in biofilm eradication compared to AHAP/TEOS (e.g., half life ~6 min).[38] Further systematic investigation is clearly necessary.

1.9 Overview of Dissertation Research

Prior work in the Schoenfisch lab have focused mainly on the development of macromolecular scaffolds (e.g., silica particles, dendrimers) with tunable NO-release kinetics and sizes. The bactericidal efficacy of *N*-diazeniumdiolate NO donor-modified silica particles and dendrimers is highly dependent on the NO-release kinetics, exterior hydrophobicity, and scaffold size.[26, 94] Nitric oxide-releasing silica particles and dendrimers proved effective at killing planktonic bacteria with minimal toxicity against mammalian cells. Unfortunately, the cytotoxicity (~80% viability reduction) of the particles remains a concern, and warrants further improvement in the design of NO-releasing scaffolds.[38] To improve the biocidal efficacy of NO release, my research has focused on the synthesis of NO-releasing macromolecular scaffolds (e.g., silica particles, dendrimers, and chitosan oligosaccharides) with tunable NO-release kinetics, sizes/molecular weights, shapes, and exterior functionalities to control hydrophobicity.

The NO-delivery efficiency and ensuing bactericidal efficacy of these materials were carefully evaluated against both planktonic bacteria and biofilms as a function of their physical and chemical properties mentioned above.

The specific aims of my research included:

1) the synthesis of *N*-diazeniumdiolate-functionalized dendrimers with controlled NO release for studying of the structure/property relationships of these materials on NO-release kinetics;

2) the design of *N*-diazeniumdiolate NO donor-functionalized dendrimers with unique exterior hydrophobicities to study how the exterior of the dendrimer impacts bactericidal efficacy against bacteria biofilms and cytotoxicity to mammalian cells;

3) the synthesis of *N*-diazeniumdiolate-NO donor-functionalized silica rods with different aspect ratios to enable the study of the shape- and NO release-dependent bactericidal efficacy against both Gram-positive and -negative bacteria;

4) the synthesis of *N*-diazeniumdiolate-functionalized chitosan oligosaccharides as new, biodegradable NO-releasing vehicles.

The research in this thesis presents the synthesis of various NO-releasing scaffolds with tunable NO-release properties, exterior functionality, and morphologies. The NO delivery efficiency and bactericidal efficacy as a functional of these chemical and physical properties were systematically studied, facilitating the future development of NO-releasing materials as antimicrobial therapeutics.

1.10 References

1. Marletta, M. A.; Tayeh, M. A.; Hevel, J. M. Unraveling the biological significance of nitric oxide. *Biofactors* **1990,** *2*, 219-225.

2. Vaughn, M. W.; Kuo, L.; Liao, J. C. Estimation of nitric oxide production and reaction rates in tissue by use of a mathematical model. *Am. J. Physiol.-Heart C* **1998,** *274*, H2163-H2176.

3. Furchgott, R. F., Endothelium-derived relaxing factor: Discovery, early studies, and identifcation as nitric oxide (Nobel lecture). *Angew. Chem. Int. Edit.* **1999,** *38*, 1870-1880.

4. Napoli, C.; Ignarro, L. J., Nitric oxide-releasing drugs. *Annu. Rev. Pharmacol.* **2003,** *43*, 97-123.

5. McMackin, C. J.; Vita, J. A. Update on nitric oxide-dependent vasodilation in human subjects. *Method Enzymol.* **2005,** *396*, 541-553.

6. Granger, H. J.; Ziche, M.; Hawker, J. R.; Meininger, C. J.; Czisny, L. E.; Zawieja, D. C. Molecular and cellular basis of myocardial angiogenesis. *Cell Mol. Biol. Res.* **1994,** *40*, 81-85.

7. Kondo, T.; Kobayashi, K.; Murohara, T. Nitric oxide signaling during myocardial angiogenesis. *Mol. Cell Biochem.* **2004,** *264*, 25-34.

8. Sanders, K. M.; Ward, S. M. Nitric-oxide as a mediator of nonadrenergic noncholinergic neurotransmission. *Am. J. Physiol.* **1992,** *262*, G379-G392.

9. Nathan, C.; Shiloh, M. U. Reactive oxygen and nitrogen intermediates in the relationship between mammalian hosts and microbial pathogens. *Proc. Natl. Acad. Sci. U. S. A.* **2000,** *97*, 8841-8848.

10. Shah, V.; Lyford, G.; Gores, G.; Farrugia, G. Nitric oxide in gastrointestinal health and disease. *Gastroenterology* **2004,** *126*, 903-913.

11. Reid, M. B. Invited Review: redox modulation of skeletal muscle contraction: what we know and what we don't. *J. Appl. Physiol.* **2001,** *90*, 724-731.

12. Stamler, J. S.; Meissner, G. Physiology of nitric oxide in skeletal muscle. *Physiol. Rev.* **2001,** *81*, 209-237.

13. Przedborski, S.; Dawson, T. M. The role of nitric oxide in Parkinson's disease. *Methods Mol. Med.* **2001,** *62*, 113-136.

14. Williams, I. L.; Wheatcroft, S. B.; Shah, A. M.; Kearney, M. T. Obesity, atherosclerosis and the vascular endothelium: mechanisms of reduced nitric oxide bioavailability in obese humans. *Int. J. Obesity* **2002,** *26*, 754-764.

15. Wink, D. A.; Vodovotz, Y.; Laval, J.; Laval, F.; Dewhirst, M. W.; Mitchell, J. B., The multifaceted roles of nitric oxide in cancer. *Carcinogenesis* **1998,** *19*, 711-721.

16. Babich, H.; Zuckerbraun, H. L. In vitro cytotoxicity of glyco-S-nitrosothiols: a novel class of nitric oxide donors. *Toxicol. in Vitro* **2001,** *15*, 181-190.

17. Hou, Y. C.; Wang, J. Q.; Andreana, P. R.; Cantauria, G.; Tarasia, S.; Sharp, L.; Braunschweiger, P. G.; Wang, P. G. Targeting nitric oxide to cancer cells: Cytotoxicity studies of glyco-S-nitrosothiols. *Bioorg. Med. Chem. Lett.* **1999,** *9*, 2255-2258.

18. de Souza, G. F. P.; Yokoyama-Yasunaka, J. K. U.; Seabra, A. B.; Miguel, D. C.; de Oliveira, M. G.; Uliana, S. R. B. Leishmanicidal activity of primary S-nitrosothiols against Leishmania major and Leishmania amazonensis: Implications for the treatment of cutaneous leishmaniasis. *Nitric Oxide-Biol. Chem.* **2006,** *15*, 209-216.

19. Fang, F. C. Antimicrobial reactive oxygen and nitrogen species: Concepts and controversies. *Nat. Rev. Microbiol.* **2004,** *2*, 820-832.

20. Schonhoff, C. M.; Matsuoka, M.; Tummala, H.; Johnson, M. A.; Estevez, A. G.; Wu, R.; Kamaid, A.; Ricart, K. C.; Hashimoto, Y.; Gaston, B.; Macdonald, T. L.; Xu, Z. S.; Mannick, J. B. S-nitrosothiol depletion in amyotrophic lateral sclerosis. *Proc. Natl. Acad. Sci. U. S. A.* **2006,** *103*, 2404-2409.

21. Schapiro, J. M.; Libby, S. J.; Fang, F. C. Inhibition of bacterial DNA replication by zinc mobilization during nitrosative stress. *Proc. Natl. Acad. Sci. U. S. A.* **2003,** *100*, 8496-8501.

22. Bell, R. M.; Maddock, H. L.; Yellon, D. M. The cardioprotective and mitochondrial depolarising properties of exogenous nitric oxide in mouse heart. *Cardiovasc. Res.* **2003,** *57*, 405-415.

23. Konorev, E. A.; Tarpey, M. M.; Joseph, J.; Baker, J. E.; Kalyanaraman, B., S-Nitrosoglutathione Improves Functional Recovery in the Isolated Rat-Heart after Cardioplegic Ischemic Arrest - Evidence for a Cardioprotective Effect of Nitric-Oxide. *J. Pharmacol. Exp. Ther.* **1995,** *274*, 200-206.

24. Schulz, R.; Kelm, M.; Heusch, G. Nitric oxide in myocardial ischemia/reperfusion injury. *Cardiovasc. Res.* **2004,** *61*, 402-413.

25. Radomski, M. W.; Rees, D. D.; Dutra, A.; Moncada, S. S-nitroso-Glutathione inhibits platelet activation in vitro and in vivo. *Brit. J. Pharmacol.* **1992,** *107*, 745-749.

26. Hetrick, E. M.; Shin, J. H.; Stasko, N. A.; Johnson, C. B.; Wespe, D. A.; Holmuhamedov, E.; Schoenfisch, M. H. Bactericidal efficacy of nitric oxide-releasing silica nanoparticles. *ACS Nano* **2008,** *2*, 235-46.

27. Carpenter, A. W.; Slomberg, D. L.; Rao, K. S.; Schoenfisch, M. H., Influence of scaffold size on bactericidal activity of nitric oxide-releasing silica nanoparticles. *ACS Nano* **2011,** *5*, 7235-7244.

28. Drago, R. S.; Paulik, F. E. The reaction of nitrogen oxide with diethylamine. *J. Am. Chem. Soc.* **1960,** *82*, 96-98.

29. Stasko, N. A.; Schoenfisch, M. H. Dendrimers as a scaffold for nitric oxide release. *J. Am. Chem. Soc.* **2006,** *128*, 8265-8271.

30. Davies, K. M.; Wink, D. A.; Saavedra, J. E.; Keefer, L. K. Chemistry of the diazeniumdiolates. 2. Kinetics and mechanism of dissociation to nitric oxide in aqueous solution. *J. Am. Chem. Soc.* **2001,** *123*, 5473-5481.

31. Coneski, P. N.; Schoenfisch, M. H. Competitive formation of N-diazeniumdiolates and N-nitrosamines via anaerobic reactions of polyamines with nitric oxide. *Org. Lett.* **2009,** *11*, 5462-5465.

32. Hrabie, J. A.; Klose, J. R.; Wink, D. A.; Keefer, L. K. New nitric oxide-releasing zwitterions derived from polyamines. *J. Org. Chem.* **1993,** *58*, 1472-1476.

33. Lu, Y.; Sun, B.; Li, C.; Schoenfisch, M. H. Structurally diverse nitric oxide-releasing poly(propylene imine) dendrimers. *Chem. Mater.* **2011,** *23*, 4227-4233.

34. Polizzi, M. A.; Stasko, N. A.; Schoenfisch, M. H. Water-soluble nitric oxide-releasing gold nanoparticles. *Langmuir* **2007,** *23*, 4938-4943.

35. Taite, L. J.; West, J. L. Poly(ethylene glycol)-lysine dendrimers for targeted delivery of nitric oxide. *J. Biomater. Sci. Polymer Edn.* **2006,** *17*, 1159-1170.

36. Zhao, H.; Serrano, M. C.; Popowich, D. A.; Kibbe, M. R.; Ameer, G. A., Biodegradable nitric oxide-releasing poly(diol citrate) elastomers. *J. Biomed. Mater. Res. A* **2010,** *93*, 356-363.

37. Zhou, Z. R.; Annich, G. M.; Wu, Y. D.; Meyerhoff, M. E. Water-soluble poly(ethylenimine)-based nitric oxide donors: Preparation, characterization, and potential application in hemodialysis. *Biomacromolecules* **2006,** *7*, 2565-2574.

38. Hetrick, E. M.; Shin, J. H.; Paul, H. S.; Schoenfisch, M. H. Anti-biofilm efficacy of nitric oxide-releasing silica nanoparticles. *Biomaterials* **2009,** *30*, 2782-9.

39. Tomalia, D. A.; Naylor, A. M.; Goddard, W. A. Starburst dendrimers - molecular-level control of size, shape, surface-chemistry, topology, and flexibility from atoms to macroscopic matter. *Angew. Chem. Int. Ed.* **1990,** *29*, 138-175.

40. Uhrich, K. E.; Cannizzaro, S. M.; Langer, R. S.; Shakesheff, K. M. Polymeric systems for controlled drug release. *Chem. Rev.* **1999,** *99*, 3181-3198.

41. Pulfer, S. K.; Ott, D.; Smith, D. J. Incorporation of nitric oxide-releasing crosslinked polyethyleneimine microspheres into vascular grafts. *J. Biomed. Mater. Res.* **1997,** *37*, 182-189.

42. Jeh, H. S.; Lu, S.; George, S. C. Encapsulation of PROLI/NO in biodegradable microparticles. *J. Microencapsul.* **2004,** *21*, 3-13.

43. Labiris, N. R.; Dolovich, M. B., Pulmonary drug delivery. Part II: The role of inhalant delivery devices and drug formulations in therapeutic effectiveness of aerosolized medications. *Brit. J. Clin. Pharmacol.* **2003,** *56*, 600-612.

44. Zhang, H. P.; Annich, G. M.; Miskulin, J.; Stankiewicz, K.; Osterholzer, K.; Merz, S. I.; Bartlett, R. H.; Meyerhoff, M. E. Nitric oxide-releasing fumed silica particles: Synthesis, characterization, and biomedical application. *J. Am. Chem. Soc.* **2003,** *125*, 5015-5024.

45. Shin, J. H.; Metzger, S. K.; Schoenfisch, M. H. Synthesis of nitric oxide-releasing silica nanoparticles. *J. Am. Chem. Soc.* **2007,** *129*, 4612-4619.

46. Champion, J. A.; Mitragotri, S. Role of target geometry in phagocytosis. *Proc. Natl. Acad. Sci. U. S. A.* **2006,** *103*, 4930-4934.

47. Yoo, J. W.; Doshi, N.; Mitragotri, S. Endocytosis and intracellular distribution of PLGA particles in endothelial cells: effect of particle geometry. *Macromol. Rapid Commun.* **2010,** *31*, 142-148.

48. Ignarro, L. J. Nitric oxide: A unique endogenous signaling molecule in vascular biology (Nobel lecture). *Angew. Chem. Int. Ed.* **1999,** *38*, 1882-1892.

49. Hogg, N. Biological chemistry and clinical potential of S-nitrosothiols. *Free Radical Biol. Med.* **2000,** *28*, 1478-1486.

50. Stamler, J. S. S-nitrosothiols in the blood - Roles, amounts, and methods of analysis. *Circ. Res.* **2004,** *94*, 414-417.

51. Riccio, D. A.; Coneski, P. N.; Nichols, S. P.; Broadnax, A. D.; Schoenfisch, M. H. Photoinitiated nitric oxide-releasing tertiary S-nitrosothiol-modified xerogels. *ACS Appl. Mater. Interfaces* **2012,** *4* (2), 796-804.

52. Achuth, H. N.; Moochhala, S. M.; Mahendran, R.; Tan, W. T. L. Nitrosoglutathione triggers collagen deposition in cutaneous wound repair. *Wound Repair Regen.* **2005,** *13* (4), 383-389.

53. Williams, D. L. H. The chemistry of S-nitrosothiols. *Acc. Chem. Res.* **1999,** *32*, 869-876.

54. Wang, P. G.; Xian, M.; Tang, X. P.; Wu, X. J.; Wen, Z.; Cai, T. W.; Janczuk, A. J. Nitric oxide donors: Chemical activities and biological applications. *Chem. Rev.* **2002,** *102*, 1091-1134.

55. Dicks, A. P.; Swift, H. R.; Williams, D. L. H.; Butler, A. R.; AlSadoni, H. H.; Cox, B. G. Identification of Cu+ as the effective reagent in nitric oxide formation from S-nitrosothiols (RSNO). *J. Chem. Soc. Perkin Trans. 2* **1996,** *4*, 481-487.

56. Al-Sa'doni, H. H.; Ferro, A. S-nitrosothiols as nitric oxide-donors: Chemistry, biology and possible future therapeutic applications. *Curr. Med. Chem.* **2004,** *11*, 2679-2690.

57. Frost, M. C.; Meyerhoff, M. E. Synthesis, characterization, and controlled nitric oxide release from S-nitrosothiol-derivatized fumed silica polymer filler particles. *J. Biomed. Mater. Res. Part A* **2005,** *72A*, 409-419.

58. Riccio, D. A.; Nugent, J. L.; Schoenfisch, M. H. Stober Synthesis of Nitric Oxide-Releasing S-Nitrosothiol-Modified Silica Particles. *Chem. Mater.* **2011,** *23*, 1727-1735.

59. Stasko, N. A.; Fischer, T. H.; Schoenfisch, M. H. S-nitrosothiol-modified dendrimers as nitric oxide delivery vehicles. *Biomacromolecules* **2008,** *9*, 834-841.

60. Stiriba, S. E.; Frey, H.; Haag, R. Dendritic polymers in biomedical applications: From potential to clinical use in diagnostics and therapy. *Angew. Chem. Int. Ed.* **2002,** *41*, 1329-1334.

61. Costerton, J. W.; Stewart, P. S.; Greenberg, E. P. Bacterial biofilms: A common cause of persistent infections. *Science* **1999,** *284*, 1318-1322.

62. Nikitkova, A. E.; Haase, E. M.; Scannapieco, F. A. Taking the starch out of oral biofilm formation: molecular basis and functional significance of salivary alpha-amylase binding to oral streptococci. *Appl. Environ. Microbiol.* **2013,** *79*, 416-23.

63. Lyczak, J. B.; Cannon, C. L.; Pier, G. B. Establishment of Pseudomonas aeruginosa infection: lessons from a versatile opportunist. *Microbes Infect.* **2000,** *2*, 1051-1060.

64. DeQueiroz, G. A.; Day, D. F., Antimicrobial activity and effectiveness of a combination of sodium hypochlorite and hydrogen peroxide in killing and removing Pseudomonas aeruginosa biofilms from surfaces. *J. Appl. Microbiol.* **2007,** *103*, 794-802.

65. Sauer, K.; Camper, A. K.; Ehrlich, G. D.; Costerton, J. W.; Davies, D. G. Pseudomonas aeruginosa displays multiple phenotypes during development as a biofilm. *J. Bacteriol.* **2002,** *184*, 1140-1154.

66. Wolcott, R. D.; Rhoads, D. D.; Dowd, S. E. Biofilms and chronic wound inflammation. *J. Wound Care* **2008,** *17*, 333-341.

67. Fux, C. A.; Costerton, J. W.; Stewart, P. S.; Stoodley, P. Survival strategies of infectious biofilms. *Trends Microbiol.* **2005,** *13*, 34-40.

68. Keren, I.; Kaldalu, N.; Spoering, A.; Wang, Y.; Lewis, K. Persister cells and tolerance to antimicrobials. *FEMS Microbiol. Lett.* **2004,** *230*, 13-18.

69. White, R. J.; Cutting, K.; Kingsley, A. Topical antimicrobials in the control of wound bioburden. *Ostomy Wound Manag.* **2006,** *52*, 26-58.

70. Wright, J. B.; Lam, K.; Burrell, R. E. Wound management in an era of increasing bacterial antibiotic resistance: a role for topical silver treatment. *Am. J. Infect. Control* **1998,** *26*, 572-577.

71. Silver, S. Bacterial silver resistance: molecular biology and uses and misuses of silver compounds. *FEMS Microbiol. Rev.* **2003,** *27*, 341-353.

72. Li, X. Z.; Nikaido, H.; Williams, K. E. Silver-resistant mutants of Escherichia coli display active efflux of Ag+ and are deficient in porins. *J. Bacteriol.* **1997,** *179*, 6127-6132.

73. Balin, A. K.; Pratt, L. Dilute povidone-iodine solutions inhibit human skin fibroblast growth. *Dermatol. Surg.* **2002,** *28*, 210-214.

74. Torricelli, R.; Wuthrich, B. Life-threatening anaphylactic shock due to skin application of chlorhexidine. *Clin. Exp. Allergy* **1996,** *26*, 112.

75. Autegarden, J. E.; Pecquet, C.; Huet, S.; Bayrou, O.; Leynadier, F. Anaphylactic shock after application of chlorhexidine to unbroken skin. *Contact Dermatitis* **1999,** *40*, 215.

76. Krautheim, A. B.; Jermann, T. H.; Bircher, A. J. Chlorhexidine anaphylaxis: case report and review of the literature. *Contact Dermatitis* **2004,** *50*, 113-116.

77. Meiller, T. F.; Kelley, J. I.; Jabra-Rizk, M. A.; Depaola, L. G.; Baqui, A. A.; Falkler, W. A., Jr. In vitro studies of the efficacy of antimicrobials against fungi. *Oral Surg. Oral Med. Oral Pathol. Oral Radiol. Endod.* **2001,** *91*, 663-670.

78. MacMicking, J.; Xie, Q. W.; Nathan, C. Nitric oxide and macrophage function. *Annu. Rev. Immunol.* **1997,** *15*, 323-350.

79. Hampl, V.; Herget, J. Role of nitric oxide in the pathogenesis of chronic pulmonary hypertension. *Physiol. Rev.* **2000,** *80*, 1337-1372.

80. Ghaffari, A.; Miller, C. C.; McMullin, B.; Ghahary, A. Potential application of gaseous nitric oxide as a topical antimicrobial agent. *Nitric Oxide-Biol. Chem.* **2006,** *14*, 21-29.

81. Jones, M. L.; Ganopolsky, J. G.; Labbe, A.; Prakash, S. A novel nitric oxide producing probiotic patch and its antimicrobial efficacy: preparation and in vitro analysis. *Appl. Microbiol. Biotech.* **2010,** *87*, 509-516.

82. Dukelow, A. M.; Weicker, S.; Karachi, T. A.; Razavi, H. M.; McCormack, D. G.; Joseph, M. G.; Mehta, S. Effects of nebulized diethylenetetraamine-NONOate in a mouse model of acute Pseudomonas aeruginosa pneumonia. *Chest* **2002,** *122*, 2127-2136.

83. Hussain, S.; Malik, M.; Shi, L. B.; Gennaro, M. L.; Drlica, K. In vitro model of mycobacterial growth arrest using nitric oxide with limited air. *Antimicrob. Agents Ch.* **2009,** *53*, 157-161.

84. Cariello, A. J.; Bispo, P. J.; de Souza, G. F.; Pignatari, A. C.; de Oliveira, M. G.; Hofling-Lima, A. L. Bactericidal effect of S-nitrosothiols against clinical isolates from keratitis. *Clin. Ophthalmol.* **2012,** *6*, 1907-1914.

85. Abu-Shakra, A. The mutagenic activity of the S-nitrosoglutathione/glutathione system in Salmonella typhimurium TA1535. *Mutat. Res.-Gen. Tox. En.* **2003,** *539*, 203-206.

86. Cariello, A. J.; de Souza, G. F. P.; Foronda, A. S.; Yu, M. C. Z.; Hofling-Lima, A. L.; de Oliveira, M. G. In vitro amoebicidal activity of S-nitrosoglutathione and S-nitroso-N-acetylcysteine against trophozoites of Acanthamoeba castellanii. *J. Antimicrob. Chemother.* **2010,** *65*, 588-591.

87. Garg, T.; Singh, O.; Arora, S.; Murthy, R. S. R. Scaffold: a novel carrier for cell and drug delivery. *Crit. Rev. Ther. Drug* **2012,** *29*, 1-63.

88. Ormerod, A. D.; Shah, A. A.; Li, H.; Benjamin, N. B.; Ferguson, G. P.; Leifert, C. An observational prospective study of topical acidified nitrite for killing methicillin-resistant Staphylococcus aureus (MRSA) in contaminated wounds. *BMC Res. Notes* **2011,** *4*, 458.

89. Friedman, A. J.; Han, G.; Navati, M. S.; Chacko, M.; Gunther, L.; Alfieri, A.; Friedman, J. M. Sustained release nitric oxide releasing nanoparticles: Characterization of a novel delivery platform based on nitrite containing hydrogel/glass composites. *Nitric Oxide-Biol. Chem.* **2008,** *19*, 12-20.

90. Martinez, L. R.; Han, G.; Chacko, M.; Mihu, M. R.; Jacobson, M.; Gialanella, P.; Friedman, A. J.; Nosanchuk, J. D.; Friedman, J. M. Antimicrobial and healing efficacy of sustained release nitric oxide nanoparticles against Staphylococcus aureus skin infection. *J. Invest. Dermatol.* **2009,** *129*, 2463-2469.

91. Swann, P. F. Carcinogenic Risk from Nitrite, Nitrate and N-Nitrosamines in Food. *Proc. R. Soc. Med.* **1977,** *70*, 113-115.

92. Lu, J.; Liong, M.; Li, Z.; Zink, J. I.; Tamanoi, F. Biocompatibility, biodistribution, and drug-delivery efficiency of mesoporous silica nanoparticles for cancer therapy in animals. *Small* **2010,** *6*, 1794-805.

93. Hetrick, E. M.; Shin, J. H.; Stasko, N. A.; Johnson, C. B.; Wespe, D. A.; Holmuhamedov, E.; Schoenfisch, M. H. Bactericidal efficacy of nitric oxide-releasing silica nanoparticles. *ACS Nano* **2008,** *2*, 235-246.

94. Sun, B.; Slomberg, D. L.; Chudasama, S. L.; Lu, Y.; Schoenfisch, M. H., Nitric oxide-releasing dendrimers as antibacterial agents. *Biomacromolecules* **2012,** *13*, 3343-3354.

95. Decuzzi, P.; Pasqualini, R.; Arap, W.; Ferrari, M. Intravascular delivery of particulate systems: does geometry really matter? *Pharm. Res.* **2009,** *26*, 235-243.

96. Champion, J. A.; Katare, Y. K.; Mitragotri, S. Making polymeric micro- and nanoparticles of complex shapes. *Proc. Natl. Acad. Sci. U. S. A.* **2007,** *104*, 11901-11904.

97. Petros, R. A.; DeSimone, J. M. Strategies in the design of nanoparticles for therapeutic applications. *Nat. Rev. Drug Discov.* **2010,** *9*, 615-627.

98. Wong, J.; Brugger, A.; Khare, A.; Chaubal, M.; Papadopoulos, P.; Rabinow, B.; Kipp, J.; Ning, J. Suspensions for intravenous (IV) injection: A review of development, preclinical and clinical aspects. *Adv. Drug Deliv. Rev.* **2008,** *60*, 939-954.

99. Huang, X. L.; Li, L. L.; Liu, T. L.; Hao, N. J.; Liu, H. Y.; Chen, D.; Tang, F. Q., The shape effect of mesoporous silica nanoparticles on biodistribution, clearance, and biocompatibility in vivo. *ACS Nano* **2011,** *5*, 5390-5399.

100. Yu, T.; Malugin, A.; Ghandehari, H. Impact of silica nanoparticle design on cellular toxicity and hemolytic activity. *ACS Nano* **2011,** *5*, 5717-5728.

101. Gratton, S. E. A.; Ropp, P. A.; Pohlhaus, P. D.; Luft, J. C.; Madden, V. J.; Napier, M. E.; DeSimone, J. M. The effect of particle design on cellular internalization pathways. *Proc. Natl. Acad. Sci. U. S. A.* **2008,** *105*, 11613-11618.

102. Huang, X. L.; Teng, X.; Chen, D.; Tang, F. Q.; He, J. Q. The effect of the shape of mesoporous silica nanoparticles on cellular uptake and cell function. *Biomaterials* **2010,** *31*, 438-448.

103. Meng, H.; Yang, S.; Li, Z. X.; Xia, T.; Chen, J.; Ji, Z. X.; Zhang, H. Y.; Wang, X.; Lin, S. J.; Huang, C.; Zhou, Z. H.; Zink, J. I.; Nel, A. E. Aspect Ratio Determines the Quantity of Mesoporous Silica Nanoparticle Uptake by a Small GTPase-Dependent Macropinocytosis Mechanism. *ACS Nano* **2011,** *5*, 4434-4447.

104. Kolhar, P.; Doshi, N.; Mitragotri, S. Polymer nanoneedle-mediated intracellular drug delivery. *Small* **2011,** *7*, 2094-2100.

105. Yoo, J. W.; Doshi, N.; Mitragotri, S. Endocytosis and Intracellular Distribution of PLGA Particles in Endothelial Cells: Effect of Particle Geometry. *Macromol. Rapid Comm.* **2010,** *3*, 142-148.

106. Qiu, Y.; Liu, Y.; Wang, L. M.; Xu, L. G.; Bai, R.; Ji, Y. L.; Wu, X. C.; Zhao, Y. L.; Li, Y. F.; Chen, C. Y. Surface chemistry and aspect ratio mediated cellular uptake of Au nanorods. *Biomaterials* **2010,** *31*, 7606-7619.

107. Champion, J. A.; Katare, Y. K.; Mitragotri, S. Particle shape: A new design parameter for micro- and nanoscale drug delivery carriers. *J. Controlled Release* **2007,** *121*, 3-9.

108. Geng, Y.; Dalhaimer, P.; Cai, S. S.; Tsai, R.; Tewari, M.; Minko, T.; Discher, D. E. Shape effects of filaments versus spherical particles in flow and drug delivery. *Nat. Nanotechnol.* **2007,** *2*, 249-255.

109. Yu, T.; Greish, K.; McGill, L. D.; Ray, A.; Ghandehari, H. Influence of Geometry, Porosity, and Surface Characteristics of Silica Nanoparticles on Acute Toxicity: Their Vasculature Effect and Tolerance Threshold. *ACS Nano* **2012,** *6*, 2289-2301.

110. Qiu, Y.; Liu, Y.; Wang, L.; Xu, L.; Bai, R.; Ji, Y.; Wu, X.; Zhao, Y.; Li, Y.; Chen, C. Surface chemistry and aspect ratio mediated cellular uptake of Au nanorods. *Biomaterials* **2010,** *31*, 7606-7619.

111. Kresge, C. T.; Leonowicz, M. E.; Roth, W. J.; Vartuli, J. C.; Beck, J. S. Ordered mesoporous molecular-sieves synthesized by a liquid-crystal template mechanism. *Nature* **1992,** *359*, 710-712.

112. Huo, Q. S.; Margolese, D. I.; Ciesla, U.; Demuth, D. G.; Feng, P. Y.; Gier, T. E.; Sieger, P.; Firouzi, A.; Chmelka, B. F.; Schuth, F.; Stucky, G. D. Organization of organic-molecules with inorganic molecular-species into nanocomposite biphase arrays. *Chem. Mater.* **1994,** *6*, 1176-1191.

113. Huo, Q. S.; Margolese, D. I.; Ciesla, U.; Feng, P. Y.; Gier, T. E.; Sieger, P.; Leon, R.; Petroff, P. M.; Schuth, F.; Stucky, G. D. Generalized synthesis of periodic surfactant inorganic composite-materials. *Nature* **1994,** *368*, 317-321.

114. Yanagisawa, T.; Shimizu, T.; Kuroda, K.; Kato, C. The preparation of alkyltrimethylammonium-kanemite complexes and their conversion to microporous materials. *Bull. Chem. Soc. Jpn.* **1990,** *63*, 988-992.

115. Beck, J. S.; Vartuli, J. C.; Roth, W. J.; Leonowicz, M. E.; Kresge, C. T.; Schmitt, K. D.; Chu, C. T. W.; Olson, D. H.; Sheppard, E. W.; Mccullen, S. B.; Higgins, J. B.; Schlenker, J. L. A new family of mesoporous molecular-sieves prepared with liquid-crystal templates. *J. Am. Chem. Soc.* **1992,** *114*, 10834-10843.

116. Yang, H.; Coombs, N.; Ozin, G. A. Morphogenesis of shapes and surface patterns in mesoporous silica. *Nature* **1997,** *386*, 692-695.

117. Ozin, G. A.; Yang, H.; Sokolov, I.; Coombs, N. Shell mimetics. *Adv. Mater.* **1997,** *9*, 662-667.

118. Israelachvili, J. N.; Mitchell, D. J.; Ninham, B. W. Theory of self-assembly of hydrocarbon amphiphiles into micelles and bilayers. *J. Chem. Soc., Faraday Trans. II* **1976,** *72*, 1525-1568.

119. Chan, H. B. S.; Budd, P. M.; Naylor, T. D. Control of mesostructured silica particle morphology. *J. Mater. Chem.* **2001,** *11*, 951-957.

120. Mou, C. Y.; Lin, H. P., Control of morphology in synthesizing mesoporous silica. *Pure Appl. Chem.* **2000,** *72*, 137-146.

121. Firouzi, A.; Kumar, D.; Bull, L. M.; Besier, T.; Sieger, P.; Huo, Q.; Walker, S. A.; Zasadzinski, J. A.; Glinka, C.; Nicol, J.; Margolese, D.; Stucky, G. D.; Chmelka, B. F. Cooperative Organization of Inorganic-Surfactant and Biomimetic Assemblies. *Science* **1995,** *267*, 1138-1143.

122. Naik, S. P.; Elangovan, S. P.; Okubo, T.; Sokolov, I. Morphology control of mesoporous silica particles. *J. Phys. Chem. C* **2007,** *111*, 11168-11173.

123. Suwalski, A.; Dabboue, H.; Delalande, A.; Bensamoun, S. F.; Canon, F.; Midoux, P.; Saillant, G.; Klatzmann, D.; Salvetat, J. P.; Pichon, C. Accelerated Achilles tendon healing by PDGF gene delivery with mesoporous silica nanoparticles. *Biomaterials* **2010,** *31*, 5237-5245.

124. Zhao, Y.; Trewyn, B. G.; Slowing, II; Lin, V. S. Mesoporous silica nanoparticle-based double drug delivery system for glucose-responsive controlled release of insulin and cyclic AMP. *J. Am. Chem. Soc.* **2009,** *131*, 8398-8400.

125. Moulari, B.; Pertuit, D.; Pellequer, Y.; Lamprecht, A. The targeting of surface modified silica nanoparticles to inflamed tissue in experimental colitis. *Biomaterials* **2008,** *29*, 4554-4560.

126. Tang, F.; Li, L.; Chen, D. Mesoporous silica nanoparticles: synthesis, biocompatibility and drug delivery. *Adv. Mater.* **2012,** *24*, 1504-1534.

127. Dash, M.; Chiellini, F.; Ottenbrite, R. M.; Chiellini, E. Chitosan-A versatile semi-synthetic polymer in biomedical applications. *Prog. Polym. Sci.* **2011,** *36*, 981-1014.

128. Jayakumar, R.; Prabaharan, M.; Nair, S. V.; Tamura, H. Novel chitin and chitosan nanofibers in biomedical applications. *Biotechnol. Adv.* **2010,** *28*, 142-150.

129. Valmikinathan, C. M.; Mukhatyar, V. J.; Jain, A.; Karumbaiah, L.; Dasari, M.; Bellamkonda, R. V. Photocrosslinkable chitosan based hydrogels for neural tissue engineering. *Soft Matter* **2012,** *8*, 1964-1976.

130. Zhang, J. L.; Xia, W. S.; Liu, P.; Cheng, Q. Y.; Tahirou, T.; Gu, W. X.; Li, B., Chitosan Modification and Pharmaceutical/Biomedical Applications. *Mar. Drugs* **2010,** *8*, 1962-1987.

131. Wan, A.; Gao, Q.; Li, H. L. Effects of molecular weight and degree of acetylation on the release of nitric oxide from chitosan-nitric oxide adducts. *J. Appl. Polym. Sci.* **2010,** *117*, 2183-2188.

132. Wan, A.; Sun, Y.; Li, H. L. Characterization of folate-graft-chitosan as a scaffold for nitric oxide release. *Int. J. Biol. Macromol.* **2008,** *43*, 415-421.

133. Smith, D. J.; Serhatkulu, S. Chitosan-based nitric oxide donor compositions. (Akron, OH) US Patent 6,261,594, July 17, 2001.

134. Du, J.; Hsieh, Y. L. Nanofibrous membranes from aqueous electrospinning of carboxymethyl chitosan. *Nanotechnology* **2008,** *19*, 125707.

135. Kim, S. K.; Rajapakse, N. Enzymatic production and biological activities of chitosan oligosaccharides (COS): A review. *Carbohydr. Polym.* **2005,** *62*, 357-368.

136. Wong, K.; Sun, G. B.; Zhang, X. Q.; Dai, H.; Liu, Y.; He, C. B.; Leong, K. W. PEI-g-chitosan, a novel gene delivery system with transfection efficiency comparable to polyethylenimine in vitro and after liver administration in vivo. *Bioconj. Chem.* **2006,** *17*, 152-158.

137. Hu, F. Q.; Liu, L. N.; Du, Y. Z.; Yuan, H. Synthesis and antitumor activity of doxorubicin conjugated stearic acid-g-chitosan oligosaccharide polymeric micelles. *Biomaterials* **2009,** *30*, 6955-6963.

138. Maghami, G. G.; Roberts, G. A. F. Evaluation of the viscometric constants for chitosan. *Macromol. Chem. Phys.* **1988,** *189*, 195-200.

139. Nichols, S. P.; Koh, A.; Brown, N. L.; Rose, M. B.; Sun, B.; Slomberg, D. L.; Riccio, D. A.; Klitzman, B.; Schoenfisch, M. H. The effect of nitric oxide surface flux on the foreign body response to subcutaneous implants. *Biomaterials* **2012,** *33*, 6305-6312.

Chapter 2

Structurally Diverse Nitric Oxide-Releasing Poly(propylene imine) Dendrimers

2.1 Introduction

Dendrimers are a family of hyperbranched macromolecules with multivalent surfaces that enable the design of targeted therapeutics agent delivery vehicles.[1-4] For example, polyamidoamines,[5] polyamines,[6] polypeptides,[7] polyesters[8] and polyethers[9] dendrimers have been utilized for a range of biomedical applications, including drug and gene delivery,[10-22] biological imaging,[23-29] and tissue engineering.[30-33] Bactericidal dendrimers have been prepared by encapsulating antibacterial agents (e.g., sulfomethoxazole[34]) within the dendrimer or at its periphery (e.g., quaternary ammonium groups[35]). Anionic amphiphilic dendrimers were also reported to possess antibacterial efficacy against Gram-positive bacteria.[36]

Nitric oxide is an endogenously produced diatomic free radical that mediates multiple processes in mammalian physiology. Due to NO's pharmacological potential, the synthesis of prodrugs capable of controlled exogeneous NO production is important in further understanding NO's role in physiology and developing NO-based therapeutics. The therapeutic effectiveness of such donors depends on the target (e.g., cell type and condition), concentration and rate of NO release.[37, 38] For example, Chakrapani and coworkers synthesized O*2*-(2,4-dinitro-5-(4-(N-methylamino)benzoyloxy)phenyl)-1-

(N,N-dimethylamino)diazen-1-ium-1,2-diolate (PABA/NO) as an anti-cancer NO prodrug with efficacy against human leukemia and A2780 human ovarian cancer xenografts.[39] Both the NO payload and release kinetics were shown to influence the anticancer activity. The study of how chemical structure impacts the rate of NO release from small molecule NO donors has been an active area of research, particularly with respect to biological activity.[40-45] Generally, stabilization of the *N*-diazeniumdiolate NO donor correlates directly with extended NO release.[46]

To enhance NO storage and release levels relative to small molecule NO donors, we previously reported the synthesis of *N*-diazeniumdiolate-functionalized poly(propylene imine) (PPI) dendrimer conjugates as macromolecular NO donors capable of storing up to ~5 μmol NO/mg with NO release kinetics dependent on the dendrimer structure.[47] Although we alluded to the multivalent exterior benefit on NO storage/release and further functionalization for imaging, controlled toxicity, and/or active targeting, for example, the study of structure/nitric oxide release relationships was not systematically pursued. In subsequent work, Stasko et al. reported the synthesis of *S*-nitrosothiol-modified polyamidoamine (PAMAM) dendrimers with alternative decomposition mechanisms for controlled NO release.[48] While capable of storing ~2 μmol NO/mg, the kinetics of NO release were found to be highly dependent on the structure of the nitrosothiol and NO release trigger (e.g., light, copper, temperature). Collectively, the dendritic effects exerted on NO donor stability and reactivity, and the benefits of multi-functionalization with imaging beacons and/or active targeting agents, highlight the tremendous potential of dendrimers as NO release therapeutics.

Herein, we describe the synthesis of *N*-diazeniumdiolate-functionalized PPI dendrimers using select exterior functionalities to diversify both the NO release kinetics and potential applications for which such materials may prove useful. In addition to assessing the roles of molecular weight (e.g., generation or size of dendrimer) and exterior chemical structure on NO release, we demonstrate the ability to tune NO release kinetics using multiple NO donor functionalization.

2.2 Experimental Section

2.2.1 Materials and General Considerations.

Ethylenediamine (EDA), acrylonitrile (ACN), propylene oxide (PO), styrene oxide (SO), poly(ethylene glycol) methyl ether acrylate (average M_n = 480) (PEG), and 1,2-epoxy-9-decene (ED) were purchased from Aldrich Chemical Company (Milwaukee, WI). 1,6-Hexanediamine (HDA) and sodium methoxide (5.4 M solution in methanol) was purchased from Acros Organics (Geel, Belgium). Sponge cobalt catalyst (A-8B46) was purchased from Johson Matthey Catalysts (London, UK). Common laboratory salts and solvents were purchased from Fisher Scientific (Pittsburgh, PA). All other materials were used as received without further purification unless otherwise noted. ^{1}H nuclear magnetic resonance (NMR) spectra were recorded on Bruker (400 MHz) and Varian (600 MHz) spectrometers. Hydrogenation reactions used for the synthesis of PPI-NH_2 (e.g., from G2 to G5) were carried out in a stainless steel high-pressure reactor purchased from Parr Instrument Company (Moline, IL). Agitation was provided by a Teflon-coated magnetic stirring bar. Heating was provided using a heating fabric wrapped around the reactor, and temperature was controlled using a temperature controller via a thermal coupler. Nitric oxide release was measured using Sievers 280i Chemiluminesce Nitric Oxide Analyzer

(Boulder, CO) as described previously.[47] The chemiluminescence analyzer was calibrated with NO gas (26.9 ppm). A parameter for converting the instrument response (ppb) to moles of NO was obtained using the conversion of nitrite standards to NO in a 0.1 M KOH/H_2SO_4 solution (1.31×10^{-13} moles NO/ppb).

2.2.2 Synthesis of [G-0.5]-PPI-CN to [G-4.5]-PPI-CN.

The synthetic approach reported here builds upon studies described previously. For the synthesis of [G-0.5]-PPI-CN, ethylenediamine (EDA, 25.0 mL, 0.374 mol) and deionized water (263 mL) were placed in a 1000 mL round-bottomed flask. Acrylonitrile (ACN, 140 mL) was added in portions of 20 mL with stirring for 15 minutes. The resulting mixture was refluxed for 2 hrs, and then cooled to room temperature overnight. ACN was removed in vacuo at 40 °C. [G-0.5]-PPI-CN was crystallized from the mixture and isolated by vacuum filtration. The crude product was recrystallized from THF/methanol as a white power. Representative ^{1}HNMR data: (300 MHz, $CDCl_3$): δ (ppm) 2.55 (8H, -NCH_2CH_2CN), 2.77 (4H, -NCH_2CH_2N-), 2.96 (t, 8H, -NCH_2CH_2CN). Synthesis of higher generation PPI-CN (e.g., from [G-1.5] to [G-4.5]) was not significantly different from the synthesis of PPI-[G-0.5]-CN as described above, with the exception that PPI-CN (e.g., from [G-1.5] to [G-4.5]) are usually viscous liquid and their purification processes would normally require the use of preparative-scale chromatography. As a result, the synthesis of higher generation PPI-CN was conducted in a slightly different manner. Higher generation PPI-CN (10.0 g) (e.g., from [G-1.5] to [G-4.5]) was dissolved in deionized water (50 mL) and THF (100 mL). To this solution was added ACN (50 mL). If phase separation of the resulting solution occurs, an additional amount of THF was added. The reaction mixture was stirred at room temperature for 3

days and a small amount was removed for analysis by ^{1}H NMR spectroscopy to determine the extent of reaction. If the reaction is not complete, an additional amount of ACN (25 mL) was added and the reaction was stirred for two to three extra days.

2.2.3 Synthesis of [G-1]-PPI-NH_2 to [G-5]-PPI-NH_2.

The synthetic approach reported here is similar to those reported in past studies. For the synthesis of [G-1]-PPI-NH_2, sponge cobalt catalyst (5.0–6.0 g) was washed with 10% KOH solution for 10 minutes, three times with de-ionized water, and twice with methanol prior to use. [G-0.5]-PPI-CN (10.0 g) was placed in a glass reactor sleeve and dissolved in THF (70 mL) and methanol (30 mL). To this solution, the sponge cobalt catalyst prepared as described above (5.0–6.0 g) was added using a pipet and the reactor sleeve was placed in the hydrogenation chamber with proper stirring. The reactor was purged with house nitrogen (60 PSI) for five times, and then with hydrogen (400 PSI) for two times. The reactor was charged with hydrogen to a pressure of 800 PSI, and heated to 100°C. The hydrogen gas pressure was maintained at 1000 PSI throughout the reaction. After 3 hours, the reaction mixture was allowed to cool down to room temperature. Hydrogen remained in the reactor was slowly removed, and the reaction chamber was purged once with house nitrogen. The resulting reaction mixture was then filtered to remove the cobalt catalyst, and solvent was removed in vacuo. The final product was dried under vacuum overnight to yield [G-1]-PPI-NH_2 as a colorless liquid. Representative $^{1}HNMR$ data: (300 MHz, $CDCl_3$): δ (ppm) 1.52 (q, 8H, $NH_2CH_2C\mathit{H}_2CH_2N$-), 2.40 (t, 8H, $NH_2CH_2CH_2C\mathit{H}_2N$-), 2.44 (s, 4H, -$NC\mathit{H}_2C\mathit{H}_2N$-), 2.64 (t, 8H, $NH_2C\mathit{H}_2CH_2CH_2N$-). The approach to synthesis of higher generation PPI-NH_2 (e.g., from [G-2] to [G-5]) was similar to that of [G-1]-PPI-NH_2 with the exception that a

mixture of EDA and THF (50:50, v/v) was used as a solvent and was removed after reaction in vacuo using 1-butanol as an azeotropic agent to assist the removal of high boiling point solvent (e.g., EDA). The resulting higher generation PPI-NH_2 (e.g., from [G-2] to [G-5]) was dried under vacuum overnight to yield as a light yellow liquid.

2.2.4 Synthesis of Secondary Amine-Functionalized PPI Dendrimers.

100 mg PPI-NH_2 (e.g., from G2 to G5) was dissolved in 2 ml methanol in a 10ml vial. One equivalent of acrylonitrile (ACN), poly(ethylene glycol) methyl ether acrylate (average M_n = 480) (PEG), propylene oxide (PO), styrene oxide (SO), or 1,2-epoxy-9-decene (ED) (e.g., with respect to molar amount of primary amine functionality) was then added to the 10 mL vial. The solution was stirred at room temperature for 4 d. Solvent was removed under reduced pressure. Dendrimers were dissolved in water followed by dialysis against water and lyophilization.

Representative ^{1}HNMR data of secondary amine-functionalized G5-PPI conjugate formed via the reactions of G5-PPI-NH_2 with ACN, PEG, PO, SO, and ED (referred to hereafter as G5-PPI-ACN **a-64**, G5-PPI-PEG **b-64**, G5-PPI-PO **c-64**, G5-PPI-SO **d-64**, G5-PPI-ED **e-64**) are as follows: G5-PPI-ACN **a-64**: ^{1}H NMR (400 MHz, CD_3OD, δ): 2.87 ($NHCH_2CH_2CN$), 2.82 ($NHCH_2CH_2CN$), 2.60 ($NCH_2CH_2CH_2NH$), 2.40 ($NCH_2CH_2CH_2NH$), 1.60 ($NCH_2CH_2CH_2NH$). ^{13}C NMR (400 MHz, CD_3OD, δ): 117, 52.4, 51.8, 44.5, 33.3, 26.1, 23.6, 16.9. G5-PPI-PEG **b-64**: ^{1}H NMR (400 MHz, CD_3OD, δ): 2.60 ($NCH_2CH_2CH_2NH$), 2.40 ($NCH_2CH_2CH_2NH$), 1.60 ($NCH_2CH_2CH_2NH$), 3.40–3.70 (OCH_2CH_2O), 2.80 ($CH_2NHCH_2CHCOOPEG$), 2.65 ($CH_2NHCH_2CHCOOPEG$), 2.42 ($CH_2NHCH_2CHCOOPEG$). ^{13}C NMR (400 MHz, CD_3OD, δ): 172, 71.6, 70.85, 69.3, 60.1, 57.0, 51.4, 43.9, 39.1, 22.9. G5-PPI-PO **c-64**: ^{1}H NMR (400 MHz, CD_3OD, δ): 3.70

($CH_2CH(OH)CH_3$), 2.60–2.62 ($CH_2CH(OH)CH_3$, $NCH_2CH_2CH_2NH$), 2.40 ($NCH_2CH_2CH_2NH$), 1.60 ($NCH_2CH_2CH_2NH$), 1.00 ($CH_2CH(OH)CH_3$). ^{13}C NMR (400 MHz, CD_3OD, δ): 66.9, 58.2, 53.7, 52.8, 41.2, 30.8, 27.6, 24.9, 21.8. G5-PPI-SO **d-64**: ^1H NMR (400 MHz, CD_3OD, δ): 7.50–7.20 ($CH_2CH(OH)Ph$), 3.70 ($CH_2CH(OH)Ph$), 2.72 ($CH_2CH(OH)Ph$), 2.60 ($NCH_2CH_2CH_2NH$), 2.40 ($NCH_2CH_2CH_2NH$), 1.60 ($NCH_2CH_2CH_2NH$). ^{13}C NMR (400 MHz, CD_3OD, δ): 140.6, 128.2, 127.5, 127.3, 125.8, 71.9, 57.1, 52.4, 45.6, 39.8, 26.3, 23.6. G5-PPI-ED **e-64**: ^1H NMR (400 MHz, CD_3OD, δ): 5.74 ($CH_2CH=CH_2$), 4.88 ($CH_2CH=CH_2$), 3.58 ($NHCH_2CH(OH)CH_2$), 2.60 ($NCH_2CH_2CH_2NH$), 2.40 ($NCH_2CH_2CH_2NH$), 1.98 ($CH_2CH=CH_2$), 1.60 ($NCH_2CH_2CH_2NH$), 1.2–1.4 ($(CH_2)_5CH_2CH=CH_2$). ^{13}C NMR (400 MHz, CD_3OD, δ): 140.0, 116.1, 70.5, 56.5, 52.4, 47.2, 39.2, 33.9, 30.2, 25.6, 24.9.

2.2.5 Synthesis of Diazeniumdiolate-Functionalized PPI Dendrimers.

One equivalent of 5.4 M sodium methoxide solution in methanol (e.g., with respect to the molar amount of primary amine functionalities in PPI-NH_2 used to synthesize these secondary amine-functionalized PPI) was added to a vial containing G1 to G5 secondary amine-functionalized PPI dendrimers in methanol (2 mL), The resulting reaction solution was charged with 10 atm of NO while stirring in a stainless steel reactor. Prior to charging with NO, the reactor was flushed three times with argon followed by a series of three longer charge/discharge cycles with argon (3 × 10 min) to remove oxygen from the stirring solutions. The reactor was then filled with 10 atm of NO (purified over KOH pellets for 30 min to remove trace NO degradation products) at ambient temperature. After 3 days, the NO was expunged using the same charge/discharge procedures described above with argon to remove unreacted NO from the reaction solution.

2.2.6 Characterization of NO Storage and Release.

Aliquots (~10–25 μL) of diazeniumdiolate-functionalized PPI as a solution in methanol (e.g., ~7–200 mM) were added to 30 mL deoxygenated phosphate buffered saline (PBS) (10 mM, pH = 7.4) at 37 °C to initiate NO release. Nitrogen was flowed through the solution at a flow rate of 70 mL/min to carry the liberated NO to the analyzer. Additional nitrogen flow was supplied to the flask to match the collection rate of the instrument at 200 mL/min. Nitric oxide analysis was terminated when levels decreased to 10 ppb NO/mg dendrimer. Chemiluminescence data for the NO-releasing dendrimers were represented as: i) total amount of NO release (t[NO], μmol NO/mg and μmol NO/μmol of secondary amine-functionalized dendrimers); ii) maximum flux of NO release ($[NO]_{max}$, ppb/mg of secondary amine-functionalized dendrimers); iii) half-life ($t_{1/2}$) of NO release; and, iv) conversion efficiency defined as percentages of amine functionalities in PPI (e.g., from G1 to G5) converted to diazeniumdiolate functionality (e.g., total moles of NO release divided by twice the molar amount of primary amine functionalities in PPI-NH_2 used initially to synthesize secondary amine-functionalized dendrimer conjugates).

2.3 Results and Discussion

2.3.1 Synthesis and Characterization of Secondary Amine-Functionalized PPI Dendrimers

Stasko et al. previously reported an approach whereby secondary amine-functionalized PPI conjugates were reacted with NO at high pressure to form NO-releasing dendritic scaffolds with large NO storage capacity[47]. Analogously, primary amine-functionalized PPI dendrimers were characterized by significantly less NO storage

and shorter NO release durations. These results suggest that the structural features of the dendrimer are critical in the design of diazeniumdiolate-functionalized scaffolds. Since chemical reaction of primary amine functionalities with organic compounds represents a simple approach for designing secondary amine-functionalized PPI conjugates, we targeted the synthesis of secondary amine-functionalized dendrimers using ring-opening and conjugate-addition reactions of PPI-NH_2 with PO, SO, ED, ACN, and PEG (Scheme 2.1) to fully unlock a series of dendrimer scaffolds with diverse exterior properties (e.g., aromatic, hydrophilic, hydrophobic). Indeed, the epoxides, acrylated and acrylonitrile selected for conjugation were based on sterics, hydrophobicity, and biocompatibility. Of note, it is also possible to yield tertiary amine adducts. In addition, we carried out a series of model kinetic studies using NMR spectroscopy for conjugate-addition reactions of first generation G1-PPI-NH_2 with ACN and ring-opening reactions of HDA with PO to determine the suitability of conjugate-addition and ring-opening reactions for the synthesis of secondary amine-functionalized PPI dendrimers.

The results of these studies revealed large differences in the rates of reactions of G1-PPI-NH_2 with ACN (i.e., k_1=1.75 M^{-1} s^{-1}, k_2=0.009 M^{-1} s^{-1}), and HDA with PO (i.e., k_1=0.13 M^{-1} s^{-1}, k_2=0.065 M^{-1} s^{-1}). The rate constants of the first conjugate-addition or ring-opening reaction (k_1) were substantially larger than those of the second reactions (k_2), providing strong support for the use of such reactions (e.g., over a period of four days, in a dilute solution, and at one equivalent of ACN, epoxides, or acrylates with respect to molar amount of PPI-NH_2) to yield secondary amine-functionalized products suitable for subsequent NO release studies.

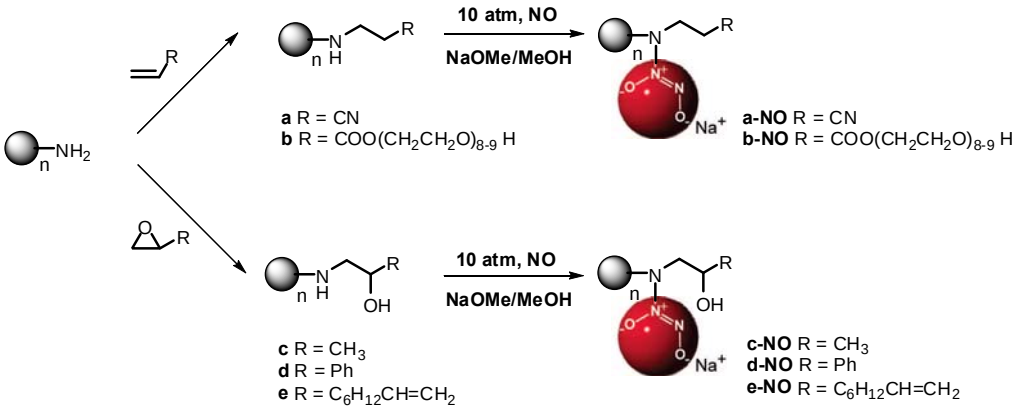

Scheme 2.1 Synthesis of secondary amine- and diazeniumdiolate-functionalized PPI conjugates for which n represents the number of primary amines on the periphery of PPI dendrimers (n = 8, 16, 32, 64).

2.3.2 Influence of Exterior Functionality on Nitric Oxide Release

The approach described above is based on dendrimer functionalization at their exterior to yield secondary amine-functionalized PPI dendrimers. Two practical advantages of this approach include that the synthesis is simple and the resulting structurally diverse exteriors greatly expand the potential applications for which these materials may find utility. Reactions of secondary amine-functionalized PPI (e.g., from G2 to G5) with NO under basic conditions (e.g., sodium methoxide) yielded *N*-diazeniumdiolate NO donor-functionalized dendrimers with diverse NO release characteristics.

Chemiluminescence was used to characterize the NO storage and release properties (e.g., in PBS, pH = 7.4, 37 °C) for the *N*-diazenuimdiolate-modified PPI dendrimers. Representative NO release profiles for these dendrimers are shown in Figure 2.1. The workup of specific NO release parameters (e.g., total NO release, maximum flux, half-life, and conversion efficiency) are provided in Table 2.1. In general, the NO release results reveal high NO storage capabilities (e.g., 0.9–3.8 μmol NO/mg) and a broad range of release kinetics (e.g., NO release half-life from 0.3–4.9 h). Further inspection of these data reveals that the conversion efficiencies (e.g., 10–40%) of the dendrimers varied substantially based on the chemical modification. As shown in Table 2.1,

G2 to G5-PPI-SO (**d-NO**) were characterized by lower NO donor formation (e.g., ~10–15%) versus the other PPI dendrimers (e.g., ~14–40%). The lower conversion efficiencies for PPI-SO (**d-NO**) may be attributed to a more sterically-hindered environment around the NO donor precursors (i.e., secondary amines), resulting in lower NO and base accessibility to the amines during the NO charging process.

The exterior modification also influenced the NO release kinetics. For example, both PPI-PO (**c-NO**) and PPI-PEG (**b-NO**) released NO rapidly (Table 2.1 and Figure 2.1). Such rapid NO release kinetics might be expected since the isopropyl and PEG groups are hydrophilic and facilitate water solvation favorable to diazeniumdiolate NO donor degradation. The data also indicate that the NO release half-lives for G2-G5 PPI-SO (**d-NO**) and PPI-ED (**e-NO**) are slightly longer than PPI-PO (**c-NO**) and PPI-PEG (**b-NO**). The longer NO release for PPI-SO (**d-NO**) and PPI-ED (**e-NO**) correlates well with the increased hydrophobic structure at the exteriors of these dendrimers.

The ACN modification for PPI dendrimer (**a-NO**) exhibited large NO storage (e.g., ~1.7–3.6 μmol NO/mg) and conversion efficiency (e.g., ~14–26%) (Table 2.1). Of note, past studies have indicated that the reaction of cyano-containing compounds with NO at high-pressures under basic conditions may yield *C*-diazeniumdiolate-functionalized products. Both NO and nitrous oxide (N_2O) may be release from *C*-diazeniumdiolates in aqueous environments at low pH.[49-51] In this context, it may be possible that the high conversion efficiencies for PPI-ACN (**a-NO**) arise from the contribution of NO released from *C*-diazeniumdiolate-functionalized products.

A series of experiments were thus carried out to probe the nature of the NO release from PPI-ACN (**a-NO**) using G0.5-PPI, a cyano-containing compound without the capacity to form N-diazeniumdiolate due to the absence of secondary amines. The NO release from G0.5-PPI was ~4.5×10^{-3} μmol NO/mg, providing strong support that the high NO storage and conversion efficiency for the ACN-modified dendrimers are indeed the result of *N*-diazeniumdiolate functionalization. The PPI-ACN (**a-NO**) analogues were also characterized as having the longest NO release half-lives (e.g., ~5 h).

Table 2.1 Nitric oxide release characteristics for PPI dendrimers in PBS (pH = 7.4) at 37 °C.

Dendrimer	t[NO] (μmol NO/mg)[a]	t[NO] (μmol NO/μmol)[b]	$[NO]_{max}$ (ppb/mg)[c]	$[NO]_{max}$ (ppb/μmol)[d]	$t_{½}$ (h)	Conversion (%)
G2-PPI-ACN-NO	3.57	4.18	1529	1788	4.81	26.1
G3-PPI-ACN-NO	3.33	8.35	1100	2758	4.84	26.1
G4-PPI-ACN-NO	2.45	12.7	1547	7977	4.82	19.9
G5-PPI-ACN-NO	1.68	17.7	881	9282	4.88	13.8
G2-PPI-PEG-NO	1.11	5.10	3771	17291	0.67	31.9
G3-PPI-PEG-NO	1.08	10.1	2309	21564	1.11	31.6
G4-PPI-PEG-NO	1.37	25.8	4088	77035	0.84	40.3
G5-PPI-PEG-NO	1.17	44.3	1886	71403	1.22	34.6
G2-PPI-PO-NO	2.99	3.63	17130	20725	0.30	22.7
G3-PPI-PO-NO	3.22	8.38	9617	24888	0.62	26.2
G4-PPI-PO-NO	3.27	17.5	7762	41481	0.78	27.3
G5-PPI-PO-NO	3.78	41.1	6839	74250	1.06	32.1
G2-PPI-SO-NO	1.14	1.95	8495	14496	1.47	12.2
G3-PPI-SO-NO	0.91	3.30	2363	8462	0.97	10.3
G4-PPI-SO-NO	1.18	8.70	1720	12609	1.43	13.6
G5-PPI-SO-NO	1.25	18.5	2215	32843	1.62	14.5
G2-PPI-ED-NO	1.95	3.87	5648	11178	0.81	24.2
G3-PPI-ED-NO	1.64	6.75	2733	11279	1.71	21.1
G4-PPI-ED-NO	1.51	12.8	2401	20217	1.34	19.9
G5-PPI-ED-NO	1.86	31.6	3190	54262	1.88	24.7

[a] total amount of NO release (μmol) per milligram of secondary amine-functionalized PPI. [b] total amount of NO release (μmol) per micromole of secondary amine-functionalized PPI. [c] maximum flux of NO release (ppb) per milligram of secondary amine-functionalized PPI. [d] maximum flux of NO release (ppb) per micromole of secondary amine-functionalized PPI.

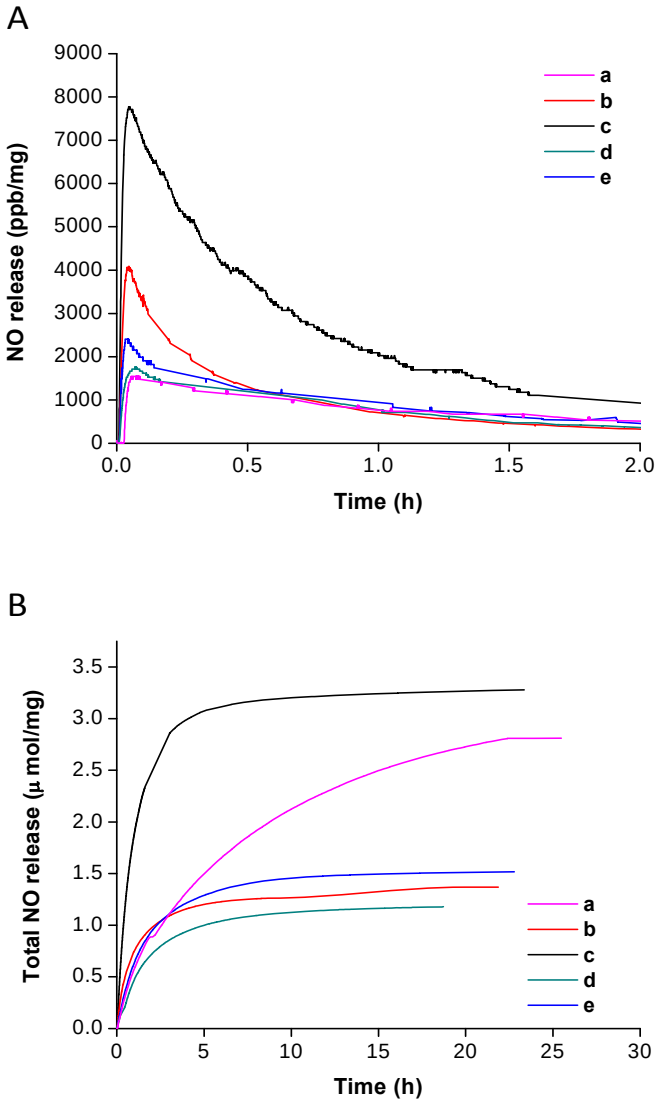

Figure 2.1 (A) Real time NO release profile for NO-releasing G4-PPI dendrimer conjugates; and (B) plot of t[NO] vs time for NO-releasing PPI dendrimer conjugates.

Given the hydrophilic nature of the cyano functionality, the extended NO release is not attributable to water uptake. For example, the long half-lives of *N*-diazeniumdiolate-functionalized small molecule derivatives (e.g., dipropylenetriamine or DPTA-NO) have previously been attributed to diazeniumdiolate stabilization by neighboring cationic ammonium functionalities as depicted in Figure 2.2A.[45,52,53] In this manner, the presence of neighboring cationic functionalities (e.g., protonated imidates) for PPI-ACN (**a-NO**) dendrimers may provide additional stabilization to the diazeniumdiolate functionality (Figure 2.2B). Since sodium methoxide was used as the base for the reaction of PPI-ACN (**a**) with NO (to yield diazeniumdiloate-functionalized products), the methoxide anion may also serve as a nucleophile to react with the cyano group in PPI-ACN (**a**) and yield imidate adducts.[54] The transfer of proton from solvent (e.g., methanol) to the relatively basic nitrogen atom in the resulting imidates might thus lead to protonated-imidate functionality (Figure 2.2B) that is similar to cationic ammonium functionality in DPTA-NO (Figure 2.2A).

As shown in Table 2.1, both the NO storage and maximum NO flux per dendrimer molecule increased as a function of dendrimer size (i.e., generation). For example, the NO payload from G5-PPI-PO-NO (**c-64-NO**) was 41.1 μmol/μmol dendrimer, much greater than G2-PPI-PO-NO (**c-8-NO**) (e.g., 3.63 μmol/μmol dendrimer). A similar trend is observed for maximum NO flux. These results reveal the capability of larger NO-releasing PPI dendrimers to deliver significant concentrations of NO, a potentially beneficial attribute for therapeutic anti-microbial and anti-cancer applications.

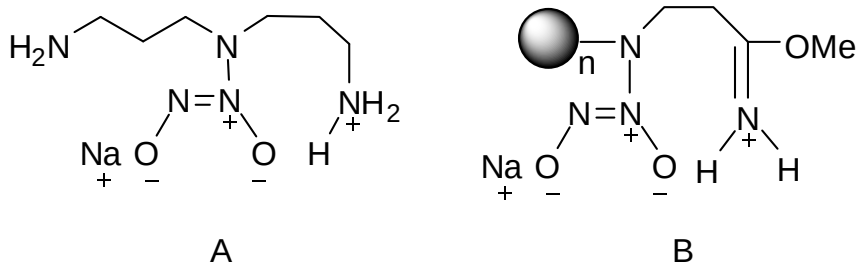

Figure 2.2 Proposed structures for stabilization of (A) diazeniumdiolate-functionalized DPTA by neighboring cationic ammonium functionality, and (B) PPI-ACN (a-NO) by neighboring cationic protonated-imidate functionality.

2.3.3 Effect of Solvent for NO Conjugation

As synthesized, the amphiphilic secondary amine-functionalized dendrimers (e.g., PPI-SO, PPI-ED) possess a hydrophilic PPI core and hydrophobic periphery of aromatic rings or long alkyl chains. Different from PPI-ACN, PPI-PO and PPI-PEG, these amphiphilic dendrimers may have more packed exterior in the charging solvent due to the poor compatibility of the aromatic rings or long alkyl chains with polar solvent (e.g., methanol). We thus sought to investigate the role of charging solvent on NO donor formation efficiency using mixtures of methanol with less polar solvent (e.g., methanol/THF (9:1, v/v), methanol/toluene (9:1, v/v) and methanol/toluene (1:1, v/v)). As shown in Figure 2.3, the NO release data reveals an adverse effect of toluene and THF on NO conjugation to PPI-SO dendrimers. Compared to toluene, use of THF compromised the NO storage to a larger extent. The lower NO conjugation efficiency may be the result of the PPI dendrimer core collapsing in the mixture of methanol and less polar solvents (e.g., toluene and THF). Indeed, this hypothesis is supported by dynamic light scattering data (data not shown). In turn, the dendrimer backbone collapse likely contributes to a greater steric hindrance around the secondary amines and concomitant lower NO conjugation efficiency.

2.3.4 Characterization of PPI Conjugates Synthesized from Defined Mixtures of PO and ACN

To evaluate the ability to define NO release, we designed multi-functionalized *N*-diazeniumdiolate-functionalized dendrimer conjugates using G5-PPI-NH_2 and defined ratios of PO and/or ACN during the functionalization step. Specifically, G5-PPI-NH_2 was reacted with either PO exclusively (e.g., **c-64**), ACN exclusively (e.g., **a-64**), or three

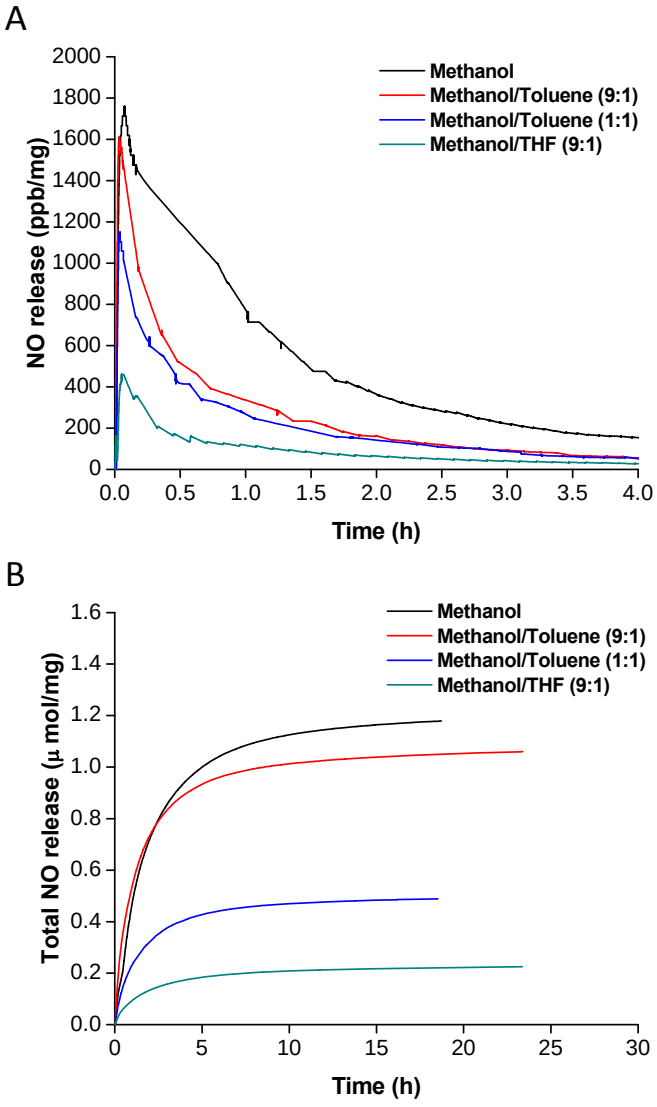

Figure 2.3 (A) Real time NO release profile and (B) plot of t[NO] vs time for G4-PPI-SO-NO synthesized in different NO conjugation solvents.

different mixtures comprised of PO and ACN at molar ratios of 3:7, 5:5, and 7:3, respectively; the PO, ACN, or defined mixtures of PO and ACN were one equivalent with respect to molar amount of primary amine functionalities in G5-PPI-NH_2. A series of ^{1}H NMR experiments were carried out on the products of these reactions to determine the actual compositions of PO and ACN conjugated to the G5-PPI-NH_2 (Figure 2.4). A distinct resonance at 1.10 ppm was apparent corresponding to the methyl protons in the isopropyl group of the products. The chemical shift of this peak was noted in the products for reactions with PO exclusively (e.g., **c-64**) and those with different mixtures of PO and ACN. Further inspection of these data indicates the presence of a second distinct peak at 2.80 ppm, formed upon G5-PPI-NH_2 dendrimer reaction with either ACN exclusively (e.g., **a-64**) or defined mixtures of PO and ACN; this peak corresponds to the methylene protons one carbon away from the cyano group of the products. The compositions of PO and ACN incorporated in the products were 27/73 (**c/a (27/73)**), 40/60 (**c/a (40/60)**), and 60/40 (**c/a (60/40)**), and indicate that the ACN was incorporated at ratios greater than that in the reaction mixtures likely due to more rapid reaction of G5-PPI-NH_2 with ACN versus PO.

The NO release from the G5-PPI-PO/ACN conjugates at PO/ACN molar ratios of 27/73, 40/60, and 60/40, respectively, were intermediate to those synthesized based upon G5-PPI-NH_2 reactions with either PO (e.g., **c-64**) or ACN (e.g., **a-64**) alone. Furthermore, the NO release profiles were influenced by the molar ratio of PO/ACN composition. For instance, the NO release was prolonged for the PPI conjugates modified with lower molar ratio of PO/ACN (half-lives of 2.90, 1.57, and 1.10 h for 27/73, 40/60, and 60/40, respectively) (Figure 2.5). A mathematical model was developed to predict the NO

release from hybrid G5-PPI-PO/ACN conjugates using the NO release data from the single G5-PPI-PO (**c-64**) and G5-PPI-ACN (**a-64**) systems. In Equation 2.1, a:b is the molar ratio of the PO and ACN modification in the hybrid G5-PPI-PO/ACN conjugate as determined by NMR spectroscopy, while y_{PO} and y_{ACN} represent the normalized NO release profiles of the G5-PPI-PO (**c-64**) and G5-PPI-ACN (**a-64**) systems, respectively. Simulated NO release from a hybrid G5-PPI-PO/ACN conjugate ($y_{a:b}$) was thus derived by averaging the normalized NO release from G5-PPI-PO (**c-64**) (y_{PO}) and G5-PPI-ACN (**a-64**) (y_{ACN}) weighted with respect to the mole percentages of PO (i.e., [a/(a+b)] × 100%) and ACN (i.e., [b/(a+b)] × 100%) modification in the hybrid G5-PPI-PO/ACN conjugate.

$$y_{a:b} = y_{PO} \times \frac{a}{a+b} + y_{ACN} \times \frac{b}{a+b} \qquad \text{Eq.2.1}$$

As shown in Figure 2.5, the simulated NO release from G5-PPI-PO/ACN conjugates were comparable with the experimental data, even though the experimental hybrid PPI conjugates were characterized by slightly faster NO release (e.g., NO release half-lives of 3.13, 2.42, and 1.65 h for **c/a (27/73)**, **c/a (40/60)**, and **c/a (60/40)**, respectively). Nevertheless, the developed mathematical model appears to be well suited for simulating dual NO release kinetics using NO release data from single NO donor systems. For dendrimers, these results demonstrate that functionalization of PPI-NH_2 with a defined mixture of PO and ACN allows for precise NO release selection with access to NO release kinetics that are intermediate to those formed upon reactions with one NO donor type exclusively.

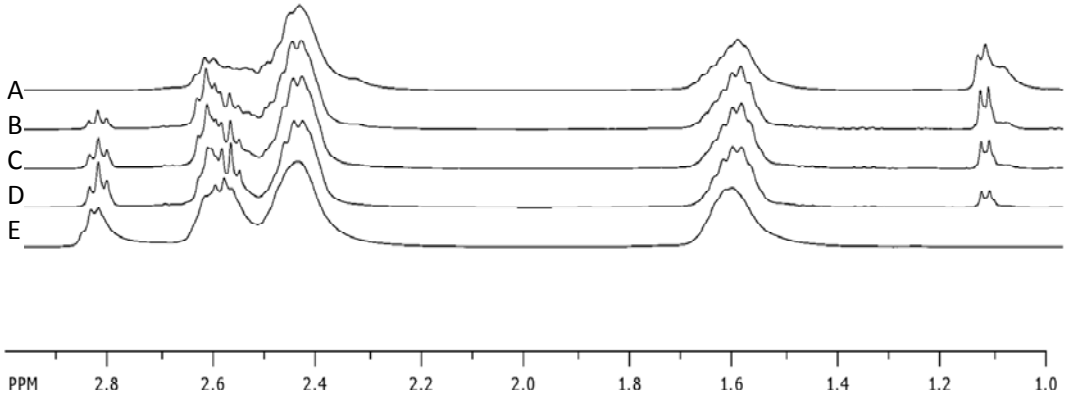

Figure 2.4 ^{1}H NMR spectra of G5-PPI-PO (c-64) (A), G5-PPI-ACN (a-64) (E), G5-PPI-PO/ACN at molar ratios of 7:3 (B), 5:5 (C), and 3:7 (D). The actual compositions of PO and ACN incorporated into these three PPI conjugates are at molar ratios of 27/73 (B), 40/60 (C), and 60/40 (D), respectively, as determined by integrating two chemical shifts at 1.10 and 2.80 ppm.

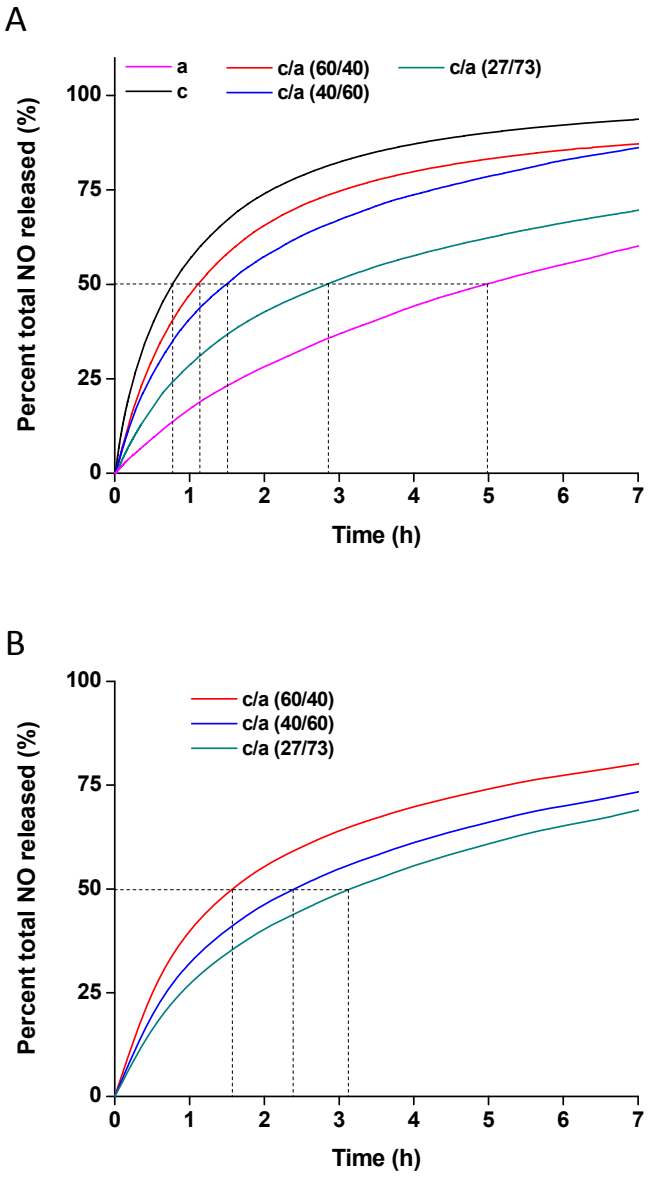

Figure 2.5 (A) Experimental plot of percent total NO released in PBS (pH = 7.4) at 37 ºC as a function of time for G5-PPI-PO (c-NO), G5-PPI-ACN (a-NO), and G5-PPI-PO/ACN conjugates; (B) Simulated plot of percent total NO released for G5-PPI-PO/ACN conjugates.

2.4 Conclusions

To expand the utility of macromolecular NO-release scaffolds as stand-alone therapeutics, dopants for biomedical polymers, or general NO-release sources, we synthesized a series of diverse NO-releasing PPI dendrimers by straightforward chemical modification of the core dendrimer using conjugation addition (ACN and PEG) or ring opening (PO, ED, and SO) reactions. The NO release from these resulting dendrimers demonstrated that size (i.e., generation number or molecular weight) and exterior structures (e.g., steric environment, hydrophobicity, etc.) play important roles in NO release kinetics. Furthermore, the use of select NO donors with unique NO release kinetics and overall payloads may be exploited by multi-NO donor/dendrimer functionalization. The combination of structural diversity and achievable NO release (i.e., up to 3.8 μmol NO/mg with half-lives from 0.3–4.9 h) should prove useful in the further study and utilization of these NO release materials for a broad range of fundamental and applied applications including pharmacological agents.

2.5 References

1. Lee, C. C.; MacKay, J. A.; Frechet, J. M. J.; Szoka, F. C. Designing dendrimers for biological applications. *Nat. Biotechnol.* **2005,** *23*, 1517-1526.

2. Mintzer, M. A.; Grinstaff, M. W. Biomedical applications of dendrimers: a tutorial. *Chem. Soc. Rev.* **2011,** *40*, 173-190.

3. Wolinsky, J. B.; Grinstaff, M. W. Therapeutic and diagnostic applications of dendrimers for cancer treatment. *Adv. Drug Delivery Rev.* **2008,** *60*, 1037-1055.

4. Joshi, N.; Grinstaff, M. Applications of dendrimers in tissue engineering. *Curr. Top. Med. Chem.* **2008,** *8*, 1225-1236.

5. Tomalia, D. A.; Naylor, A. M.; Goddard, W. A. Starburst dendrimers - molecular-level control of size, shape, surface-chemistry, topology, and flexibility from atoms to macroscopic matter. *Angew. Chem., Int. Ed.* **1990,** *29*, 138-175.

6. Debrabandervandenberg, E. M. M.; Meijer, E. W. Poly(propylene Imine) dendrimers - large-scale synthesis by hetereogeneously catalyzed hydrogenations. *Angew. Chem., Int. Ed.* **1993,** *32*, 1308-1311.

7. Sadler, K.; Tam, J. P. Peptide dendrimers: applications and synthesis. *Rev. Mol. Biotechnol.* **2002,** *90*, 195-229.

8. Ihre, H.; Hult, A.; Soderlind, E. Synthesis, characterization, and H-1 NMR self-diffusion studies of dendritic aliphatic polyesters based on 2,2-bis(hydroxymethyl)propionic acid and 1,1,1-tris(hydroxyphenyl)ethane. *J. Am. Chem. Soc.* **1996,** *118*, 6388-6395.

9. Hawker, C. J.; Frechet, J. M. J. Preparation of polymers with controlled molecular architecture - a new convergent approach to dendritic macromolecules. *J. Am. Chem. Soc.* **1990,** *112*, 7638-7647.

10. Allen, T. M.; Cullis, P. R. Drug delivery systems: Entering the mainstream. *Science* **2004,** *303*, 1818-1822.

11. Malik, N.; Evagorou, E. G.; Duncan, R. Dendrimer-platinate: a novel approach to cancer chemotherapy. *Anti-Cancer Drugs* **1999,** *10*, 767-776.

12. Matsumura, Y.; Maeda, H. A new concept for macromolecular therapeutics in cancer-chemotherapy - mechanism of tumoritropic accumulation of proteins and the antitumor agent smancs. *Cancer Res.* **1986,** *46*, 6387-6392.

13. Kukowska-Latallo, J. F.; Candido, K. A.; Cao, Z. Y.; Nigavekar, S. S.; Majoros, I. J.; Thomas, T. P.; Balogh, L. P.; Khan, M. K.; Baker, J. R. Nanoparticle targeting of anticancer drug improves therapeutic response in animal model of human epithelial cancer. *Cancer Res.* **2005,** *65*, 5317-5324.

14. Wooley, K. L.; Hawker, C. J.; Frechet, J. M. J. Unsymmetrical 3-dimensional macromolecules - preparation and characterization of strongly dipolar dendritic macromolecules. *J. Am. Chem. Soc.* **1993,** *115*, 11496-11505.

15. Gillies, E. R.; Frechet, J. M. J. Designing macromolecules for therapeutic applications: Polyester dendrimer-poly(ethylene oxide) "bow-tie" hybrids with tunable molecular weight and architecture. *J. Am. Chem. Soc.* **2002,** *124*, 14137-14146.

16. Steffensen, M. B.; Simanek, E. E. Synthesis and manipulation of orthogonally protected dendrimers: Building blocks for library synthesis. *Angew. Chem., Int. Ed.* **2004,** *43*, 5178-5180.

17. Li, Y. G.; Cu, Y. T. H.; Luo, D. Multiplexed detection of pathogen DNA with DNA-based fluorescence nanobarcodes. *Nat. Biotechnol.* **2005,** *23*, 885-889.

18. Haensler, J.; Szoka, F. C. Polyamidoamine cascade polymers mediate efficient transfection of cells in culture. *Bioconjugate Chem.* **1993,** *4*, 372-379.

19. Tang, M. X.; Redemann, C. T.; Szoka, F. C. In vitro gene delivery by degraded polyamidoamine dendrimers. *Bioconjugate Chem.* **1996,** *7*, 703-714.

20. Vincent, L.; Varet, J.; Pille, J. Y.; Bompais, H.; Opolon, P.; Maksimenko, A.; Malvy, C.; Mirshahi, M.; Lu, H.; Soria, J. P. V. C.; Li, H. Efficacy of dendrimer-mediated angiostatin and TIMP-2 gene delivery on inhibition of tumor growth and angiogenesis: In vitro and in vivo studies. *Int. J. Cancer* **2003,** *105*, 419-429.

21. Thomas, T. P.; Shukla, R.; Kotlyar, A.; Kukowska-Latallo, J.; Baker, J. R. Dendrimer-based tumor cell targeting of fibroblast growth factor-1. *Bioorg. Med. Chem. Lett.* **2010,** *20*, 700-703.

22. Majoros, I. J.; Myc, A.; Thomas, T.; Mehta, C. B.; Baker, J. R. PAMAM dendrimer-based multifunctional conjugate for cancer therapy: Synthesis, characterization, and functionality. *Biomacromolecules* **2006,** *7*, 572-579.

23. Wiener, E. C.; Brechbiel, M. W.; Brothers, H.; Magin, R. L.; Gansow, O. A.; Tomalia, D. A.; Lauterbur, P. C. Dendrimer-based metal-chelates - a new class of magnetic-resonance-imaging contrast agents. *Magnet. Reson. Med.* **1994,** *31*, 1-8.

24. Margerum, L. D.; Campion, B. K.; Koo, M.; Shargill, N.; Lai, J. J.; Marumoto, A.; Sontum, P. C. Gadolinium(III) DO3A macrocycles and polyethylene glycol coupled to dendrimers - Effect of molecular weight on physical and biological properties of macromolecular magnetic resonance imaging contrast agents. *J. Alloy Compd.* **1997,** *249*, 185-190.

25. Kobayashi, H.; Kawamoto, S.; Choyke, P. L.; Sato, N.; Knopp, M. V.; Star, R. A.; Waldmann, T. A.; Tagaya, Y.; Brechbiel, M. W. Comparison of dendrimer-based macromolecular contrast agents for dynamic micro-magnetic resonance lymphangiography. *Magnet. Reson. Med.* **2003,** *50*, 758-766.

26. Ziemer, L. S.; Lee, W. M. F.; Vinogradov, S. A.; Sehgal, C.; Wilson, D. F. Oxygen distribution in murine tumors: characterization using oxygen-dependent quenching of phosphorescence. *J. Appl. Physiol.* **2005,** *98*, 1503-1510.

27. Dunphy, I.; Vinogradov, S. A.; Wilson, D. F. Oxyphor R2 and G2: phosphors for measuring oxygen by oxygen-dependent quenching of phosphorescence. *Anal. Biochem.* **2002,** *310*, 191-198.

28. Brinas, R. P.; Troxler, T.; Hochstrasser, R. M.; Vinogradov, S. A. Phosphorescent oxygen sensor with dendritic protection and two-photon absorbing antenna. *J. Am. Chem. Soc.* **2005,** *127*, 11851-11862.

29. Floyd, W. C.; Klemm, P. J.; Smiles, D. E.; Kohlgruber, A. C.; Pierre, V. C.; Mynar, J. L.; Frechet, J. M. J.; Raymond, K. N. Conjugation effects of various linkers on Gd(III) MRI contrast agents with dendrimers: optimizing the hydroxypyridinonate (HOPO) ligands with nontoxic, degradable esteramide (EA) dendrimers for high relaxivity. *J. Am. Chem. Soc.* **2011,** *133*, 2390-2393.

30. Rozhkov, V.; Wilson, D.; Vinogradov, S. Phosphorescent Pd porphyrin-dendrimers: Tuning core accessibility by varying the hydrophobicity of the dendritic matrix. *Macromolecules* **2002,** *35*, 1991-1993.

31. Cloninger, M. J. Biological applications of dendrimers. *Curr. Opin. Chem. Biol.* **2002,** *6*, 742-748.

32. Wathier, M.; Jung, P. J.; Camahan, M. A.; Kim, T.; Grinstaff, M. W. Dendritic macromers as in situ polymerizing biomaterials for securing cataract incisions. *J. Am. Chem. Soc.* **2004,** *126*, 12744-12745.

33. Velazquez, A. J.; Carnahan, M. A.; Kristinsson, J.; Stinnett, S.; Grinstaff, M. W.; Kim, T. New dendritic adhesives for sutureless ophthalmic surgical procedures - In vitro studies of corneal laceration repair. *Arch. Ophthalmol-Chic.* **2004,** *122*, 867-870.

34. Ma, M. L.; Cheng, Y. Y.; Xu, Z. H.; Xu, P.; Qu, H.; Fang, Y. J.; Xu, T. W.; Wen, L. P. Evaluation of polyamidoamine (PAMAM) dendrimers as drug carriers of anti-bacterial drugs using sulfamethoxazole (SMZ) as a model drug. *Eur. J. Med. Chem.* **2007,** *42*, 93-98.

35. Chen, C. Z. S.; Beck-Tan, N. C.; Dhurjati, P.; van Dyk, T. K.; LaRossa, R. A.; Cooper, S. L. Quaternary ammonium functionalized poly(propylene imine) dendrimers as effective antimicrobials: Structure-activity studies. *Biomacromolecules* **2000,** *1*, 473-480.

36. Meyers, S. R.; Juhn, F. S.; Griset, A. P.; Luman, N. R.; Grinstaff, M. W. Anionic amphiphilic dendrimers as antibacterial gents. *J. Am. Chem. Soc.* **2008,** *130*, 14444-14445.

37. Hofseth, L. J.; Hussain, S. P.; Wogan, G. N.; Harris, C. C. Nitric oxide in cancer and chemoprevention. *Free Radical Bio. Med.* **2003,** *34*, 955-968.

38. Pacher, P.; Beckman, J. S.; Liaudet, L. Nitric oxide and peroxynitrite in health and disease. *Physiol. Rev.* **2007,** *87*, 315-424.

39. Chakrapani, H.; Wilde, T. C.; Citro, M. L.; Goodblatt, M. M.; Keefer, L. K.; Saavedra, J. E. Synthesis, nitric oxide release, and anti-leukemic activity of glutathione-activated nitric oxide prodrugs: Structural analogues of PABA/NO, an anti-cancer lead compound. *Bioorg. Med. Chem.* **2008,** *16*, 2657-2664.

40. Velazquez, C. A.; Chen, Q. H.; Citro, M. L.; Keefer, L. K.; Knaus, E. E. Second-generation aspirin and indomethacin prodrugs possessing an O-2-(Acetoxymethyl)-1-(2-carboxypyrrolidin-1-yl)diazenium-1,2-diolate nitric oxide donor moiety: Design, synthesis, biological evaluation, and nitric oxide release studies. *J. Med. Chem.* **2008,** *51*, 1954-1961.

41. Chakrapani, H.; Showalter, B. M.; Kong, L.; Keefer, L. K.; Saavedra, J. E. V-PROLI/NO, a prodrug of the nitric oxide donor, PROLI/NO. *Org. Lett.* **2007,** *9*, 3409-3412.

42. Velazquez, C. A.; Rao, P. N. P.; Citro, M. L.; Keefer, L. K.; Knaus, E. E. O-2-Acetoxymethyl-protected diazeniumdiolate-based NSAIDs (NONO-NSAIDs): Synthesis, nitric oxide release, and biological evaluation studies. *Bioorg. Med. Chem.* **2007,** *15*, 4767-4774.

43. Keefer, L. K.; Flippen-Anderson, J. L.; George, C.; Shanklin, A. P.; Dunams, T. A.; Christodoulou, D.; Saavedra, J. E.; Sagan, E. S.; Bohle, D. S. Chemistry of the diazeniumdiolates - 1. Structural and spectral characteristics of the [N(O)NO](-) functional group. *Nitric Oxide-Biol. Chem.* **2001,** *5*, 377-394.

44. Davies, K. M.; Wink, D. A.; Saavedra, J. E.; Keefer, L. K. Chemistry of the diazeniumdiolates. 2. Kinetics and mechanism of dissociation to nitric oxide in aqueous solution. *J. Am. Chem. Soc.* **2001,** *123*, 5473-5481.

45. Keefer, L. K.; Nims, R. W.; Davies, K. M.; Wink, D. A. "NONOates" (1-substituted diazen-1-ium-1,2-diolates) as nitric oxide donors: Convenient nitric oxide dosage forms. *Method Enzymol.* **1996,** *268*, 281-293.

46. Hrabie, J. A.; Klose, J. R.; Wink, D. A.; Keefer, L. K. New Nitric oxide-releasing zwitterions derived from polyamines. *J. Org. Chem.* **1993,** *58*, 1472-1476.

47. Stasko, N. A.; Schoenfisch, M. H. Dendrimers as a scaffold for nitric oxide release. *J. Am. Chem. Soc.* **2006,** *128*, 8265-8271.

48. Stasko, N. A.; Fischer, T. H.; Schoenfisch, M. H. S-nitrosothiol-modified dendrimers as nitric oxide delivery vehicles. *Biomacromolecules* **2008,** *9*, 834-841.

49. DeRosa, F.; Kibbe, M. R.; Najjar, S. F.; Citro, M. L.; Keefer, L. K.; Hrabie, J. A. Nitric oxide-releasing fabrics and other acrylonitrile-based diazeniumdiolates. *J. Am. Chem. Soc.* **2007,** *129*, 3786-3787.

50. Arnold, E. V.; Citro, M. L.; Keefer, L. K.; Hrabie, J. A. A nitric oxide-releasing polydiazeniumdiolate derived from acetonitrile. *Org. Lett.* **2002,** *4*, 1323-1325.

51. Arnold, E. V.; Keefer, L. K.; Hrabie, J. A. Reaction of nitric oxide with benzyl cyanide to yield a bis-diazeniumdiolated imidate. *Tetrahedron Lett.* **2000,** *41*, 8421-8424.

52. Shin, J. H.; Schoenfisch, M. H. Inorganic/organic hybrid silica nanoparticles as a nitric oxide delivery scaffold. *Chem. Mater.* **2008**, *20*, 239-249.

53. Kim, J.; Lee, Y.; Singha, K.; Kim, H. Y.; Shin, J. H.; Jo, S.; Han, D. K.; Kim. W. J. NONOates-polyethylenimine hydrogel for controlled nitric oxide release and cell proliferation modulation. *Bioconjugate Chem.* **2011**, *22*, 1031-1038.

54. Schaefer, F. C.; Peters, G. A. Base-catalyzed reaction of nitriles with alcohols-a convenient route to imidates and amidine salts. *J. Org. Chem.* **1961,** *26*, 412-418.

Chapter 3

Nitric Oxide-Releasing Amphiphilic Poly(amidoamine) (PAMAM) Dendrimers as Anti-biofilm Agents

3.1 Introduction

Bacteria in nature exist in two states – free-floating planktonic bacteria and bacterial biofilms.[1] While many antimicrobial agents have proven effective against planktonic bacteria, medically relevant infections including those associated with medical implants, diabetes mellitus, and cystic fibrosis are often caused by bacterial biofilms.[1-3] In contrast to planktonic bacteria, biofilms are communities of microorganisms adhered to a surface and protected by a self-secreted exopolysaccharides (EPS) matrix.[4] Along with inhibiting the penetration of antibiotics, biofilms exhibit several other defense mechanisms such as overexpression of stress-responsive genes, oxygen gradients within the biofilm matrix, and differentiation of a subpopulation of biofilm bacteria into resistant dormant species.[4] Collectively, these effects result in greater resistance of bacteria within biofilms to antimicrobial agents compared to their planktonic counterparts. It has been shown that killing bacteria in biofilms may require up to 1000 times the antibiotic dose necessary for killing planktonic bacteria.[1] As such, new antimicrobial agents capable of eradicating mature biofilms are urgently needed.

Dendrimers, a family of macromolecular scaffolds with hyper-branched architectures and multivalent surfaces,[5-13] have exhibited antibacterial activity against

both planktonic bacteria[14-18] and biofilms.[19-21] For example, quaternary ammonium-functionalized poly(propylenimine) (PPI) dendrimers[15] and primary amine-functionalized poly(amidoamine) (PAMAM) dendrimers[14] were shown to be biocidal against planktonic *Pseudomonas aerugionsa* and *Staphylococcus aureus*. Unfortunately, the inherent toxicity of these materials to eukaryotic (e.g., mammalian) cells has slowed their development as therapeutics.[22] To reduce overall toxicity to mammalian cells, Grinstaff et al. synthesized anionic amphiphilic polyester dendrimers that were potent against Gram-positive *Bacillus subtilis* but not human umbilical vein endothelial cells (HUVECs).[16] Likewise, hydroxyl-, carboxyl-, and poly(ethylene glycol) (PEG)-functionalized PAMAM dendrimers have been designed to minimize toxicity towards mammalian cells while retaining their antibacterial efficacy against bacterial species.[17, 23] Although most work to date has focused on the planktonic antibacterial activity of dendrimers, the efficacy of dendritic scaffolds against more challenging systems, including antibiotic-resistant bacteria and biofilms, has become an important focus in the design of antimicrobial dendrimers. Several studies have demonstrated the dispersion and inhibition of *Pseudomonas aeruginosa* and *Escherichia coli* biofilms by amphiphilic dendritic glycopeptides.[19-21, 23] As opposed to linear antimicrobial peptides, these dendritic peptides exhibited enhanced inhibition of biofilm growth.[19] However, additional work is required to elucidate the potential of dendrimers as effective agents for both inhibiting biofilm growth and eradicating mature biofilms.

Nitric oxide (NO), an endogenously-produced diatomic free radical, plays a key role in the natural immune response to pathogens.[24-26] Both NO and its reactive byproducts (e.g., peroxynitrite and dinitrogen trioxide) exert significant oxidative and nitrosative

stress on bacterial cells to facilitate killing. Nitrosative stress occurs when thiols on proteins and DNA are nitrosated, impairing normal function. Oxidative stress is mostly observed through lipid peroxidation, which destroys the bacterial membrane integrity.[26] Nitric oxide exhibited broad-spectrum antimicrobial efficacy and its short-lived nature allows for local bactericidal action.[26] As such, macromolecular vehicles (e.g., gold nanoparticles, silica nanoparticles, and dendrimers) have been developed to store and controllably release NO.[27-31] These materials have proven highly effective against both Gram–positive and –negative bacteria.[32-35] Nitric oxide-releasing dendrimes in particular have exhibited highly promising bactericidal action due to large NO payloads and dendrimer–bacteria association.[33] The biocidal activity of NO-releasing dendrimers was found to be highly dependent on both the size (i.e., generation) and the exterior functionality with hydrophobic functionalizations (e.g., via styrene oxide modification of primary amines) proving most effective against Gram-positive and –negative bacteria.[33] Unfortunately, the utility of these dendrimers for eradicating established biofilms presents toxicity concerns due to the larger concentration required (vs. planktonic assays) membrane disrupting properties of the hydrophobic exterior.[36] Herein, we report the synthesis of NO-releasing amphiphilic dendrimers with varied exterior hydrophobicity as a new class of anti-biofilm agents capable of eradicating bacterial biofilms with reduced toxicity to mammalian cells.

3.2 Experimental Section

3.2.1 Materials.

Phenazine methosulfate (PMS), 3-(4,5-dimethylthiazol-2-yl)-5-(3-carboxymethoxyphenyl)-2-(4-sulfophenyl)-2H-tetrazolium inner salt (MTS), trypsin,

phosphate buffered saline (PBS), penicillin streptomycin (PS), rhodamine B isothiocyanate (RITC), Dulbecco's modified Eagle's medium (DMEM), and propidium iodide (PI) were purchased from Sigma-Aldrich (St. Loius, MO). Sodium methoxide (5.4 M solution in methanol), propylene oxide (PO), and 1,2-epoxy-9-decene (ED) were obtained from Acros Organics (Geel, Belgium). Tryptic soy broth (TSB) and tryptic soy agar (TSA) were obtained from Becton, Dickison and Company (Franklin Lakes, NJ). Spectra/Por Float-A-Lyzers for dialysis of the dendrimers were purchased from Spectrum Laboratories, Inc. (Rancho Dominguez, CA). 4,5-Diaminofluorescein diacetate (DAF-2 DA) was purchased from Calbiochem (San Diego, CA). Syto 9 green fluorescent nucleic acid stain was purchased from Life Technologies (Grand Island, NY). Glass bottom microscopy dishes were received from MatTek Corporation (Ashland, MA). Common laboratory salts and solvents were purchased from Fisher Scientific (Pittsburgh, PA). Unless noted otherwise, these and other materials were used as received without further purification.

3.2.2 Synthesis of Secondary Amine- and N-Diazeniumdiolate-Functionalized PAMAM Dendrimers.

Secondary amine-functionalized PAMAM dendrimers (generation 1 or G1 and generation 3 or G3) were synthesized as described previously.[27] Briefly, primary amine-functionalized G1-PAMAM dendrimer (100 mg) was dissolved in methanol (2 mL). One molar equivalent of PO, ED, or a mixture of PO and ED relative to the primary amines was then added to the G1-PAMAM-NH_2 solution under constant stirring at room temperature for 4 d to yield the secondary amine-functionalized G1-PAMAM conjugates. Similarly, secondary amine-functionalized G3-PAMAM conjugates were formed via the reaction of G3-PAMAM-NH_2 with PO, ED, or a mixture of PO and ED, respectively.

Following 3 d of reaction, solvent was removed under reduced pressure. The dendrimers were then washed with ethanol, followed by dialysis against water and lyophilization. The resulting secondary amine-functionalized dendrimers (G1 and G3) were characterized by nuclear magnetic resonance (NMR) spectroscopy in deuterated methanol.

Representative ^{1}H NMR data of secondary amine-functionalized G1-PAMAM conjugates formed via the reactions of G1-PAMAM-NH_2 with PO, ED and PO/ED mixtures yielded the following peaks: **G1-PAMAM-PO**: ^{1}H NMR (400 MHz, CD_3OD, δ): 3.82 ($CH_2NHCH_2CH(OH)CH_3$), 3.10–3.20 ($CONHCH_2CH_2$), 2.75 ($CH_2N(CH_2CH_2CO)_2$), 2.60 ($CH_2NHCH_2CH(OH)CH_3$), 2.55 ($CH_2N(CH_2CH_2CO)_2$), 2.37 ($CH_2N(CH_2CH_2CO)_2$), 1.00 ($CH_2NHCH_2CH(OH)CH_3$). **G1-PAMAM-ED**: ^{1}H NMR (400 MHz, CD_3OD, δ): 5.80 ($CH_2CH=CH_2$), 4.88 ($CH_2CH=CH_2$), 3.58 ($NHCH_2CH(OH)CH_2$), 3.10–3.20 ($CONHCH_2CH_2$), 2.73 ($CH_2N(CH_2CH_2CO)_2$), 2.67 ($NH(CH_2)_2$), 2.55 ($CH_2N(CH_2CH_2CO)_2$), 2.36 ($CH_2N(CH_2CH_2CO)_2$), 1.98 ($CH_2CH=CH_2$), 1.2–1.4 ($(CH_2)_5CH_2CH=CH_2$). **G1-PAMAM-PO/ED**: ^{1}H NMR (400 MHz, CD_3OD, δ): 5.80 ($CH_2CH=CH_2$), 4.88 ($CH_2CH=CH_2$), 3.82 ($CH_2NHCH_2CH(OH)CH_3$), 3.58 ($NHCH_2CH(OH)CH_2$), 3.10–3.20 ($CONHCH_2CH_2$), 2.75 ($CH_2N(CH_2CH_2CO)_2$), 2.60 ($CH_2NHCH_2CH(OH)CH_3$), 2.55 ($CH_2N(CH_2CH_2CO)_2$), 2.37 ($CH_2N(CH_2CH_2CO)_2$), 1.98 ($CH_2CH=CH_2$), 1.2–1.4 ($(CH_2)_5CH_2CH=CH_2$), 1.00 ($CH_2NHCH_2CH(OH)CH_3$).

N-diazeniumdiolate-functionalized PAMAM dendrimers were synthesized by adding one equivalent of 5.4 M sodium methoxide solution in methanol (with respect to the molar amount of primary amine functionality in PAMAM-NH_2 used to synthesize

dendrimers) to a vial containing dendrimers (100 mg) in methanol (1 mL). The glass vials were then inserted in a stainless steel reactor, and the headspace in the reactor was subsequently flushed with argon three times followed by three longer purges with argon (3 × 10 min) to remove oxygen from the stirred solution. The reactor was then filled with NO (purified over KOH pellets for 30 min to remove trace NO degradation products) to 10 atm for 3 d. Unreacted NO was then removed using the same argon flushing procedure described above to obtain the *N*-diazeniumdiolate-modified PAMAM dendrimers.

3.2.3 Characterization of NO Storage and Release.

Nitric oxide release was measured using a Sievers 280i Chemiluminesce Nitric Oxide Analyzer (Boulder, CO) by adding NO-releasing dendrimers (1 mg) to a sample containing deoxygenated PBS (30 mL) (pH = 7.4, 37 ^{o}C). Nitrogen was purged through the sample vessel solution to carry liberated NO to the analyzer at a flow rate of 70 mL/min. Additional nitrogen flow was supplied to the vessel to match the collection rate of the analyzer (200 mL/min). Nitric oxide release was measured in real time, thus allowing for the determination of NO release total (t[NO]), half-life ($t_{1/2}$), and maximum NO flux ($[NO]_{max}$). The analysis was terminated when the NO release levels fell to below 10 ppb NO/mg dendrimer.

3.2.4 Planktonic Bactericidal Assays Under Static Conditions.

Bacterial cultures were grown from a frozen (-80 ^{o}C) stock overnight in TSB at 37 ^{o}C. A 500 μL aliquot of the resulting suspension was added to fresh TSB (50 mL) and incubated at 37 ^{o}C for ~2 h until the concentration reached 1×10^{8} colony forming units (CFU)/mL, as confirmed by the OD_{600}. A working bacterial stock was generated by plating the bacterial suspension on TSA and incubating at 37 ^{o}C overnight. Subsequent

TSA bacterial stocks were prepared weekly and stored at 4 ^{o}C. For bactericidal assays, colonies of *P. aeruginosa* were taken from the TSA plate, dispersed in TSB (3 mL), and then incubated at 37 ^{o}C overnight. A 500 μL aliquot of culture was added to fresh TSB (50 mL) and incubated to a concentration of ~1×10^{8} CFU/mL. The bacteria was then collected by centrifugation (3645 × *g* for 10 min), resuspended in PBS, and diluted 100-fold to obtain a final concentration of 1×10^{6} CFU/mL. The bactericidal efficacy of NO-releasing dendrimers against the bacteria was evaluated by incubating the bacteria suspension with NO-releasing dendrimers over a range of concentrations in PBS at 37 ^{o}C. At 4 h, 100 μL aliquots of the bacteria suspensions were removed, diluted 10-fold in PBS, plated on TSA, and incubated overnight at 37 ^{o}C. The minimum concentration of NO-releasing dendrimers that resulted in a 3-log reduction in bacterial viability was defined as the planktonic minimum bactericidal concentration (MBC).

3.2.5 Growth of P. aeruginosa Biofilms.

A standard US centers for disease control (CDC) bioreactor (Biosurface Technologies, Bozeman, MT) was used to grow *P. aeruginosa* biofilms over a 48 h period. Briefly, medical grade silicone rubber substrates were mounted in coupon holders prior to assembling the reactor. The assembled reactor was then autoclaved. The reactor effluent line was clamped and 1% (v/v) sterile TSB (500 mL) was added aseptically. Subsequently, the reactor was inoculated with an aliquot (1 mL) of *P. aeruginosa* (10^{8} CFU/mL in TSB) to achieve a final concentration ~2×10^{5} CFU/mL. The reactor was then incubated at 37 °C for 24 h with stirring (150 rpm). Following this "batch phase" growth, the reactor media was refreshed continuously with 0.33% (v/v) TSB at 6 mL/min for another 24 h.

3.2.6 Treatment of P. aeruginosa Biofilms with NO-releasing Dendrimers.

P. aeruginosa biofilms grown on silicone rubber substrates were exposed to dendrimers in PBS with slight agitation (37 °C, 24 h) to determine the minimum bactericidal concentration (MBC) necessary to elicit a 5-log reduction in viability of the biofilm-based bacteria. At 24 h, samples were sonicated and vortexed to disrupt the biofilm. Aliquots (100 μL) of the cell/dendrimer suspensions were diluted and plated on TSA and incubated overnight. Bacterial viability was determined by counting observed colonies. Of note, the limit of detection for this selected plate counting method is 2.5×10^3 CFU/mL. As such, biofilm growth conditions were selected to accurately represent a 5-log reduction in viability.

3.2.7 In vitro Cytotoxicity.

L929 mouse fibroblasts were grown in DMEM supplemented with 10% (v/v) fetal bovine serum (FBS) and 1 wt% penicillin/streptomycin, and incubated in 5% (v/v) CO_2 under humidified conditions at 37 ^oC. After reaching confluency (80%), the cells were trypsinized, seeded onto tissue-culture treated polystyrene 96-well plates at a density of 3×10^4 cells/mL, and incubated at 37 ^oC for 48 h. The supernatant was then aspirated prior to adding 200 μL fresh DMEM and 50 μL of NO-releasing dendrimers in PBS to each well. After incubation at 37 ^oC for 24 h, the supernatant was aspirated and a 120 μL mixture of DMEM/MTS/PMS (105/20/1, v/v/v) was added to each well. The absorbance of the resulting colored solution after 1.5 h incubation at 37 ^oC was quantified using a Thermoscientific Multiskan EX plate reader at 490 nm. The mixture of DMEM/MTS/PMS and untreated cells were used as a blank and control, respectively. Cell viability was calculated as follows (Eq. 3.1):

$$\text{Cell Viability} = \frac{(\text{Absorbance}_{\text{treated cell}} - \text{Absorbance}_{\text{blank}})}{(\text{Absorbance}_{\text{untreated cell}} - \text{Absorbance}_{\text{blank}})} \qquad \text{Eq. 3.1}$$

3.2.8 Confocal Microscopy for Association of Dendrimers with Bacteria Cells.

Fluorescently-labeled control and NO-releasing dendrimers were prepared following a previously reported procedure.[33] Briefly, G1-PAMAM-NH_2 (100 mg) and rhodamine B isothiocyanate (RITC) (3 mg) were dissolved in 2 mL methanol. The solution was stirred for 3 d in the dark. The product solution was dialyzed against 0.1 M NaCl (2 L) for 24 h, and ultrapure Milli-Q water for 3 d (3 × 2 L). Subsequent lyophilization yielded RITC-labeled G1-PAMAM-NH_2. The fluorescently-labeled G1-PAMAM-NH_2 dendrimers were modified with one molar equivalent of PO or ED alone, or a PO/ED mixture, and further reacted with NO at 10 atm under basic conditions as described above to yield NO-releasing G1-PAMAM dendrimers. *P. aeruginosa* was cultured in TSB to a concentration of 1 × 10^8 CFU/mL, collected *via* centrifugation (3645 × *g* for 10 min), resuspended in sterile PBS, and adjusted to 1 × 10^6 CFU/mL. Aliquots of the bacteria solution were incubated in a glass bottom confocal dish for 2 h at 37 °C. A Zeiss 510 Meta inverted laser scanning confocal microscope with a 543 nm HeNe excitation laser and a LP 585 nm filter was used to obtain fluorescence images of the RITC-modified dendrimers. The bright field and fluorescence images were collected using a N.A. 1.2 C-apochromat water immersion lens with a 20× objective. Solutions of RITC-labeled NO-releasing (400 μg/mL) dendrimers in PBS (1.5 mL) were added to the bacteria solution (1.5 mL) in the glass confocal dish to achieve a final concentration of 200 μg/mL. Images were collected at 2 h incubation to characterize the association, if any, of the dendrimers with *P. aerugionsa*. Dendrimer–bacteria association within biofilms was also characterized using confocal microscopy. Established biofilms stained with Syto 9 (10 μM) were incubated

with RITC-labeled NO-releasing dendrimers (50 μg/mL) for 1 h before imaging. A 488 nm Ar excitation laser with BP 505-530 nm filter was used to image Syto 9 fluorescence. The bright field and fluorescence images were collected simultaneously using a N.A. 1.2 C-apochromat water immersion lens with a 10× objective.

3.2.9 Confocal Microscopy for the Detection of Intracellular NO and Cell Death.

The efficiency of NO delivery and resulting bacteria death were evaluated as a function of dendrimer exterior hydrophobicity using confocal microscopy. Bacteria (*P. aeruginosa*) were cultured in TSB to a concentration of 1×10^8 CFU/mL, collected via centrifugation (3645 × *g* for 10 min), resuspended in sterile PBS, and adjusted to 1×10^6 CFU/mL in PBS supplemented with 10 μM DAF-2 DA and 30 μM PI. The bacteria solution (2.5 mL) was incubated in a glass bottom confocal dish for 45 min at 37 °C. A Zeiss 510 Meta inverted laser scanning confocal microscope with a 488 nm Ar excitation laser and a BP 505–530 nm filter was used to obtain DAF-2 (green) fluorescence images. Red fluorescence images for PI were obtained using a 543 nm HeNe excitation laser with a BP 560–615 nm filter. The bright field and fluorescence images were collected by a N.A. 1.2 C-apochromat water immersion lens with a 40× objective. An aliquot (1.5 mL) of NO-releasing dendrimers (10 μg/mL) in PBS (supplemented with 10 μM DAF-2 DA and 30 μM PI) was added to the bacteria solution (1.5 mL) in the glass confocal dish. Images were collected every 5 min to observe intracellular NO concentrations (green fluorescence) and compromised bacteria membrane (red fluorescence) temporally. The efficiency of NO delivery to bacteria within biofilms was also evaluated as a function of dendrimer composition by incubating the *P. aeruginosa* biofilm with NO-releasing dendrimers (20 μg/mL) in PBS supplemented with 10 μM DAF-2 DA and 30 μM PI for 1

h. Bright field and fluorescence images were collected using a N.A. 1.2 C-apochromat water immersion lens with a 20× objective.

3.3 Results and Discussion

Sun et al. previously reported on the planktonic bactericidal activity of NO-releasing dendrimers as a function of exterior functionality.[33] Functionalization with hydrophobic groups at the dendrimer exterior improved bactericidal efficacy but also resulted in significant toxicity towards mammalian cells. Indeed, even low concentration (~34 μg/mL) of hydrophobic dendrimer resulted in ~80% killing of L929 mouse fibroblast cells.[33] We thus sought to synthesize NO-releasing dendrimers with tunable exterior hydrophobicity in order to evaluate the impact of surface energy (hydrophobicity/hydrophilicity) on both bactericidal action and cytotoxicity.

3.3.1 Synthesis of Nitric Oxide Donor-Modified PAMAM Dendrimers.

We prviously has reported the synthesis of secondary amine-functionalized dendrimers with diverse exterior functionalities using the ring opening of epoxides to the primary amines on the dendrimer exterior.[27] *N*-diazeniumdiolate NO donors were formed by the reaction of the resulting secondary amines with NO gas under basic conditions.[27]

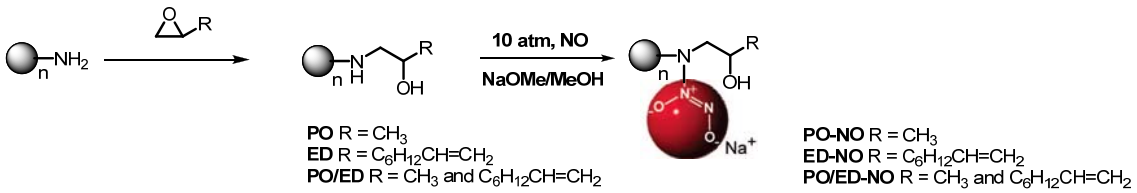

Scheme 3.1 Synthesis of secondary amine- and *N*-diazeniumdiolate-functionalized PAMAM conjugates for which n represents the number of primary amines on the periphery of PAMAM dendrimers (n = 8, 32).

To synthesize secondary amine-functionalized dendrimer with varied exterior hydrophobicicty, poly(amidoamine) (PAMAM) dendrimers were modified by a similar ring opening reaction with either hydrophilic PO exclusively, hydrophobic ED exclusively, or varying molar ratios of PO and ED (Scheme 3.1). The PO, ED, and PO/ED mixtures were added in a total of one equivalent with respect to the molar concentration of PAMAM primary amine functionality. The actual ratio of PO and ED conjugated to the PAMAM dendrimers was determined using ^{1}H NMR spectroscopy. As shown in Figure 3.1, a distinct resonance at 3.82 ppm corresponded to the methyne protons adjacent to the hydroxyl group of the product. This chemical shift was observed in the products of dendrimer reacting with PO exclusively, as well as those with the PO/ED mixture. Further inspection of the NMR spectra reveals the presence of a second distinct peak at 5.80 ppm, formed upon reaction of the dendrimer with either ED exclusively or the PO/ED mixtures. The 5.80 ppm peak corresponds to the methyne protons of the unsaturated ED double bond. The integration of the 3.82 and 5.80 ppm peaks allowed for the determination of the molar ratio of PO and ED. For PO/ED bifunctionalized dendrimers, the feed molar ratio of PO and ED was tuned to yield PO/ED ratios of 7:3 (i.e., **G1-PE 73**, **G3-PE 73**), 5:5 (i.e., **G1-PE 55**), and 3:7 (i.e., **G1-PE 37**). In this manner, we were able to study the effects of hydrophobicity on bactericidal activity and cytotoxicity (Table 3.1). In addition, recent research suggests that dendrimer size (i.e., dendrimer generation) plays an important role in the bactericidal efficacy of NO-releasing dendrimers, with higher generation (i.e., larger) NO-releasing dendrimers being more effective at killing bacteria due to the delivery of greater NO payloads.[33] Multivalent dendrimer-bound NO donors with 8 (G1) and 32 (G3) terminal

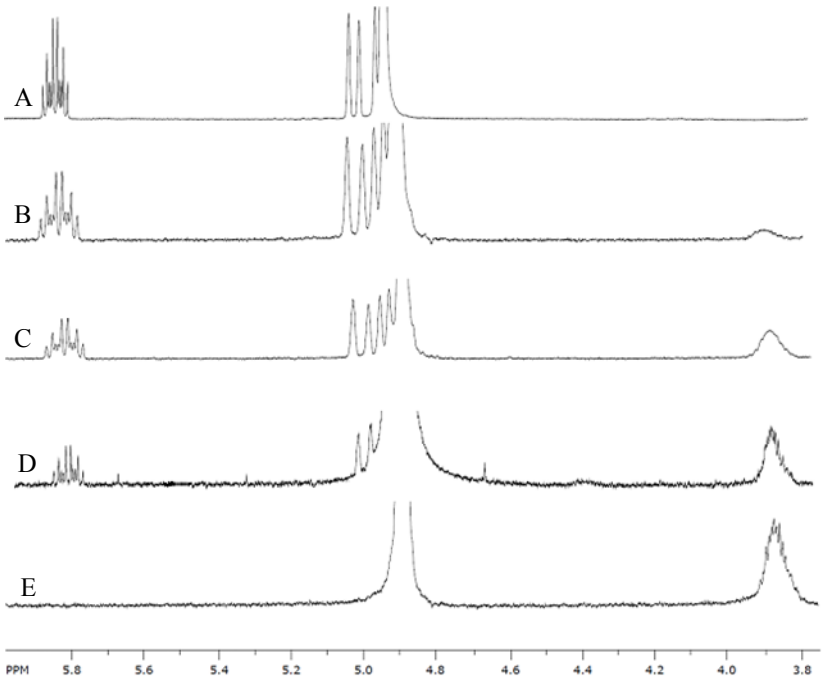

Figure 3.1 ^{1}H NMR spectra of A) **G1-PAMAM-ED**, B) **G1-PAMAM-PE 37**, C) **G1-PAMAM-PE 55**, D) **G1-PAMAM-PE 73**, and E) **G1-PAMAM-PO**. The actual composition of ED and PO was determined by the integration of peaks at 5.80 (-C*H*=CH_2) and 3.82 (-C*H*(OH)CH_3) ppm.

functional groups were thus synthesized to understand the influence of dendrimer size on the anti-biofilm efficacy against *P. aeruginosa* biofilms.

Subsequent reaction of the secondary amine-functionalized dendrimers (e.g., **PO**, **ED**, **PE**) with NO at 10 atm under basic conditions (Scheme 3.1) produced *N*-diazeniumdiolate-functionalized dendritic scaffolds (e.g., **PO-NO**, **ED-NO**, **PE-NO**).

The dendrimers exhibited similar NO storage (~1 μmol/mg) and NO-release kinetics (i.e., half life ~1 h) regardless of modification (Table 3.1). Of note, similar total NO storage and NO-release kinetics for the PO/ED (PE)-functionalized dendrimers was expected since both 100% PO or ED-functionalized dendrimers exhibited a total NO storage of ~1 μmol/mg and a half-life of ~1 h. These NO-release properties facilitate the evaluation of how surface hydrophobicity (via the PO to ED ratio) and dendrimer generation impact NO delivery and bacteria killing.

3.3.2 Bactericidal studies: Planktonic Bacteria.

Planktonic Gram-negative *P. aeruginosa* were exposed to control and NO-releasing dendrimers to evaluate the effects of the PO/ED ratio on bacterial killing. Bacterial viability assays were conducted over a 4-h period under static conditions to quantify the concentration of dendrimer required to reduce bacteria viability by 3-logs. This concentration is hereafter referred to as the planktonic minimum bactericidal concentration or MBC. The bactericidal NO dose for the NO-releasing dendrimers was also determined by multiplying total NO dose over 4 h (i.e., t[NO]^{a}) and the corresponding MBC (Table 3.2). As expected, the amphiphilic control dendrimers functionalized with ED exclusively or a PO/ED mixture (e.g., **G1-ED**, **G1-PE 37**, **G1-PE**

Table 3.1 Nitric oxide-release properties for G1 and G3 PAMAM dendrimers in PBS (pH = 7.4 at 37 °C) as measured by a chemiluminescence NO analyzer.

	Feed molar ratio (PO/ED)	t[NO][a] (μmol/mg)	t[NO][b] (μmol/mg)	$[NO]_{max}$ (ppb/mg)	$t_{1/2}$ (h)
G1-ED	0:1	0.71	1.23	3295	0.94
G1-PE 37	5:5	0.93	1.10	5666	0.87
G1-PE 55	7:3	1.10	1.23	5000	0.95
G1-PE 73	9:1	0.88	1.04	3000	1.01
G1-PO	1:0	0.92	1.03	3800	0.75
G3-PE 73	9:1	0.89	1.06	2400	1.02

[a] the NO released over 4 h (μmol per milligram of secondary amine-functionalized dendrimers).
[b] the NO released over 24 h (μmol per milligram of secondary amine-functionalized dendrimers).

Table 3.2 Comparison of the minimum bactericidal concentration (MBC) and bactericidal NO doses of control and NO-releasing dendrimers against planktonic Gram-negative *P. aeruginosa* after 4 h exposure for 3-log reduction in bacterial viability.

Dendrimers	MBC[a] (μg/mL)	MBC[b] (μg/mL)	Bactericidal NO Doses (nmol/mL)
G1-ED	8	5	3.55
G1-PE 37	5	4	3.72
G1-PE 55	10	7	7.70
G1-PE 73	30	20	17.6
G1-PO	3000	200	182
G3-PE 73	20	15	13.4

[a]concentration of control dendrimer required to reduce bacterial viability by 3-logs.
[b]concentration of NO-releasing dendrimer required to reduce bacterial viability by 3-logs.
Each parameter was analyzed with multiple replicates (n=3).

55, **G1-PE 73**) exhibited enhanced biocidal activity against planktonic *P. aeruginosa* compared to the hydrophilic control dendrimer (**G1-PO**). This behavior can in part be attributed to the enhanced perturbation and disruption of the bacteria membrane by the amphiphilic structures.[37] For example, functionalizing 30% of the dendrimer primary amines with ED (i.e., **G1-PE 73**) improved the biocidal action of the dendrimer scaffold by 99% (i.e., the MBC for **G1-PE 73** and **G1-PO** was 30 and 3000 μg/mL, respectively) compared to dendrimers functionalized solely with PO (i.e., **G1-PO**).

Further inspection of the results revealed lower MBCs for NO-releasing dendrimers compared to their non-NO-releasing counterpart, indicating enhanced bactericidal activity with NO. This increase in bactericidal efficacy is attributed to the oxidative and nitrosative stresses resulting from NO byproducts (e.g., peroxynitrite and dinitrogen trioxide).[26] As shown in Table 3.2, the bactericidal NO dose required to elicit the 3-log reduction in bacterial viability decreased with increasing dendrimer hydrophobicity (i.e., ED content), suggesting enhanced bacterial killing. For example, the bactericidal NO doses for **G1-ED-NO** and **G1-PO-NO** were 3.55 and 182 nmol/mL, respectively. Since dendrimer association with the outer surface (i.e., membrane) of bacteria followed by penetration through the bacteria membrane has been identified previously as important killing mechanisms,[18] we hypothesized that increasing the ED (hydrophobic) content of the dendrimer exterior would improved dendrimer association with the bacteria and facilitate more efficient NO delivery. Confocal microscopy was thus used to characterize the association of RITC-labeled **G1-PE 73-NO**, **G1-PE 55-NO**, **G1-PE 37-NO**, and **G3-PE 73-NO** with planktonic *P. aeruginosa* (Figure 3.2). (Dendrimers were labeled with RITC following a previous report.[33]) The impact of the RITC label on the dendrimer–

bacteria association was minimized by using a low amount of RITC (i.e., 1:100 molar ratio to total primary amines). As expected, based on hydrophobicity, the red fluorescence intensity was the greatest from RITC-labeled **G1-PE 55-NO** and **G1-PE 37-NO** indicating more rapid association of these dendrimers with *P. aeruginosa* than **G1-PE 73-NO**. However, the association of **G1-PE 37-NO** and **G1-PE 55-NO** with *P. aeruginosa* were similar, illustrating that the improvement of dendrimer association due to hydrophobicity plateaus at ~50% ED functionality (**G1-PE-55-NO**). Additional ED modification had negligible influence on the dendrimer-bacteria association kinetics. Furthermore, the association of the larger dendrimer (**G3-PE 73-NO**) was similar to that of **G1-PE 73-NO**, indicating that the hydrophobicity of the dendritic scaffolds plays a greater role in bacteria association than size, at least for G1 vs. G3 dendrimers. Other sizes and bacteria may result in altered behavior in dendrimer–bacteria association.

Based on enhanced dendrimer–bacteria association for dendrimers with greater ED character, we predicted more effective NO delivery and greater bacteria damage (i.e., membrane disruption). Fluorescence from DAF-2 (green) and PI (red) molecular probes were employed to study the intracellular NO levels and ensuing membrane disruption, respectively, using confocal microscopy. Green fluorescence (DAF-2) was nearly always observed first, indicating a buildup of intracellular NO. Red fluorescence (PI) followed as the bacteria membrane became compromised, with concomitant diminished green fluorescence. The buildup of measurable intracellular NO for bacteria incubated with **G1-PE 37-NO**, **G1-PE 55-NO**, and **G3-PE 73-NO** was observed at 35 min (Figure 3.3), significantly earlier than bacteria incubated with **G1-PE 73-NO** (60 min). The more rapid association (**G1-PE 37-NO** and **G1-PE 55-NO**) with bacteria and greater localized NO

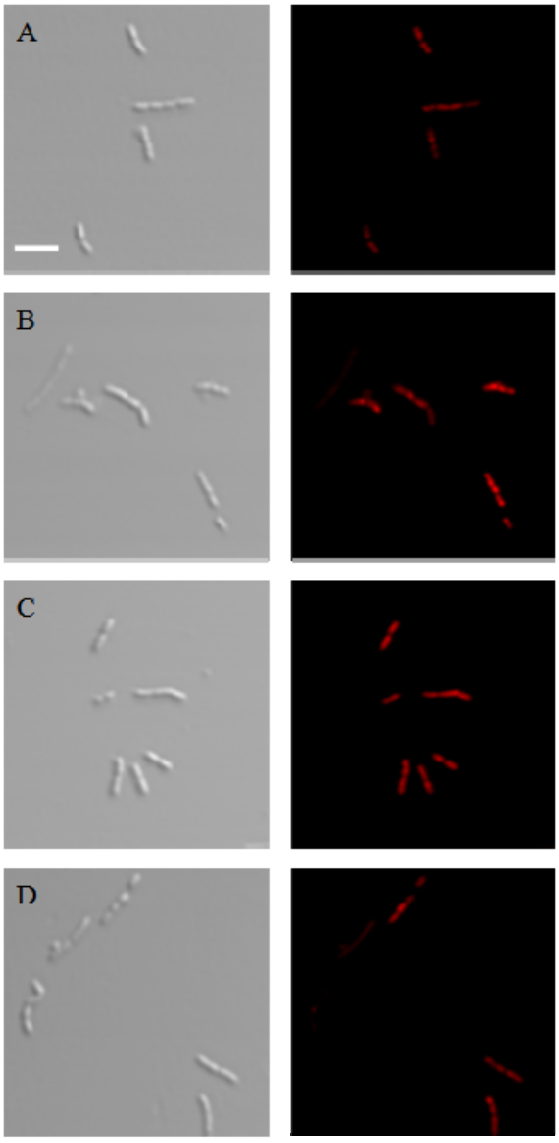

Figure 3.2 Bright field/fluorescent overlay and fluorescent images of RITC-label NO-releasing dendrimers association with *P. aeruginosa*. A) **G1-PE 73**; B) **G1-PE 55**; C) **G1-PE 37**; D) **G3-PE 73**. Scale bar 5 μm.

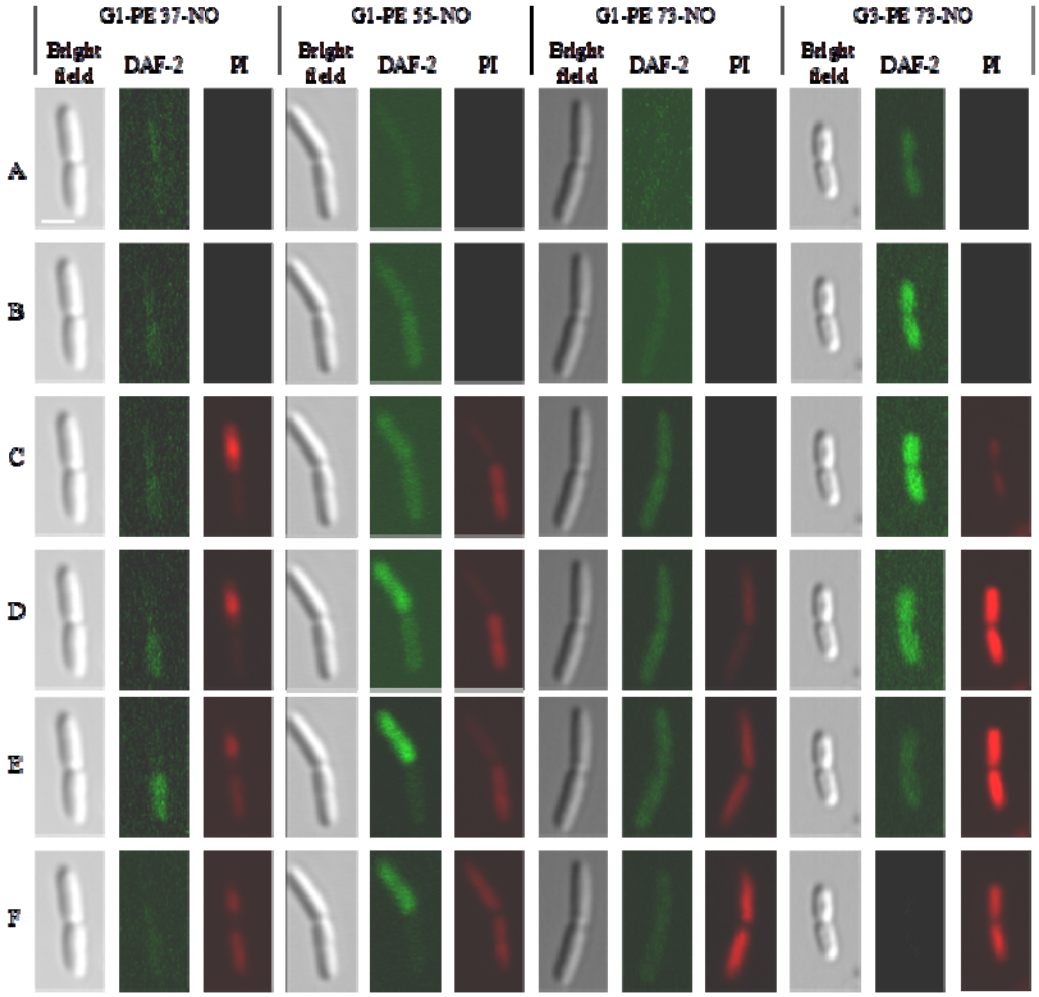

Figure 3.3. Intracellular DAF-2 (green) and PI (red) fluorescence from *P. aeruginosa* exposed to NO-releasing dendrimers **G1-PE 37-NO** (at A-35, B-50, C-55, D-65, E-105, F-110 min), **G1-PE 55-NO** (at A-35, B-60, C-75, D-85, E-115, F-150 min), **G1-PE 73-NO** (at A-60, B-85, C-125, D-135, E-140, F-150 min), and **G3-PE 73-NO** (at A-35, B-50, C-65, D-70, E-100, F-130 min). Intracellular NO is indicated by the DAF-2 green fluorescence, whereas PI red fluorescence points to compromised membranes. Scale bar: 2 μm.

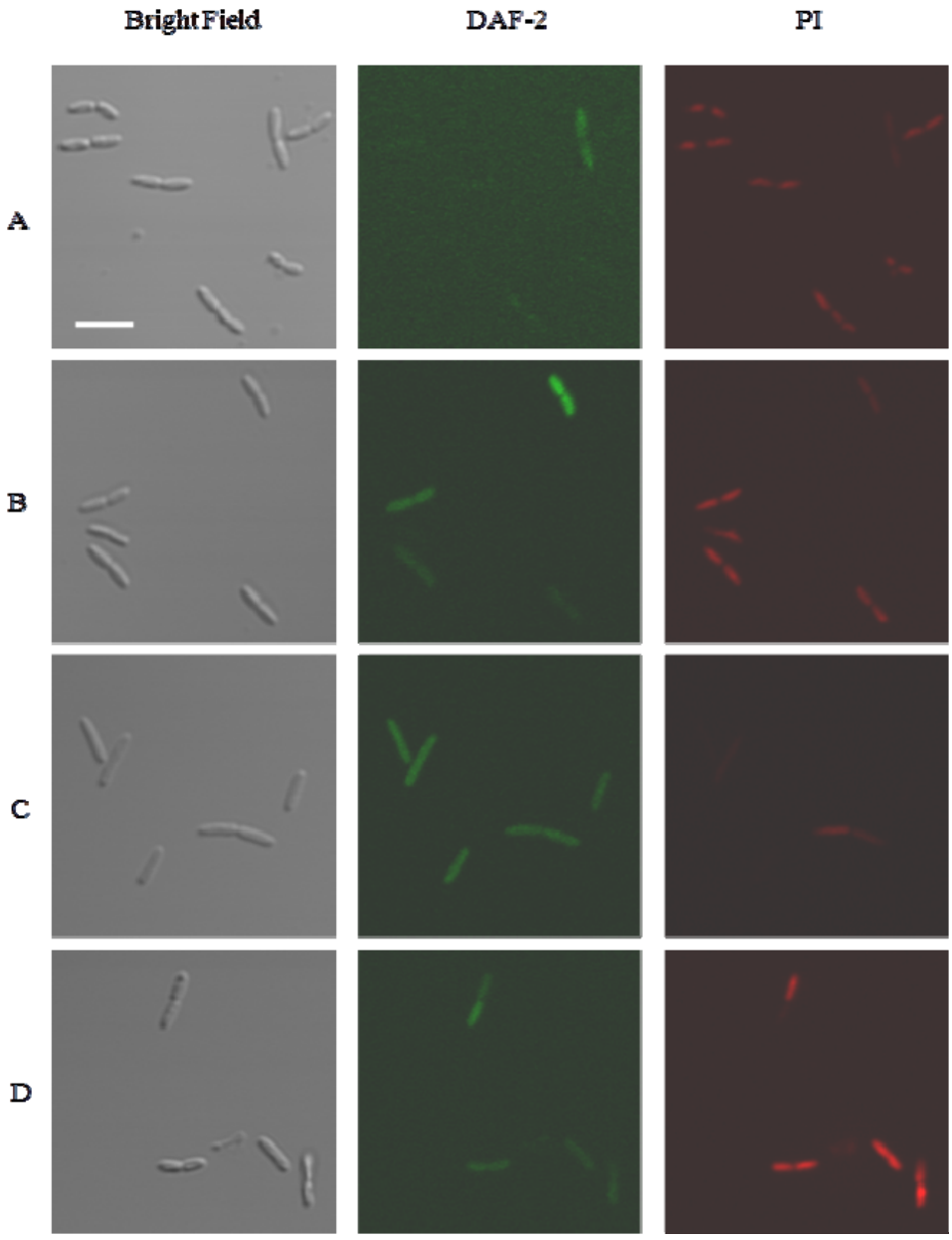

Figure 3.4. Intracellular DAF-2 (green) and PI (red) fluorescence from *P. aeruginosa* exposed to NO-releasing dendrimers at 135 min incubation A) **G1-PE 37-NO**; B) **G1-PE 55-NO**; C) **G1-PE 73-NO**; and D) **G3-PE 73-NO**. Scale bar: 5 µm.

release (**G3-PE 73-NO**) allowed for faster NO localization and biocidal action. Indeed, red fluorescence (PI) was observed at 55, 75, 135, and 70 min for **G1-PE 37-NO**, **G1-PE 55-NO**, **G1-PE 73-NO**, and **G3-PE 73-NO**, respectively. The confocal images of bacteria incubated with **G1-PE 37-NO**, **G1-PE 55-NO**, **G1-PE 73-NO**, and **G3-PE 73-NO** at 135 min were also used to compare the bactericidal activity of the dendrimers. As shown in Figure 3.4, bacteria incubated with **G1-PE 37-NO**, **G1-PE 55-NO**, and **G3-PE 73-NO** generally exhibited compromised membranes. Conversely, bacteria incubated with **G1-PE 73-NO** exhibited DAF-2 fluorescence, but without a compromise in membrane integrity (i.e., low PI fluorescence), confirming the enhanced bactericidal activity of larger generation dendrimers and those with greater exterior hydrophobicity.

3.3.3 Bactericidal Studies: Biofilm Eradication.

Although planktonic killing assays are helpful in determining a drug or antibacterial agent's potential biomedical utility, most bacteria establish biofilms as a protective mechanism against therapeutics.[1] To evaluate the effects of PO/ED ratio and dendrimer size on the anti-biofilm activity of NO-releasing amphiphilic dendrimers, *P. aeruginosa* biofilms were exposed to a range of NO-releasing dendrimer concentrations (10–800 μg/mL) for 24 h (Table 3.3). Following treatment, the biofilm was forced off of the substrate and dispersed by vortexing and sonication to enable viability quantification. Control experiments were performed to confirm both the growth of *P. aeruginosa* biofilms under the selected conditions and the negligible effect of vortexing/sonication on bacteria viability when incubated only in PBS. The viability of bacteria embedded in biofilms was ~2×10^8 CFU per biofilm. Considering the detection limit of 2,500 CFU/mL for this selected plate counting method, a maximum of 5-log reduction in bacterial

viability can be achieved. The lowest concentration for a 5-log reduction in bacterial viability (minimum bactericidal concentration or MBC) was then used to characterize the antibacterial efficacy of amphiphilic dendrimers. The bactericidal NO dose for each of the NO-releasing dendrimers was also derived by multiplying total NO release over 24 h ($t[NO]^b$) and the corresponding MBCs (Table 3.3).

Analogous to the inherent bacterial killing observed for planktonic *P. aeruginosa*, the amphiphilic control dendrimers (**G1-PE 73**, **G1-PE 55**, **G1-PE 37**, and **G1-ED**) proved more effective at killing bacterial biofilms than the hydrophilic dendrimer (**G1-PO**) due to the membrane disruption properties by amphiphilic structures. Indeed, the dendrimer MBCs for biofilm eradication (5-log killing) were 10000, 150, 30, 15, and 25 μg/mL for **G1-PO**, **G1-PE 73**, **G1-PE 55**, **G1-PE 37**, and **G1-ED**, respectively. As expected, NO release improved the bactericidal activity of the dendrimers with reduced MBCs (i.e., 800, 80, 20, 10, and 15 μg/mL for **G1-PO-NO**, **G1-PE 73-NO**, **G1-PE 55-NO**, **G1-PE 37-NO**, and **G1-ED-NO**, respectively). Of the dendrimer systems studied, **G1-PE 37-NO** exhibited the greatest anti-biofilm efficacy indicated by the lowest MBC (10 μg/mL) and corresponding bactericidal NO dose (11 nmol/mL). To evaluate the enhanced bactericidal activity of **G1-PE 37-NO** and whether it could be attributed to more rapid association with bacteria embedded within the biofilms, the association of **G1-PE 73-NO**, **G1-PE 37-NO**, and **G1-ED-NO** with bacteria in *P. aeruginosa* biofilms was characterized using confocal microscopy. As shown in Figure 3.5, a greater number of bacteria in the biofilms exhibited red fluorescence upon incubation with RITC-labeled **G1-PE 37-NO** compared to **G1-PE 73-NO**. As for planktonic bacteria, the enhanced hydrophobic interaction between the dendrimer and bacteria membrane likely facilitates more efficient

Table 3.3. Comparison of the minimum bactericidal concentration and bactericidal NO doses of control and NO-releasing dendrimers required to achieve 5-log reduction in bacteria viability of Gram-negative *P. aeruginosa* biofilms after 24 h exposure.

	MBC[a] (μg/mL)	MBC[b] (μg/mL)	Bactericidal NO Doses (nmol/mL)
G1-ED	25	15	18.5
G1-PE 37	15	10	11.0
G1-PE 55	30	20	24.6
G1-PE 73	150	80	83.2
G1-PO	10000	800	824
G3-PE 73	150	60	63.6

[a] concentration of control dendrimer required to reduce bacterial viability by 5-logs.
[b] concentration of NO-releasing dendrimer required to reduce bacterial viability by 5-logs.
Each parameter was analyzed with multiple replicates (n=3).

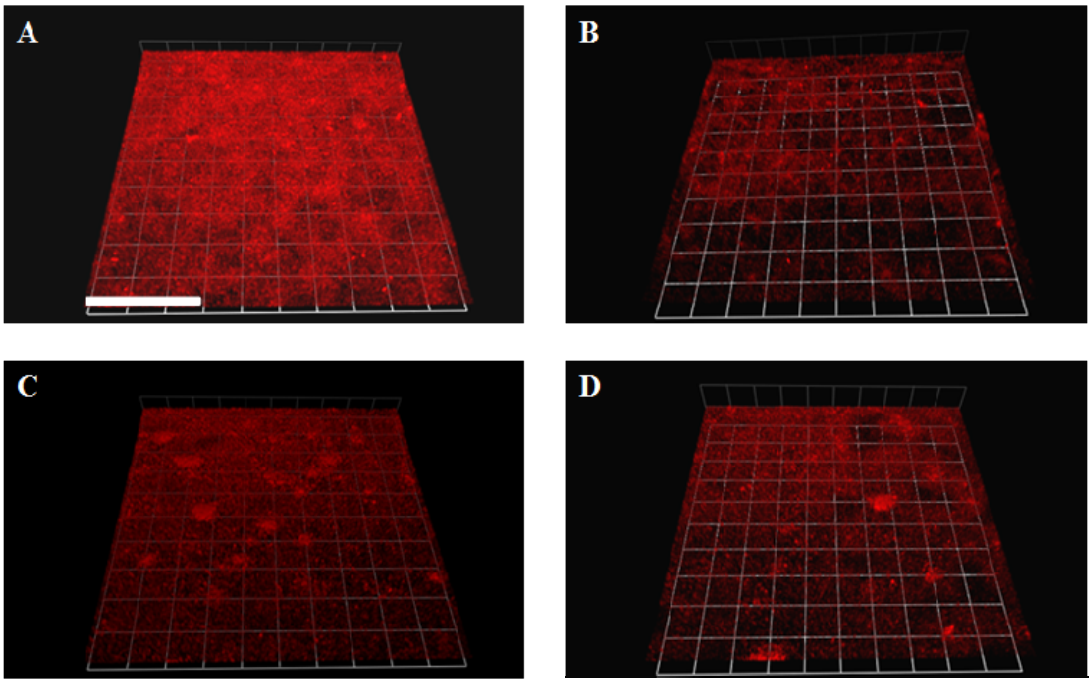

Figure 3.5. Three dimentional scanning confocal microscopy images of *P. aeruginosa* biofilms exposed to A) **G1-PE-37-NO**; B) **G1-ED-NO**; C) **G1-PE 73-NO**; and D) **G3-PE 73-NO** RITC-labeled NO-releasing dendrimers for 1 h incubation. Greater red fluorescence indicates more efficient dendrimer–bacteria association. Scale bar: 300 μm.

NO delivery and killing bacteria (e.g., membrane disruption). However, less dendrimer–bacteria association was noted for **G1-ED-NO** compared to **G1-PE 37-NO** despite the greater hydrophobicity of **G1-ED-NO**. At this stage, we associate this result to less efficient EPS penetration due to the greater hydrophobicity of **G1-ED-NO**.[38] Indeed, Wicke et al. reported the inhibited diffusion of hydrophobic organic molecules within microbial biofilms compared to hydrophilic derivatives.[38] **G1-PE 37-NO** proved to be the most effective dendrimer construct for eradicating the biofilm bacteria because of its rapid penetration into the biofilm and association with embedded bacteria.

Perhaps unexpectedly, dendrimer size (i.e., dendrimer generation) only slightly impacted the association with bacteria in the *P. aeruginosa* biofilms. Although **G3-PE 73-NO** exhibited similar association with bacteria in *P. aeruginosa* biofilms compared to **G1-PE 73-NO**, the DAF-2 fluorescence from biofilms incubated with the larger (G3) dendrimer indicated greater intracellular NO delivery. The increased NO payload and delivery from the larger generation dendrimer (**G3-PE 73-NO**) proved more bactericidal, as noted by the lower required dose to eradicate the bacteria.

3.3.4 Toxicity of NO-Releasing Dendrimers against L929 Mouse Fibroblast Cells.

Although effective at eradicating biofilms, Sun et al. previously reported that amphiphilic NO-releasing dendrimers were toxic to mammalian cells.[33] For example, polypropylenimine dendrimers modified with styrene oxide elicited substantial toxicity (i.e., >80% reduction in viability at >34 μg/mL) towards L929 mouse fibroblast cells, whereas dendrimers modified with hydrophilic PO elicited no toxicity at concentrations up to 500 μg/mL. Based on these results, we hypothesize that the ratio of hydrophobic

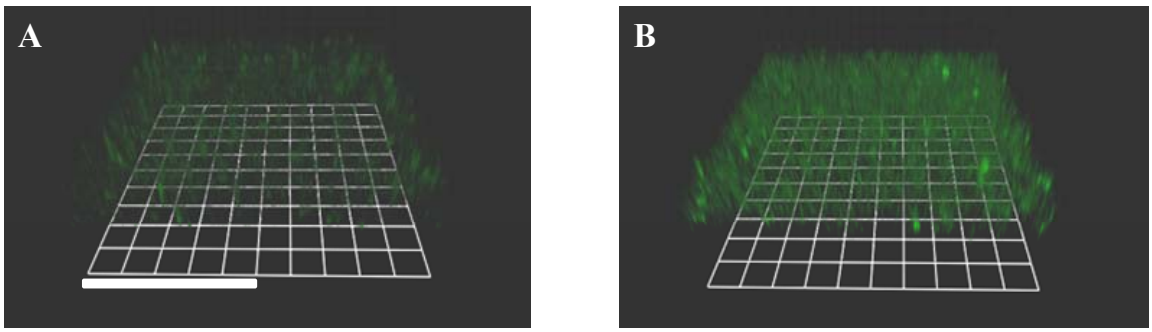

Figure 3.6. Three dimensional intracellular DAF-2 fluorescence images of *P. aeruginosa* biofilms incubated with A) **G1-** and B) **G3-PE 73-NO** for 1 h. Scale bar: 20 μm. Green fluorescence indicates the intracellular NO levels.

(ED)/hydrophilic (PO) functionalization likely influences the cytotoxicity of the amphiphilic NO-releasing dendrimers reported herein. Cytotoxicity to L929 mouse fibroblast cells was thus evaluated at the dendrimer concentrations necessary for 3- and 5-log reductions in bacteria viability against planktonic and biofilm *P. aeruginosa* bacteria, respectively, using the MTS assay (24 h incubation).

Normalized L929 mouse fibroblast cell viabilities of NO-releasing and control dendrimers at the planktonic and biofilm bacteria MBCs are shown in Figure 3.7A and 7B, respectively. In general, the NO-releasing dendrimers were less toxic than their control counterparts due to the lower concentration of NO-releasing dendrimers required for planktonic killing and biofilm eradication. As expected, dendrimers with increased hydrophobic character (e.g., **G1-ED-NO** and **G1-PE 37-NO**) exhibited greater toxicity (i.e., ~70% cell viability reduction) after 24 h incubation at the MBCs against *P. aeruginosa* biofilms, likely resulting from membrane disruption by the large density of hydrophobic chains on the dendrimer periphery. The most hydrophilic dendrimer, **G1-PO-NO**, was also toxic at its corresponding MBC (800 μg/mL) as a result of the large concentration required to eradicate the biofilm-embedded bacteria. Dendrimers with intermediate ratios of PO/ED (e.g., **G1-PE 55-NO** and **G1-PE 73-NO**) exhibited significantly lower toxicity to the mammalian cells at the MBCs required to kill the biofilm bacteria. The reduced toxicity is clearly the result of the lower concentrations of dendrimers required to deliver sufficient levels of NO and the lower ED content on the dendrimer exterior compared to **G1-ED-NO** and **G1-PE 37-NO**. Clearly, the PO/ED ratio at the dendrimer exterior had a significant impact on overall cytotoxity.

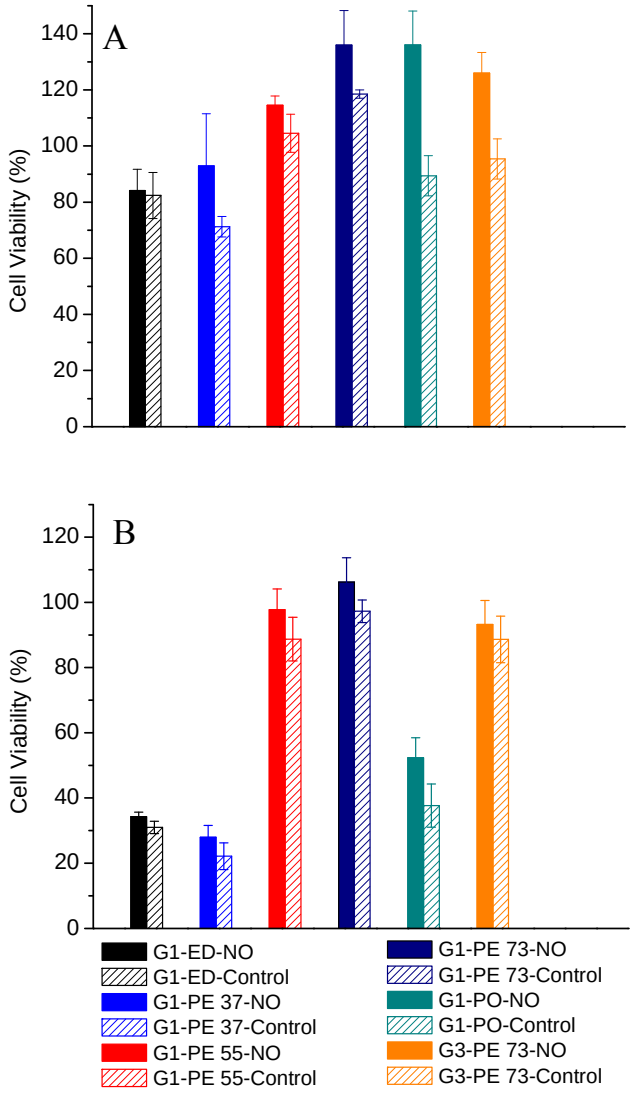

Figure 3.7. Cytotoxicity of NO-releasing dendrimers to L929 fibroblast cells at the MBCs against A) planktonic and B) biofilm-based *P. aeruginosa*.

Despite the enhanced biocidal activity against biofilms, **G1-PE 37-NO** and **G1-ED-NO** also elicited toxicity towards L929 cells as a result of the ED-induced membrane disruption properties. The larger dendrimer constructs (e.g., **G3-PE 73-NO**) were found to be slightly more toxic (~10% reduction in cell viability) to the L929 mouse fibroblast cells compared to **G1-PE 73-NO** at their respective MBCs, corroborating results by Sun et al. who reported similar generation dependent-cytotoxicity of NO-releasing dendrimers to L929 cells (larger generation being more toxic).[33] The favorable toxicity of the antibacterial **G1-PE 55-NO**, **G1-PE 73-NO**, and **G3-PE 73-NO** dendrimers over previously reported hydrophobic polypropylenimine dendrimers[33] indicate the advantage of using amphiphilic NO-releasing vehicles with intermediate exterior hydrophobicity (e.g., **G1-PE 55-NO**, **G1-PE 73-NO**) to maximize bacteria killing while minimizing toxicity to mammalian cells.

3.4 Conclusions

The utility of amphiphilic NO-releasing dendrimers as antibacterial/anti-biofilm agents was demonstrated through the systematic study of killing efficiency as a function of NO-releasing dendrimer hydrophobicity and dendrimer size (i.e., dendrimer generation). The hydrophobicity of, in particular, dendrimer surface groups were found to significantly influence dendrimer association with Gram-negative bacteria, the efficiency of intracellular NO delivery, the extent of bacteria membrane disruption, and the cytotoxicity to mammalian cells. Optimal anti-biofilm activity with minimal toxicity toward mammalian cells was achieved by modifying the dendrimer exterior with a mixture of hydrophilic (PO) and hydrophobic (ED) functionalities. Roughly equal PO/ED modification amounts proved most effectively at eradicating *P. aeruginosa* biofilms at

minimally lethal concentrations to L929 mouse fibroblast cells. Future studies should include testing of these materials against polymicrobial biofilms, biofilms formed from clinically-isolated bacteria, and detailed pharmacological toxicity testing of the NO-releasing dendrimers with human cells/tissues.

3.5 References

1. Costerton, J. W.; Stewart, P. S.; Greenberg, E. P. Bacterial biofilms: A common cause of persistent infections. *Science* **1999,** *284*, 1318-1322.

2. Nikitkova, A. E.; Haase, E. M.; Scannapieco, F. A. Taking the starch out of oral biofilm formation: molecular basis and functional significance of salivary alpha-amylase binding to oral streptococci. *Appl. Environ. Microbiol.* **2013,** *79*, 416-423.

3. Lyczak, J. B.; Cannon, C. L.; Pier, G. B. Lung infections associated with cystic fibrosis. *Clin. Microbiol. Rev.* **2002,** *15*, 194-222.

4. Mah, T. F.; O'Toole, G. A. Mechanisms of biofilm resistance to antimicrobial agents. *Trends Microbiol.* **2001,** *9*, 34-39.

5. Boas, U.; Heegaard, P. M. Dendrimers in drug research. *Chem. Soc. Rev.* **2004,** *33* , 43-63.

6. Lee, C. C.; MacKay, J. A.; Frechet, J. M.; Szoka, F. C. Designing dendrimers for biological applications. *Nat. Biotechnol.* **2005,** *23*, 1517-1526.

7. Mintzer, M. A.; Grinstaff, M. W. Biomedical applications of dendrimers: a tutorial. *Chem. Soc. Rev.* **2011,** *40*, 173-190.

8. Debrabandervandenberg, E. M. M.; Meijer, E. W. Poly(propylene imine) dendrimers - large-scale synthesis by hetereogeneously catalyzed hydrogenations. *Angew. Chem. Int. Ed.* **1993,** *32*, 1308-1311.

9. Tomalia, D. A.; Naylor, A. M.; Goddard, W. A. Starburst dendrimers - molecular-level control of size, shape, surface-chemistry, topology, and flexibility from atoms to macroscopic matter. *Angew. Chem. Int. Ed.* **1990,** *29*, 138-175.

10. Fox, M. E.; Szoka, F. C.; Frechet, J. M. J. Soluble Polymer Carriers for the Treatment of Cancer: The Importance of Molecular Architecture. *Acc. Chem. Res.* **2009,** *42*, 1141-1151.

11. Bosman, A. W.; Janssen, H. M.; Meijer, E. W. About dendrimers: Structure, physical properties, and applications. *Chem. Rev.* **1999,** *99*, 1665-1688.

12. Grayson, S. M.; Frechet, J. M. J. Convergent dendrons and dendrimers: from synthesis to applications. *Chem. Rev.* **2001,** *101*, 3819-3867.

13. Carlmark, A.; Hawker, C. J.; Hult, A.; Malkoch, M. New methodologies in the construction of dendritic materials. *Chem. Soc. Rev.* **2009,** *38*, 352-362.

14. Calabretta, M. K.; Kumar, A.; McDermott, A. M.; Cai, C. Z., Antibacterial activities of poly(amidoamine) dendrimers terminated with amino and poly(ethylene glycol) groups. *Biomacromolecules* **2007,** *8*, 1807-1811.

15. Chen, C. Z. S.; Beck-Tan, N. C.; Dhurjati, P.; van Dyk, T. K.; LaRossa, R. A.; Cooper, S. L. Quaternary ammonium functionalized poly(propylene imine) dendrimers as effective antimicrobials: Structure-activity studies. *Biomacromolecules* **2000,** *1*, 473-480.

16. Meyers, S. R.; Juhn, F. S.; Griset, A. P.; Luman, N. R.; Grinstaff, M. W., Anionic Amphiphilic Dendrimers as Antibacterial Agents. *J. Am. Chem. Soc.* **2008,** *130*, 14444-14445.

17. Lopez, A. I.; Reins, R. Y.; McDermott, A. M.; Trautner, B. W.; Cai, C. Z. Antibacterial activity and cytotoxicity of PEGylated poly(amidoamine) dendrimers. *Mol. BioSyst.* **2009,** *5*, 1148-1156.

18. Chen, C. Z. S.; Cooper, S. L. Recent advances in antimicrobial dendrimers. *Adv. Mater.* **2000,** *12*, 843-846.

19. Hou, S. Y.; Zhou, C. H.; Liu, Z. G.; Young, A. W.; Shi, Z. H.; Ren, D. C.; Kallenbach, N. R. Antimicrobial dendrimer active against Escherichia coli biofilms. *Bioorg. Med. Chem. Lett.* **2009,** *19*, 5478-5481.

20. Reymond, J. L.; Darbre, T. Peptide and glycopeptide dendrimer apple trees as enzyme models and for biomedical applications. *Org. Biomol. Chem.* **2012,** *10*, 1483-1492.

21. Johansson, E. M. V.; Crusz, S. A.; Kolomiets, E.; Buts, L.; Kadam, R. U.; Cacciarini, M.; Bartels, K. M.; Diggle, S. P.; Camara, M.; Williams, P.; Loris, R.; Nativi, C.; Rosenau, F.; Jaeger, K. E.; Darbre, T.; Reymond, J. L. Inhibition and Dispersion of Pseudomonas aeruginosa Biofilms by Glycopeptide Dendrimers Targeting the Fucose-Specific Lectin LecB. *Chem. Biol.* **2008,** *15*, 1249-1257.

22. Hong, S. P.; Bielinska, A. U.; Mecke, A.; Keszler, B.; Beals, J. L.; Shi, X. Y.; Balogh, L.; Orr, B. G.; Baker, J. R.; Holl, M. M. B. Interaction of poly(amidoamine) dendrimers with supported lipid bilayers and cells: Hole formation and the relation to transport. *Bioconj. Chem.* **2004,** *15*, 774-782.

23. Wang, B.; Navath, R. S.; Menjoge, A. R.; Balakrishnan, B.; Bellair, R.; Dai, H.; Romero, R.; Kannan, S.; Kannan, R. M., Inhibition of bacterial growth and intramniotic infection in a guinea pig model of chorioamnionitis using PAMAM dendrimers. *Int. J. Pharm.* **2010,** *395*, 298-308.

24. Marletta, M. A.; Tayeh, M. A.; Hevel, J. M. Unraveling the biological significance of nitric oxide. *Biofactors* **1990,** *2*, 219-225.

25. MacMicking, J.; Xie, Q. W.; Nathan, C. Nitric oxide and macrophage function. *Annu. Rev. Immunol.* **1997,** *15*, 323-350.

26. Fang, F. C. Perspectives series: host/pathogen interactions. Mechanisms of nitric oxide-related antimicrobial activity. *J. Clin. Invest.* **1997,** *99*, 2818-2825.

27. Lu, Y.; Sun, B.; Li, C.; Schoenfisch, M. H. Structurally diverse nitric oxide-releasing poly(propylene Imine) dendrimers. *Chem. Mater.* **2011,** *23*, 4227-4233.

28. Riccio, D. A.; Nugent, J. L.; Schoenfisch, M. H. Stober synthesis of nitric oxide-releasing S-nitrosothiol-modified silica particles. *Chem. Mater.* **2011,** *23*, 1727-1735.

29. Stasko, N. A.; Schoenfisch, M. H., Dendrimers as a scaffold for nitric oxide release. *J. Am. Chem. Soc.* **2006,** *128*, 8265-8271.

30. Shin, J. H.; Metzger, S. K.; Schoenfisch, M. H. Synthesis of nitric oxide-releasing silica nanoparticles. *J. Am. Chem. Soc.* **2007,** *129*, 4612-4619.

31. Rothrock, A. R.; Donkers, R. L.; Schoenfisch, M. H. Synthesis of nitric oxide-releasing gold nanoparticles. *J. Am. Chem. Soc.* **2005,** *127*, 9362-9363.

32. Carpenter, A. W.; Slomberg, D. L.; Rao, K. S.; Schoenfisch, M. H. Influence of scaffold size on bactericidal activity of nitric oxide-releasing silica nanoparticles. *ACS Nano* **2012,** *5*, 7235-7244.

33. Sun, B.; Slomberg, D. L.; Chudasama, S. L.; Lu, Y.; Schoenfisch, M. H. Nitric oxide-releasing dendrimers as antibacterial agents. *Biomacromolecules* **2012,** *13*, 3343-3354.

34. Hetrick, E. M.; Shin, J. H.; Paul, H. S.; Schoenfisch, M. H. Anti-biofilm efficacy of nitric oxide-releasing silica nanoparticles. *Biomaterials* **2009,** *30*, 2782-2789.

35. Hetrick, E. M.; Shin, J. H.; Stasko, N. A.; Johnson, C. B.; Wespe, D. A.; Holmuhamedov, E.; Schoenfisch, M. H. Bactericidal efficacy of nitric oxide-releasing silica nanoparticles. *ACS Nano* **2008,** *2*, 235-246.

36. van 't Hof, W.; Veerman, E. C. I.; Helmerhorst, E. J.; Amerongen, A. V. N., Antimicrobial peptides: Properties and applicability. *Biol. Chem.* **2001,** *382*, 597-619.

37. Denyer, S. P., Mechanisms of action of antibacterial biocides. *Int. Biodeter. Biodegr.* **1995,** *36*, 227-245.

38. Wicke, D.; Bockelmann, U.; Reemtsma, T., Environmental influences on the partitioning and diffusion of hydrophobic organic contaminants in microbial Biofilms. *Environ. Sci. Technol.* **2008,** *42*, 1990-1996.

Chapter 4

Shape- and Nitric Oxide-Flux Dependent Bactericidal Activity of Nitric Oxide-Releasing Silica Nanorods

4.1 Introduction

Nitric oxide (NO), a diatomic free radical produced endogenously by macrophages and other inflammatory cells, plays a key role in the natural immune response to pathogens.[1-3] NO-releasing materials have been widely used in different biomedical applications. [4-9] Both NO and its reactive byproducts (e.g., peroxynitrite and dinitrogen trioxide) exert significant oxidative and nitrosative stress on bacterial cells to facilitate their killing.[1-3] Nitrosative stress acts to nitrosate thiols influencing protein and DNA function, while lipid peroxidation via oxidative stress destroys the bacterial membrane integrity.[3] Methods for delivering exogenous NO are thus actively being developed against both Gram–positive and Gram–negative bacteria.[10-12] While gaseous NO from a cylinder and NO delivered from small molecule NO donors have proven to be antimicrobial,[11, 13] macromolecular scaffolds are more potent due to their ability to deliver large localized concentrations of NO.[11, 12] Indeed, we have previously reported the ability to achieve larger NO payloads and improved bactericidal efficacy using NO-releasing dendrimers and silica particles, relative to small molecule NO donors.[11, 14, 15] To date, the bacterial toxicity of NO-releasing particles has been shown to be dependent on chemical composition, NO-release kinetics and particle size.[16] For example, the bactericidal activity of NO-releasing silica particles correlated directly with particle size,

with the smallest particles tested (i.e., 50 nm) exhibiting the greatest antibacterial efficacy.[16]

Given the dependence of bactericidal efficacy on the physicochemical properties of NO-releasing particles, we hypothesized that particle shape might influence particle-bacteria interactions and potentially the biocidal activity. Recent work on particle design for drug delivery to mammalian cells indicated the importance of particle shape on particle-cell adhesion strength, internalization rate, biodistribution, cytotoxicity, phagocytosis and circulation time. [17-31] In particular, rod-like nanoparticles have been shown to significantly influence mammalian cell internalization and circulation time compared to their spherical or cubic counterparts.[23-27] Herein, we describe the synthesis and evaluation of the bactericidal efficacy of NO-releasing silica nanorods (SNRs) of ~1–8 aspect ratios but similar size (e.g., particle volume) against Gram–negative and –positive bacteria.

4.2 Experimental section

4.2.1 Materials.

Tetraethyl orthosilicate (TEOS), *N*-(2-aminoethyl)-3-amino-isobutyl-dimethyl-methoxysilane (AEAI), aminopropyldimethylethoxysilane (APDE) and 3-aminopropyltrimethoxysilane (APTMS) were purchased from Gelest (Morrisville, PA). Cetyltrimethylammonium bromide (CTAB) was obtained from Acros Organics (Geel, Belgium). Rhodamine B isothiocyanate (RITC), poly(ethylene glycol) methyl ether acrylate (average M_n = 480) (PEG), propidium iodide (PI), fetal bovine serum (FBS), Dulbecco's Modified Eagle's Medium (DMEM), phenazine methosulfate (PMS), 3-(4,5-

dimethylthiazol-2-yl)-5-(3-carboxymethoxyphenyl)-2-(4-sulfophenyl)-2H-tetrazolium inner salt (MTS), trypsin, phosphate buffered saline (PBS) used for cell culture, and penicillin streptomycin (PS) were purchased from the Aldrich Chemical Company (Milwaukee, WI). *Pseudomonas aeruginosa* (ATCC #19143) and *Staphylococcus aureus* (ATCC# 29231) were obtained from the American Type Culture Collection (Manassas, VA). L929 mouse fibroblasts (ATCC #CCL-1) were purchased from the University of North Carolina Tissue Culture Facility (Chapel Hill, NC). Distilled water was purified with a Millipore Milli-Q Gradient A-10 water purification system (Bedford, MA). 4,5-Diaminofluorescein diacetate (DAF-2 DA) was purchased from Calbiochem (San Diego, CA). Common laboratory salts and solvents were purchased from Fisher Scientific (Pittsburgh, PA). All materials were used as received without further purification unless noted otherwise.

4.2.2 Surfactant-Templated Synthesis of Silica Nanorods.

The silica nanorods (SNRs) were synthesized via a surfactant-templated method and tuning the aspect ratio by varying temperature, ammonia concentration, and solution volume (Table 4.1). In a representative synthesis, 0.11 mL tetraethyl orthosilicate (TEOS) was added to a solution of 0.29 g cetyltrimethylammonium bromide (CTAB) in 50 mL of 0.5 M ammonia at 50 ^{o}C. A subsequent addition of TEOS (0.60 mL) was added after 5 h of stirring, followed by aging for 24 h at 50 ^{o}C. The resulting SNRs were collected by centrifugation and washed twice with 50 mL of ethanol, recollected via centrifugation, and dried under vacuum at ambient temperature. To remove the CTAB templates, the SNRs were resuspended in a mixture of ethanol and concentrated HCl (9:1; v/v) and stirred at 60 ^{o}C for 24 h. Finally, the particles were re-collected by centrifugation and

washed twice with ethanol before drying under vacuum at ambient temperature. Complete removal of CTAB was confirmed by CHN elemental analysis.

4.2.3 Preparation of Nitric Oxide-Releasing Silica Nanorods with Functionality c.

A suspension of 50 mg SNRs and 0.5 mL AEAI in 10 mL anhydrous THF was refluxed under nitrogen overnight. The resulting amine-functionalized SNRs **a** were collected by centrifugation, washed twice with ethanol and dried under vacuum at ambient temperature. Elemental analysis (CHN) was performed to determine the amount of aminoalkoxysilane anchored onto the surface of the SNRs. To modify the SNRs for NO release, 15 mg AEAI-functionalized SNRs (**a**) were resuspended in a mixture of 2.7 mL anhydrous DMF and 0.3 mL methanol and 50 μL of 5.4M NaOMe/MeOH. The suspension was added to vials in a Parr hydrogenation vessel, purged rapidly (5–10 s) with argon three times, and then three longer cycles (10 min) of argon purges to remove residual oxygen from the solution. The Parr hydrogenation vessel was then filled with 10 atm of NO gas purified over KOH pellets to remove any impurities (NO degradation products) and maintained at 10 atm for 3 d. The same argon purging protocol was performed to remove unbound NO prior to removing the vials from the vessel. The SNRs were recollected by centrifugation, washed twice with anhydrous ethanol, dried under vacuum and stored at -20 ^{o}C until future use.

4.2.4 Preparation of Nitric Oxide-Releasing Nanosilica Rods with Functionality d.

Aminopropyldimethylethoxysilane (APDE)-functionalized SNRs were synthesized as described previously for SNRs **a** by simply replacing AEAI with APDE. Subsequently, poly(ethylene glycol) methyl ether acrylate (PEG) was added to a suspension of APDE-functionalized SNRs in ethanol with equimolar PEG corresponding to the amine content

of the SNRs. After stirring at room temperature for 2 d, the PEG-modified SNRs (**b**) were collected by centrifugation, washed twice with anhydrous ethanol and dried at ambient temperature. The resulting secondary-amine functionalized SNRs **b** were modified with NO in the same manner described above.

4.2.5 Characterization of Functionalized Nanosilica Rods.

Scanning electron micrographs were recorded with a Hitachi S-4700 scanning electron microscope (Pleasanton, CA) to determine size and aspect ratios of the SNRs. Elemental (CHN) analysis was performed using a PerkinElmer CHN/S O Elemental Analyzer Series 2400 (Waltham, MA) instrument to quantify the amine content of each SNR, that would be proportional to the aminosilane surface coverage. The zeta potential of the silica particles was determined using a Zetasizer Nano ZS (Malvern, U.K.). Samples (~1 mg/mL) were prepared in phosphate buffer (10 mM, pH = 7.4) and immediately injected into a folded capillary cell for zeta potential analysis. Nitric oxide release was measured using a Sievers 280i Chemiluminescence Nitric Oxide Analyzer (Boulder, CO) by adding NO-releasing SNRs to deoxygenated PBS (pH = 7.4 and 37 ^{o}C). Nitrogen was purged through the solution to carry liberated NO to the analyzer at a flow rate of 70 mL/min. Additional nitrogen flow was supplied to match the collection rate of the analyzer at 200 mL/min. Real-time NO release profiles were recorded, allowing for the determination of NO release totals (t[NO]), half-lives ($t_{1/2}$), and maximum NO fluxes ($[NO]_{max}$). For surface area measurement, N_2 adsorption-desorption isotherms were obtained on a Micromeritics Tristar II analyzer. The BET model was applied to evaluate the specific surface areas and the Barret-Joyner-Halenda (BJH) method was used to calculate the pore volume.

4.2.6 Bactericidal Assays.

Cultures of *P. aeruginosa* and *S. aureus* were prepared as described previously.[6] Briefly, bacterial cultures were grown from a frozen (-80 ^{o}C) stock overnight in TSB at 37 ^{o}C. A 100 μL aliquot of the resulting suspension was added into 5 mL fresh TSB and incubated at 37 ^{o}C for ~2 h until the concentration reached 1×10^{8} colony forming units (CFU)/mL, as confirmed by the OD_{600} and replicate plating and enumeration on nutrient agar. A working bacterial stock was prepared by plating the bacterial suspension on TSA and incubating at 37 ^{o}C overnight. The TSA bacterial stocks were prepared weekly and stored at 4 ^{o}C. For bactericidal assays, colonies of *P. aeruginosa* and *S. aureus* were taken from the TSA plate and dispersed in 3 mL TSB and then incubation at 37 ^{o}C overnight. A 100 μL aliquot of culture was added to 5 mL fresh TSB and incubated to a concentration of ~1×10^{8} CFU/mL. The bacteria was collected by centrifugation and resuspended in 3 mL PBS or 1% (v/v) tryptic soy broth (TSB)-supplemented PBS. The resulting suspension was diluted 100-fold in PBS or 1% TSB-supplemented PBS to obtain a final concentration of 1×10^{6} CFU/mL. The bactericidal efficacy of NO-releasing SNRs against the bacteria was evaluated after 4 h incubation over a range of concentrations. Bacteria suspensions in PBS or 1% (v/v) TSB-supplemented PBS were added to premeasured NO-releasing silica nanorods and incubated at 37 ^{o}C for 4 h. Following incubation, 100 μL aliquots of the bacteria suspensions were removed, diluted 10-fold in PBS, deposited on TSA plates, and incubated overnight at 37 ^{o}C. The minimum concentration of NO-releasing SNRs that resulted in a 3-log reduction of bacterial viability after 4 h exposure was defined as the minimum bactericidal concentration (MBC).

4.2.7 In Vitro Toxicity.

L929 mouse fibroblasts were grown in DMEM supplemented with 10% (v/v) fetal bovine serum (FBS) and 1 wt% penicillin/streptomycin, and incubated in 5% (v/v) CO_2 under humidified conditions at 37 ^{o}C. After reaching 80% confluency, the cells were trypsinized, seeded onto tissue-culture treated polystyrene 96-well plates at a density of 3×10^4 cells/mL and incubated at 37 ^{o}C for 48 h. The supernatant was then aspirated prior to adding 200 μL fresh DMEM and 50 μL of a NO-releasing SNR suspension in PBS to each well. After incubation at 37 ^{o}C for 24 h, the supernatant was aspirated and 120 μL mixture of DMEM/MTS/PMS (105/20/1, v/v/v) was added to each well. The absorbance of the resulting colored solution after 1.5 h incubation at 37 ^{o}C was quantified at 490 nm using a Thermoscientific Multiskan EX plate reader. The mixture of DMEM/MTS/PMS and untreated cells were used as blank and control, respectively. The cell viability was calculated by equation 4.1.

$$\text{Cell Viability} = \frac{(\text{Absorbance}_{\text{treated cell}} - \text{Absorbance}_{\text{blank}})}{(\text{Absorbance}_{\text{untreated cell}} - \text{Absorbance}_{\text{blank}})} \qquad \text{Eq. 4.1}$$

4.2.8 Confocal Microscopy for Detection of Intracellular Nitric Oxide.

Bacteria (*P. aeruginosa* and *S. aureus*) were cultured in TSB to a concentration of 1×10^8 CFU/mL, collected via centrifugation ($3645 \times g$ for 10 min), resuspended in sterile PBS, and adjusted to 1×10^6 CFU/mL in PBS supplemented with 10 μM DAF-2 DA and 30 μM PI. The bacteria solution (2.5 mL) was incubated in a glass bottom confocal dish for 45 min at 37 °C. A Zeiss 510 Meta inverted laser scanning confocal microscope with a 488 nm Ar excitation laser (2.0%) and a BP 505–530 nm filter was used to obtain DAF-2 (green) fluorescence images. Red fluorescence images for PI were obtained using a 543

nm HeNe excitation laser (25.3%) with a BP 560–615 nm filter. The bright field and fluorescence images were collected using a N.A. 1.2 C-apochromat water immersion lens with a 40× objective. Suspensions (1.5 mL) of **AR1-c** or **AR8-c** NO-releasing silica nanorods (44 μg/mL) in PBS (supplemented with 10 μM DAF-2 DA and 30 μM PI) were added to the bacteria solution (1.5 mL) in the glass confocal dish. Images were collected every 5 min to observe intracellular NO concentrations and cell death.

4.2.9 Synthesis of Fluorescently Labeled Silica Nanorods.

Rhodamine B isothiocyanate (RITC, 1.52 mg) and 3-aminopropyltrimethoxysilane (ATPMS, 0.5 mL) were dissolved in 0.5 mL ethanol and stirred for 2 d to form RITC-APTMS. A mixture of TEOS and RITC-APTMS (100:1) was used in a typical surfactant-templated synthesis to form RITC-modified SNRs. The resulting fluorescently labeled SNRs were subjected to the same washing and CTAB removal protocols as non-labeled SNRs.

4.2.10 Confocal Microscopy for Association of Particles with Bacteria Cells.

P. aeruginosa was cultured in TSB to a concentration of 1×10^8 CFU/mL, collected *via* centrifugation (3645 × *g* for 10 min), resuspended in sterile PBS, and adjusted to 1×10^6 CFU/mL. Aliquots of the bacteria solution were incubated in a glass bottom confocal dish for 2 h at 37 °C. A Zeiss 510 Meta inverted laser scanning confocal microscope with a 543 nm HeNe excitation laser (80% intensity) and a LP 585 nm filter was used to obtain fluorescence images of the RITC-modified dendrimers. The bright field and fluorescence images were collected using a N.A. 1.2 C-apochromat water immersion lens with a 20× objective. Solutions of RITC-labeled NO-releasing (200 μg/mL) particles in PBS (1.5 mL) were added to the bacteria solution (1.5 mL) in the glass confocal dish to

achieve a final concentration of 100 μg/mL. Images were collected every 2 min to monitor association of the particles with *P. aerugionsa* temporally.

4.3 Results and Discussion

Surfactant-templated synthesis of silica materials were first developed by Mobil Oil Corporation.[32] To date, both acidic[33, 34] and alkaline[32, 35, 36] routes have been used to synthesize these silica materials.[37-41] According to a mechanism proposed by Stucky and coworkers,[33, 34, 42] mesophase formation arises from the multidentate binding of silicate species to surfactant micelle interfaces *via* electrostatic interactions. The resulting liquid crystal phases self-assemble by charge density matching across the interface and continuously grow end to end or side to side through accretion into well-formed particles.[43] Ozin suggested that any defects in the liquid crystal seeds direct the formation of specific particle morphologies (e.g., spirals, toroids, discoids or worm-like particles).[44] In addition, reaction conditions may be tuned to purposefully induce different particle morphology.[43] For example, Sokolov demonstrated control over the aspect ratio of micron-sized silica rods synthesized under acidic condition by adjusting silane concentration and pH.[43] Following the above reports, we synthesized silica rods with different aspect ratios (1.1–9.4) under alkaline conditions by varying the temperature and concentration of ammonia and silane.

4.3.1 Aspect Ratios (AR) and Sizes Control of Silica Particles.

As reported by Sokolov and coworkers, the aspect ratio of our silica rods also increased with reaction temperature.[43] As shown in Figure 4.1 and Table 4.1, the observed particle morphology revealed a positive correlation between reaction temperature and SNR aspect ratio. For example, synthesis at 20 ^{o}C yielded particles with

a AR of ~4.5 (**SNR A**) while 30 and 50 ^{o}C resulted in particles with increased AR of ~8.0 (**SNR B**) and ~9.4 (**SNR C**), respectively. Temperature also proved to affect the morphology of the SNRs. In contrast to **SNR A** and **B**, **SNR C** exhibited more twisted and curved morphology that has been previously attributed to defects in the liquid crystal seeds.[44] The thermal energy available at increased reaction temperature likely allows for greater defect stabilization in the liquid crystal, leading to the formation of twisted and curved silica rods.

Although the aspect ratio of the silica rods proved tunable via reaction temperature, the aspect ratio of the resulting particles was large (e.g., >4) for silane and ammonia concentrations of 64.0 mM and 0.5 M, respectively. To further adjust the aspect ratio, we also evaluated the role of pH and total silane concentration on particle morphology. Due to the influence of electrostatic interactions between the surfactant molecules and the silica species on silica rod formation,[45] we hypothesized varying the reaction pH would alter rod morphology. Indeed, the use of more ammonia (1 M) resulted in SNRs with an aspect ratio of ~1.23 (**SNR D**), attributable to the cooperative assembly of surfactant and silica species. At high pH, the formation of silica oligomers that vary in degree of polymerization and charge represent more efficient multidentate ligands for the cationic surfactant molecules, and thus result in stronger interaction between the two species.[45] The ensuing multidentate binding contributes to preferential side-to-side growth of liquid crystals and a lower aspect ratio.

Table 4.1 Influence of reaction temperature, pH, and concentration of silane on the size and aspect ratio of silica nanorods.

Rod	T (^{o}C)	TEOS (mM)	CTAB (mM)	Ammonia (M)	Length (nm)	Width (nm)	AR
SNR A	20	64.0	16.0	0.5	757 ± 42	168 ± 36	4.5 ± 0.9
SNR B	30	64.0	16.0	0.5	1120 ± 69	140 ± 34	8.0 ± 1.0
SNR C	50	64.0	16.0	0.5	1077 ± 105	115 ± 15	9.4 ± 0.7
SNR D	20	64.0	16.0	1.0	671 ± 102	543 ± 106	1.2 ± 0.5
SNR E	20	32.0	8.0	1.0	302 ± 35	280 ± 26	1.1 ± 0.1
SNR F	50	42.7	10.7	0.5	241 ± 32	78 ± 6	3.1 ± 0.3

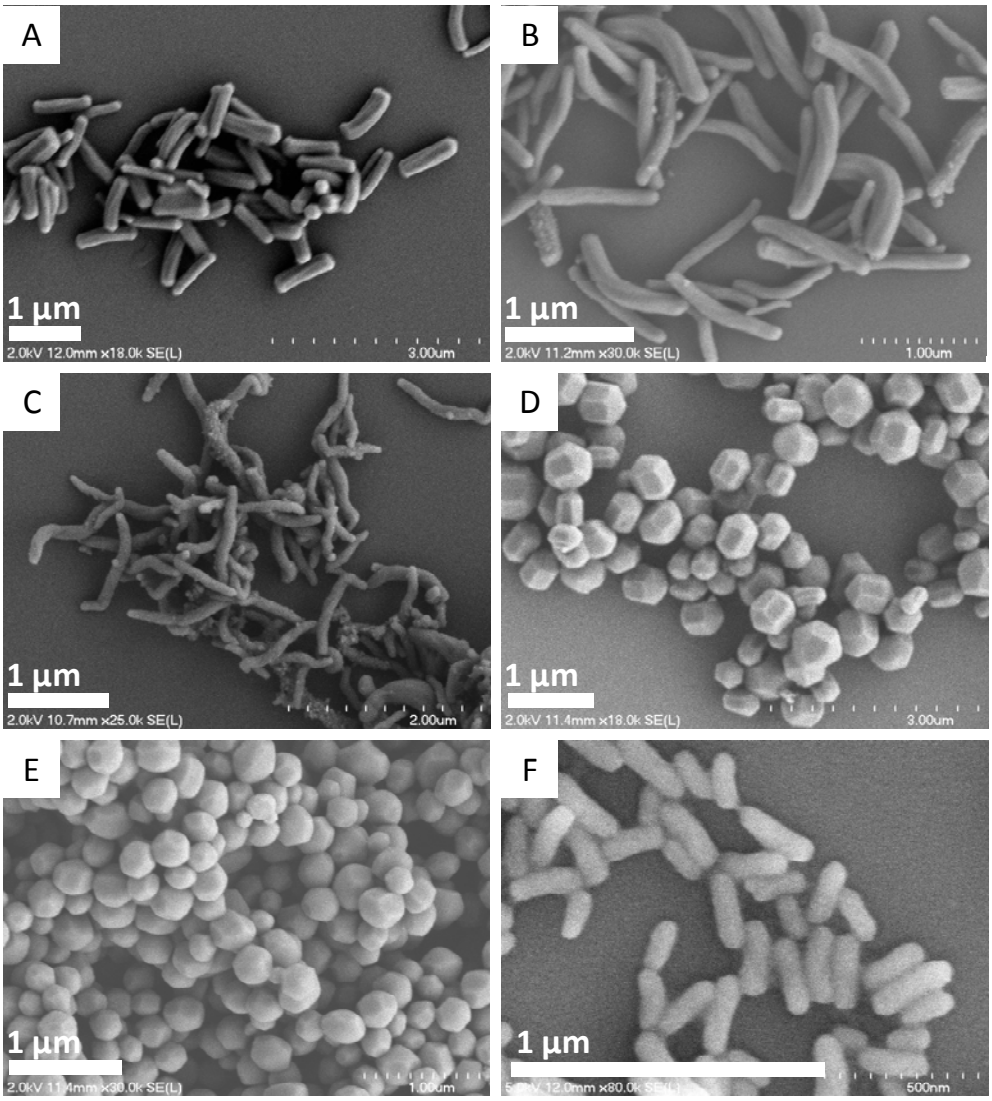

Figure 4.1 Scanning electron microscopy (SEM) images of silica nanorods with different morphologies. Aspect ratios of these particles were 4.5 ± 0.9 (A), 8.0 ± 1.0 (B), 9.4 ± 0.7 (C), 1.2 ± 0.5 (D), 1.1 ± 0.1 (E), and 3.1 ± 0.3 (F), respectively.

Both the size and aspect ratio of SNRs were also adjustable as a function of silane concentration. Decreasing the silane concentration from 64.0 mM (**SNR D**) to 32.0 mM yielded particles (**SNR E**) of smaller size (~0.02 μm^3) and aspect ratio (1.10).

A similar trend also observed between **SNR C** (aspect ratio of 9.4) and **SNR F** (aspect ratio of 3.1). Collectively, SNRs of a wide range of aspect ratios (~1–10) and volumes (~0.02 and 0.19 μm^3) were synthesized by tuning temperature, pH, and silane concentration. **SNRs E**, **A**, and **B** were selected to study the role of aspect ratio on bactericidal activity due to their similar particle size (e.g., particle volume ~0.02 μm^3), yet distinct aspect ratios (i.e., 1.1, 4.5, and 8.0).

4.3.2 Synthesis of Diazeniumdiolate-Functionalized Silica Nanorods.

Following SNR synthesis, the materials were functionalized with polyamine ligands to enable subsequent NO donor formation (Scheme 4.1). The environment surrounding *N*-diazeniumdiolate NO donors can greatly influence NO-release kinetics particularly if manipulating water uptake and local pH.[15] Two distinct secondary amine functionalities were employed in this work to allow study of SNR NO-release kinetics on bactericidal activity. Monoalkoxysilanes (i.e., *N*-(2-aminoethyl)-3-amino-isobutyl-dimethyl-methoxysilane (AEAI) and aminopropyldimethylethoxysilane (APDE)) were anchored onto the surface of **SNR E**, **A**, and **B**, denoted as **AR1**, **AR4**, and **AR8**, following a previously published modification procedure.[46] Aminopropyldimethylethoxysilane (APDE)-functionalized rods containing only primary amines were further functionalized with acrylate-functionalized PEG, resulting in the formation of secondary amines (Scheme 4.1).[15] Varied NO-release kinetics were expected from these two functionalities, as the degradation of *N*-diazeniumdiolate NO donors is related to the protonation of the

polyamine that binds the NO. We hypothesized that more rapid water uptake/hydration by hydrophilic PEG chains on the surface of APDE-PEG functionalized SNRs would lead to faster *N*-diazeniumdiolate decomposition and NO release (i.e., higher $[NO]_{max}$ and shorter $t_{1/2}$).[15] Elemental analysis (Table 4.2) was used to determine the secondary amine content for **AR1-a**, **AR4-a**, **AR8-a**, **AR4-b**.

As shown in Scheme 4.1, **AR1-a**, **AR4-a**, **AR8-a**, **AR4-b** were reacted or "charged" with NO at high pressures in methanol under basic conditions to form *N*-diazeniumdiolate-functionalized nanorods (i.e., **AR1-c**, **AR4-c**, **AR8-c**, **AR4-d)**. Next, chemiluminescence was used to characterize the NO storage and release properties of the *N*-diazeniumdiolate-modified SNRs (i.e., **AR1-c**, **AR4-c**, **AR8-c**, **AR4-d**) in PBS (pH 7.4, 37 °C). As shown in Table 4.3, the NO release totals and half-lives for **AR1-c**, **AR4-c**, and **AR8-c** were analogous (~0.70 μmol/mg and ~0.70 h, respectively) even though the porosity was different for these three particles (e.g., the pore volume for **AR1-c**, **AR4-c** and **AR8-c** was 3.3×10^{-3}, 4.3×10^{-3}, and 1.4×10^{-1} cm^3/g, respectively). In contrast, **AR4-d** had lower NO storage and a shorter half-life due to less secondary amine content (See Table 4.2). Nevertheless, the secondary amine-to-diazeniumdiolate conversion efficiency was similar (~20%) regardless of precursor concentration. Similar NO donor conversion values were previously reported for *N*-diazeniumdiolated-modified dendrimers.[15] The NO release profile of **AR4-d** showed the greatest initial flux (i.e., $[NO]_{max}$ ~14000 ppb/mg) and fastest decay (i.e., $t_{1/2}$=0.16 h), due to greater water uptake facilitated by the hydrophilic PEG groups. The distinct NO-release kinetics between **AR4-c** and **AR4-d** SNRs could thus be used to study NO flux-dependent bactericidal activity in addition to nanorod aspect ratio.

Scheme 4.1 Synthesis of secondary amine- (functionalities a and b) control and *N*-diazeniumdiolate-functionalized (functionalities c and d) silica nanorods.

Table 4.2 Elemental analysis and zeta potential characterization of the secondary amine-functionalized silica nanorods.

	C (%)	H (%)	N (%)	2^{o}-amine content (μmol/mg)	Zeta Potential (mV)
AR1-a	23.99 ± 1.41	5.38 ± 0.27	6.07 ± 0.18	2.19 ± 0.06	34.1 ± 1.6
AR4-a	23.16 ± 3.38	5.22 ± 1.20	5.77 ± 1.40	1.74 ± 0.42	35.2 ± 3.6
AR8-a	25.23 ± 5.50	5.47 ± 1.07	6.21 ± 1.22	2.43 ± 0.47	38.4 ± 1.2
AR4-b	18.80 ± 1.24	4.04 ± 0.45	2.14 ± 0.22	1.53 ± 0.16	-8.1 ± 0.9

Table 4.3 Nitric oxide-release properties and surface charge (i.e., zeta potential) of *N*-diazeniumdiolate NO donor-functionalized SNRs.

	t[NO]^{a} (μmol/mg)	**t[NO]^{b} (μmol/mg)**	**$[NO]_{max}$ (ppb/mg)**	**$t_{1/2}$ (h)**	**Zeta Potential (mV)**
AR1-c	0.76 ± 0.12	0.63 ± 0.07	5400 ± 1100	0.77 ± 0.10	-18.9 ± 0.7
AR4-c	0.69 ± 0.09	0.59 ± 0.07	5000 ± 800	0.70 ± 0.09	-17.1 ± 0.9
AR8-c	0.77 ± 0.13	0.64 ± 0.09	5380 ± 700	0.76 ± 0.10	-15.3 ± 0.4
AR4-d	0.36 ± 0.04	0.27 ± 0.03	14000 ± 1200	0.16 ± 0.01	-20.8 ± 0.6

[a] total NO storage per milligram particles. [b] total NO released after 4 h per milligram particles.

4.3.3 Bactericidal Activity as a function of SNR Aspect Ratio.

Since the porosity of **AR1-c**, **AR4-c**, and **AR8-c** did not affect the NO-release kinetics of the nanorods, the direct comparison of **AR1-c**, **AR4-c**, and **AR8-c** allows for the study of how particle aspect ratio affects bactericidal activity. Bacteria killing assays were evaluated in nutrient-free ("static") solutions with *P. aeruginosa*, a Gram–negative pathogen involved in burn and chronic wound infections.[47-49] The minimum bactericidal concentration (MBC) reported represents the lowest dose of NO-releasing SNRs resulting in a 3 log reduction in bacteria viability after 4 h exposure. The corresponding dose of NO released from the SNRs over the 4 h is provided in Figure 4.2B.

As shown in Figure 4.2, particles of higher aspect ratio killed bacteria at lower concentrations than lower-aspect ratio particles. For example, the MBCs for **AR1-c**, **AR4-c**, and **AR8-c** were 500, 250, and 150 μg/mL, respectively. The NO dose required to achieve a 3 log reduction in bacteria viability for **AR8-c** was ~0.10 μmol/mL, lower than that of **AR1-c** (~0.32 μmol/mL) or **AR4-c** (~0.15 μmol/mL). Given that NO-releasing silica particles associate with bacteria (Figure 4.3), the enhanced activity of **AR8-c** against *P. aeruginosa* may be attributed to greater contact area between the particle and the bacteria membrane, resulting in a greater NO dose delivered to the membrane.[11] Confocal microscopy was used to confirm the greater NO delivery by **AR8-c** to the bacteria using 4,5-diaminofluorescein diacetate (DAF-2 DA), an intracellular NO sensitive dye. Briefly, the membrane-permeable DAF2-DA is hydrolyzed to the impermeable form, 4,5-diaminofluorescein (DAF-2), by intracellular esterases. In the presence of oxygen and NO, DAF-2 is converted to the green fluorescent derivative, triazolofluorescein.[11]

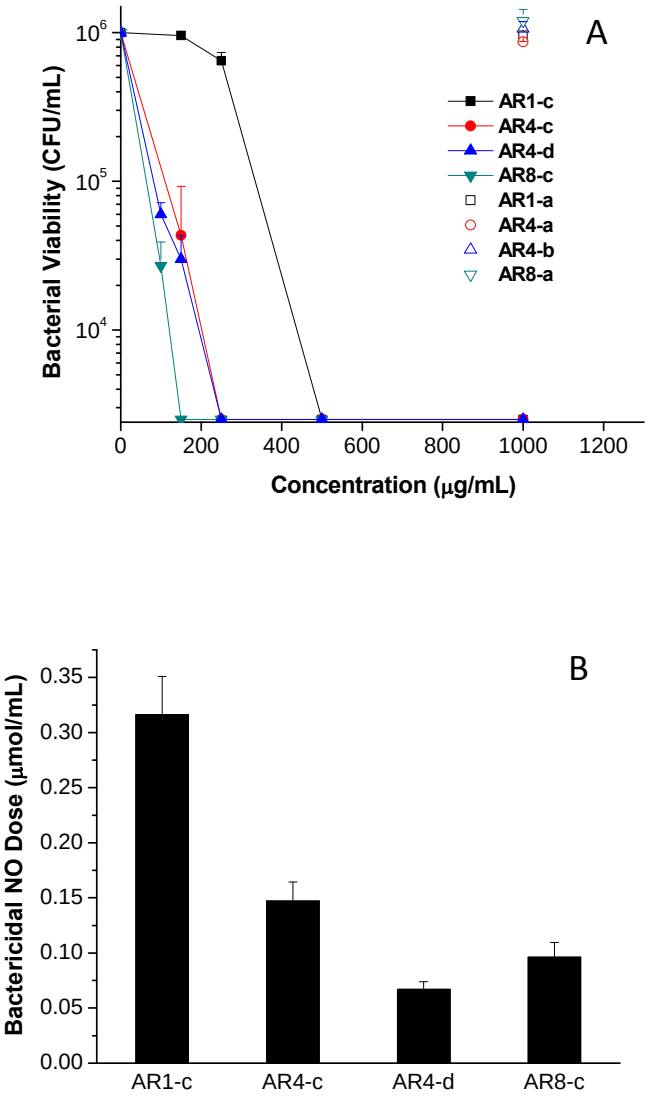

Figure 4.2 *P. aeruginosa* viability (in PBS) as a function of particle (A) and bactericidal NO (B) doses using the NO-releasing (solid symbols) SNRs. Control particles (open symbols) did not impact bacteria viability at SNR concentrations up to 1000 μg/mL, the maximum concentration tested.

As shown in Figure 4.4, the intracellular NO delivered from **AR8-c** was observed at 95 min via DAF-2 fluorescence (Figure 4.4E), ~25 min earlier than bacteria incubated with **AR1-c** (Figure 4.4B). At 125 min, a greater number of bacteria incubated with **AR8-c** exhibited DAF-2 fluorescence compared to those incubated with **AR1-c** (Figure 4.5). When bacteria were incubated with **AR8-c** for 125 min, over half of the bacteria exhibited green DAF-2 fluorescence indicating the presence of intracellular NO. The NO delivered from **AR8-c** also resulted in cell death at 125 min. However, only one bacterium exhibited green fluorescence from intracellular NO after exposure to **AR1-c** and cell death was not observed. The greater fluorescence intensity from bacteria incubated with **AR8-c** indicated larger intracellular NO concentrations (Figure 4.4F). As described previously by Fang,[3] some of NO's antibacterial action is the result of NO reacting with superoxide, a product of bacteria respiration, to form peroxynitrite, a potent oxidative species that induces lipid peroxidation. The delivery of larger NO payloads to bacteria (e.g., by **AR8-c**) would accordingly lead to increased bactericidal activity. As expected, the corresponding secondary amine-functionalized control particles (**AR1-a**, **AR4-a**, **AR8-a** depleted of NO) exhibited no killing of *P. aeruginosa* at the MBCs of their NO-releasing counterparts (e.g., **AR1-c**, **AR4-c**, **AR8-c**).

4.3.4 Influence of Nitric Oxide-Release Kinetics.

In addition to studying shape-dependence, we sought to understand the influence of SNR NO-release kinetics on bactericidal activity. **AR4-d** and **AR4-c** SNRs with distinct NO-release profiles were thus exposed to *P. aeruginosa*. As shown in Figure 4.6, **AR4-d** displayed greater initial NO flux ($[NO]_{max}$ ~14000 ppb/mg) and faster decay ($t_{1/2}$ =0.16 h) due to the PEG modification and faster *N*-diazeniumdiolate breakdown.

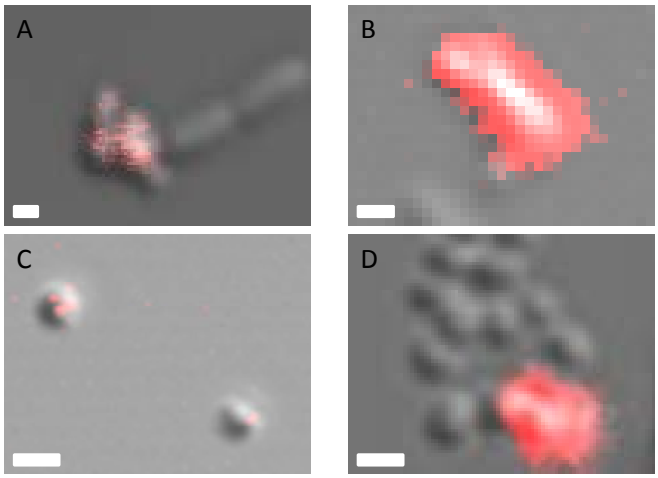

Figure 4.3 Association of fluorescently-labeled particles with bacteria. (A) AR1 with *P. aeruginosa*; (B) AR8 with *P. aeruginosa*; (C) AR1 with *S. aureus*; (D) AR8 with *S. aureus*.

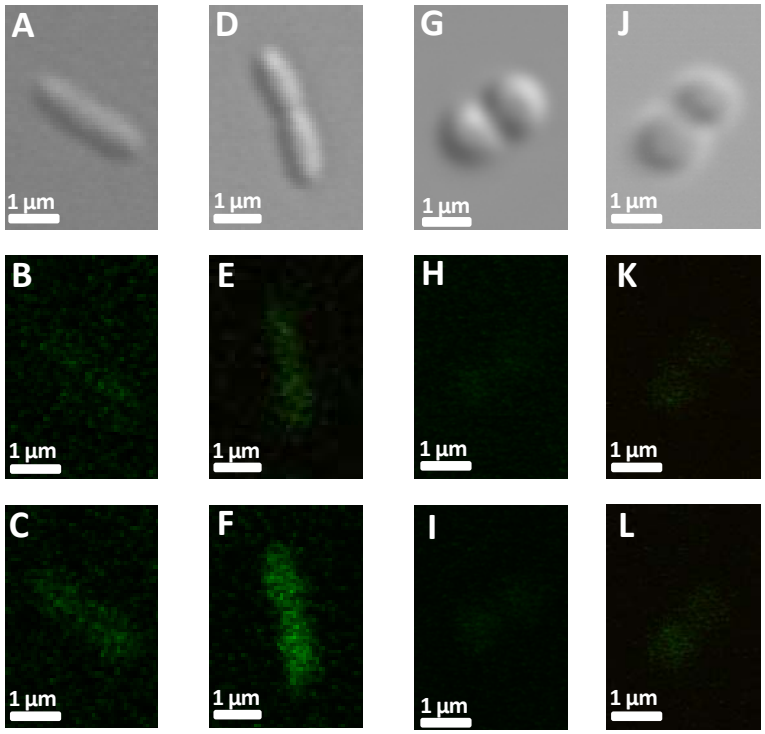

Figure 4.4 Intracellular DAF-2 fluorescence from *P. aeruginosa* bacterial cells incubated with 22 µg/mL AR1-c (Bright field (A), 120 min (B), 125 min (C)) and AR8-c (Bright field (D), 95 min (E), 100 min (F)) and from *S. aureus* bacterial cells incubated with AR1-c (Bright field (G), 135 min (H), 155 min (I)) AR8-c (Bright field (J), 100 min (K), 130 min (L)). Intensity of DAF-2 fluorescence indicates the intracellular concentration of NO and reactive nitrogen species.

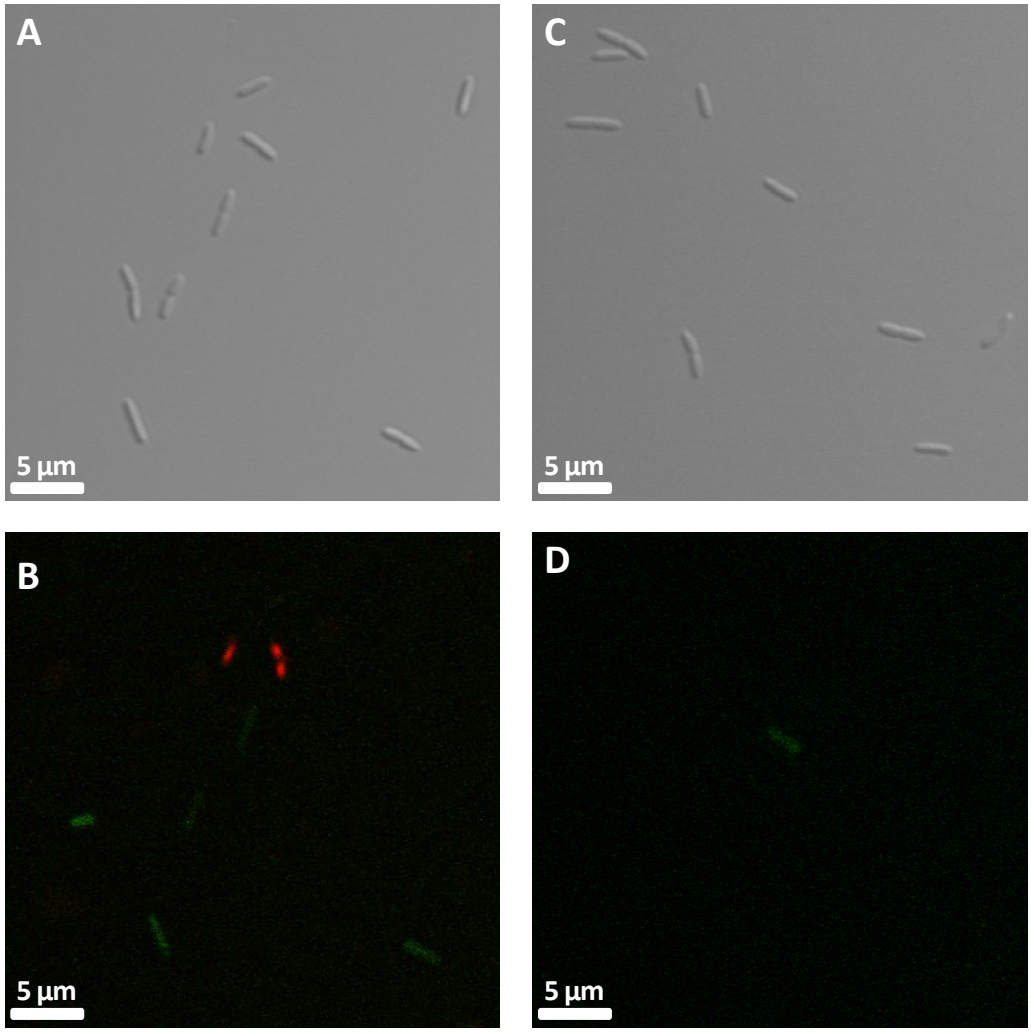

Figure 4.5 Bright field (A, C) and overlay images of intracellular DAF-2 (green) and PI (red) fluorescence from *P. aeruginosa* cells incubated with 22 µg/mL AR8-c (B) and AR1-c (D) for 125 min. DAF-2 fluorescence indicates the presence of NO and reactive nitrogen species, while PI fluorescence indicates membrane destruction and cell death.

Bacteria killing assays against *P. aeruginosa* indicated that the bactericidal NO dose for **AR4-d** was approximately half that for **AR4-c** (~0.07 vs ~0.15 μmol/ml, respectively), suggesting that greater initial NO flux is favorable for killing *P. aeruginosa*. However, the total NO storage (e.g., t[NO]) for **AR4-c** was also greater than **AR4-d**. To rule out possible influence of NO release total, SNRs with similar t[NO] to **AR4-d** were prepared but with different $[NO]_{max}$, denoted as **AR4-c***. As reported by Carpenter et al.,[16] the total NO storage from a *N*-diazeniumdiolate macromolecule scaffold is easily tuned by altering the concentration of sodium methoxide. In this study, reduced amounts of sodium methoxide (25 μL of 5.4 M sodium methoxide in methanol per 15 mg **AR4-a** particles) were used to prepare **AR4-c***, thus matching the total NO storage of **AR4-d** (~0.27 μmol/mg).

Since the resulting $[NO]_{max}$ for **AR4-c*** (~2000 ppb/mg) was substantially lower than that of **AR4-d** (~14000 ppb/mg), the comparison between **AR4-d** and **AR4-c*** revealed the effect of NO flux on killing efficacy. As expected, the MBC for **AR4-c*** in a 4 h bacteria killing assay against *P. aeruginosa* was 4 mg/mL, substantially greater than that for **AR4-d** (0.25 mg/mL), illustrating the significance of a large initial NO flux (e.g., $[NO]_{max}$) for killing this bacterium.

4.3.5 Bactericidal Assays Against S. aureus.

In contrast to *P. aeruginosa*, *S. aureus* is a Gram–positive bacteria with a thicker peptidoglycan layer and spherical morphology.[50] Privett et al. previously reported that NO produced from small molecule NO donors (e.g., 1-[2-(carboxylato)pyrrolidin-1-yl]diazen-1-ium-1,2-diolate (PROLI/NO)) was less effective at killing *S. aureus* compared to *P. aeruginosa*.[12]

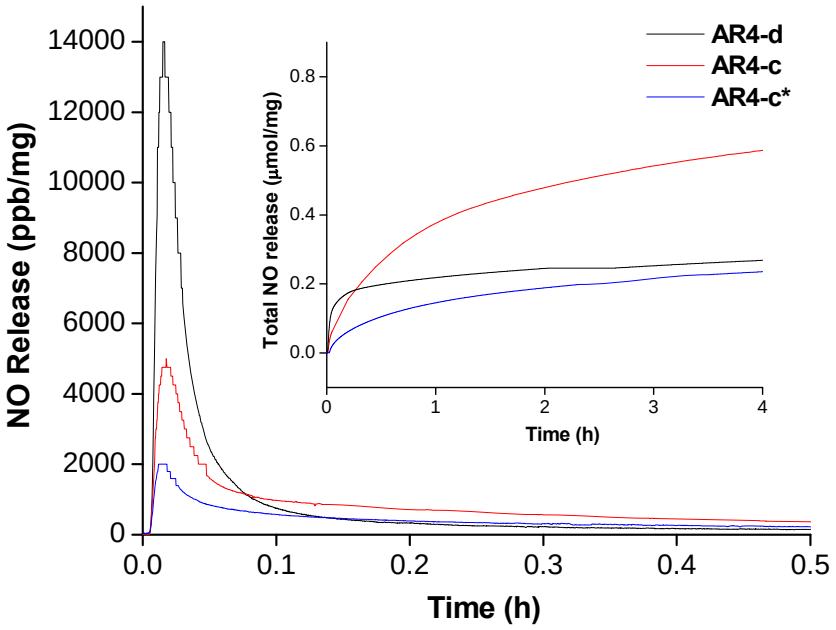

Figure 4.6 Nitric oxide-release profiles for AEAI (c)- and APDE-PEG (d)-functionalized AR4 silica nanorods. Inset: total NO release of AR4-c, AR4-c* and AR4-d as a function of time.

A working hypothesis describing this phenomenon involves the thicker peptidoglycan layer decreasing NO diffusion to the inside of the bacterium. In this regard, high-aspect ratio SNRs may improve the bactericidal activity of the silica-based NO-releasing scaffolds against *S. aureus* by delivering NO more efficiently due to their shape.

As shown in Figure 4.7, the MBCs for **AR1-c**, **AR4-c**, and **AR8-c** against *S. aureus* were 2000, 1000, and 300 μg/mL, respectively, greater than that against *P. aeruginosa*. We hypothesize that this behavior may be the result of decreased NO diffusion into the bacterium due to the more substantial (i.e., thicker) peptidoglycan layer for *S. aureus*. Confocal microscopy was used to characterize the NO diffusion to the inside of *P. aeruginosa* and *S. aureus* cells by monitoring the intracellular NO concentration as a function of time. As shown in Figure 4.4, intracellular NO was observed more quickly for *P. aeruginosa* (Figure 4.4E) than *S. aureus* (Figure 4.4K). Furthermore, the intracellular NO levels for *S. aureus* did not change between 110 (Figure 4.4K) and 130 min (Figure 4.4L) indicating slower NO diffusion.

Analogous to *P. aeruginosa*, **AR8-c** also delivered NO into the *S. aureus* cells more rapidly than **AR1-c**. As shown in Figure 4.4, DAF-2 fluorescence appeared at 110 min (Figure 4.4K) compared to 135 min for **AR1-c** (Figure 4.4H). As such, the **AR8-c** exhibited the greatest bactericidal activity. Overall, a more dramatic shape dependence of MBCs was observed against *S. aureus*, illustrating the influence of greater NO doses from high-aspect ratio particles (Figure 4.4). As expected, the comparison between **AR4-c** and **AR4-d** again reinforced the benefits of greater initial NO flux on bactericidal activity. Compared to PROLI/NO,[12] each of the NO-releasing SNRs studied exhibited enhanced bactericidal activity against *S. aureus*. The bactericidal NO doses against *S.*

aureus for **AR1-c** and **AR4-c** were 1.264 and 0.586 μmol/mL, respectively, roughly four times greater than that against *P. aeruginosa*. For **AR8-c** and **AR4-d**, the bactericidal NO doses against *S. aureus* were 0.191 and 0.134 μmol/mL, only twice that against *P. aeruginosa*. These results suggest that the more effective NO delivery (e.g., greater NO dose and flux) to the bacterium from NO-releasing SNRs may compensate for the lower bactericidal action of NO against Gram–positive *S. aureus*.

4.3.6 Bactericidal Assays in Protein (Nutrient)-Containing Medium.

To confirm the efficacy of the NO-releasing silica rods in a protein-containing media, *P. aeruginosa* killing assays were conducted in PBS supplemented with 1% (v/v) trypsin soy broth (TSB) nutrient-containing medium.[51] After 4 h incubation, the bacteria viability in 1% (v/v) TSB supplemented PBS in the absence of silica rods was ~10^6 CFU/mL. In contrast, the MBCs for **AR1-c** and **AR8-c** were 250 and 750 μg/mL, respectively, demonstrating the shape-dependent bactericidal action of NO-releasing silica rods in the protein- and nutrient-containing medium. Of note, greater concentrations of particles (e.g., **AR1-c** and **AR8-c**) were required to achieve 3-log killing under nutrient-supplemented condition (e.g., 1% v/v TSB supplemented PBS). As we reported previously, this behavior is attributed to NO scavenging by proteins.[11]

4.3.7 Mammalian Cell Cytotoxicity of Nitric Oxide.

MTS assays were performed against L929 mouse fibroblasts over 24 h to evaluate the toxicity of the NO-releasing SNRs at the MBCs from the bactericidal assays. Particle concentrations were selected from 150 to 2000 μg/mL to encompass the bactericidal concentrations of the NO-releasing SNRs in PBS.

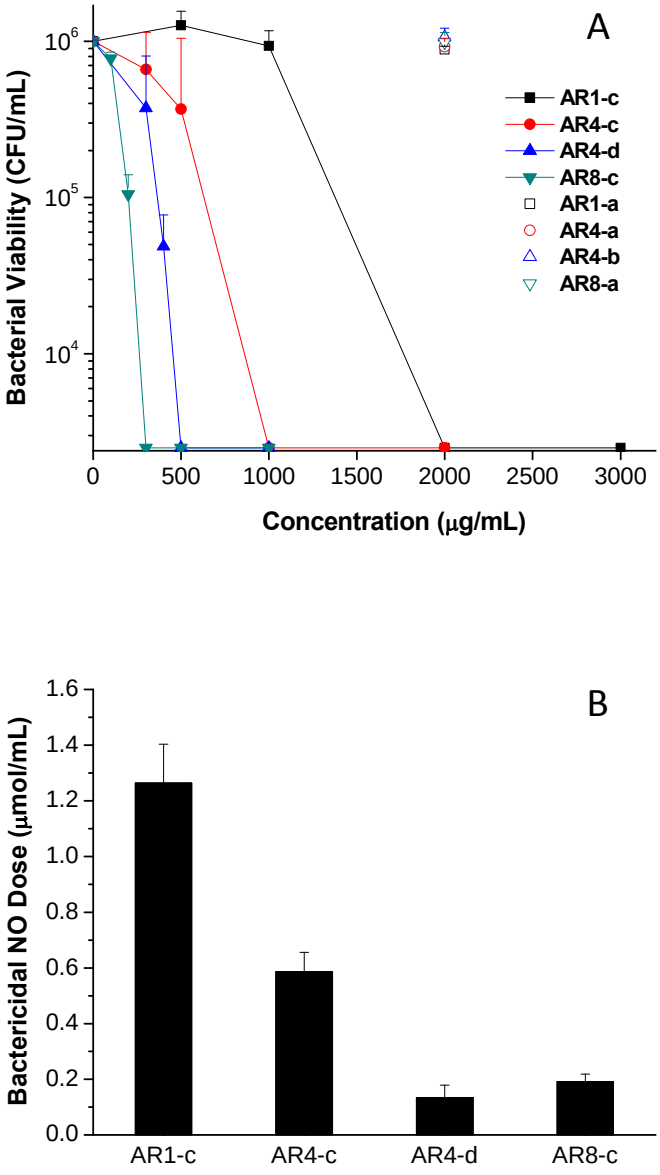

Figure 4.7 *S. aureus* viability (in PBS) as a function of particle (A) and bactericidal NO (B) doses using the NO-releasing (solid symbols) SNRs. Control particles (open symbols) did not impact bacteria viability at SNR concentrations up to 2000 μg/mL, the maximum concentration tested.

The normalized cell viabilities after 24 h as a function of particle concentration are shown in Figure 4.8. Nitric oxide-releasing SNRs (i.e., **AR1-c**, **AR4-c**, **AR8-c**, **AR4-d**) were not toxic at concentrations < 500 μg/mL, while toxicity was observed at 1000 and 2000 μg/mL. Further inspection of the cytotoxicity and bactericidal assay results revealed that **AR8-c** and **AR4-d** were nontoxic at the MBCs against both *P. aeruginosa* and *S. aureus*. Although **AR1-c** and **AR4-c** were also nontoxic at the *P. aeruginosa* MBCs, reduced L929 cell viability was observed at the *S. aureus* MBCs. MTS assays were also used to assess the cytotoxicity of secondary-amine functionalized control particles. As shown in Figure 4.8B, control particles also exhibited cytotoxicity at 1000 and 2000 μg/mL, explaining the toxicity of the NO-releasing SNRs. Collectively, the cytotoxicity results reinforce the advantage of **AR4-d** (e.g., high initial NO flux) and **AR8-c** (e.g., large aspect ratio) as antibacterial agents relative to **AR4-c** and **AR1-c** SNRs.

4.4 Conclusions

The bactericidal activity of NO-releasing silica nanorods against Gram–negative (*P. aeruginosa*) and –positive (*S. aureus*) bacteria appear to depend on both the NO flux and particle morphology. For example, we found that significantly less NO is required to kill bacteria from NO-releasing silica nanorods with higher aspect ratio or greater NO flux due to more efficient NO delivery to the bacterium. Regardless of morphology or NO flux, the NO-releasing silica nanorods were nontoxic to L929 mouse fibroblast cells at bactericidal concentration against *P. aeruginosa*. In contrast, high aspect ratio (e.g., 8) NO-releasing SNRs were necessary to eradicate *S. aureus* at non-cytotoxic concentrations to L929 fibroblasts, demonstrating the variance in bactericidal efficacy and toxicity.

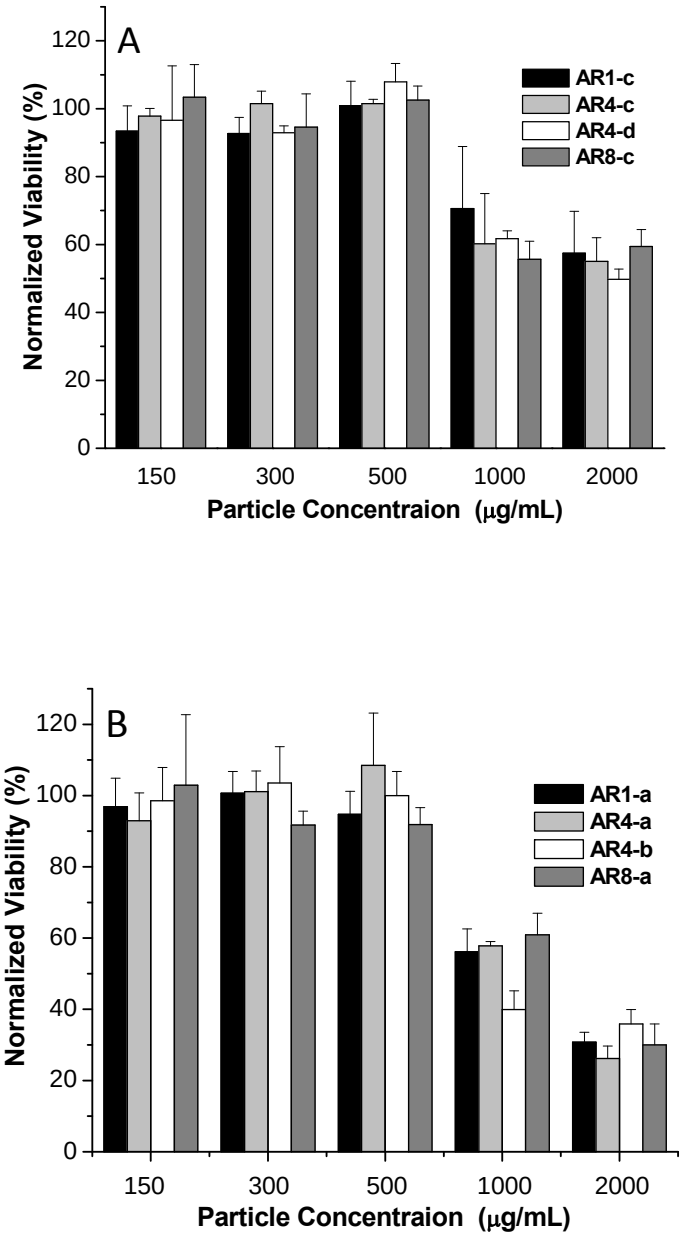

Figure 4.8 Cytotoxicity of NO-releasing (A) and control (B) SNRs to L929 mouse fibroblasts.

Of note, effective killing was nevertheless achievable at nontoxic (mammalian cells) concentrations. Future studies will evaluate the antibacterial efficacy of these particles in different biological media as NO scavenging by proteins and cells may require more NO delivery to achieve similar results. Antibiofilm efficacy studies should also be carried out as >99% of all bacteria live in biofilm communities that offer protection against antimicrobial agents.[52]

4.5 References

1. Marletta, M. A.; Tayeh, M. A.; Hevel, J. M. Unraveling the biological significance of nitric oxide. *Biofactors* **1990,** *2*, 219-225.

2. MacMicking, J.; Xie, Q. W.; Nathan, C. Nitric oxide and macrophage function. *Annu. Rev. Immunol.* **1997,** *15*, 323-350.

3. Fang, F. C. Mechanisms of nitric oxide-related antimicrobial activity. *J. Clin. Invest.* **1997,** *99*, 2818-2825.

4. Nichols, S. P.; Storm, W. L.; Koh, A.; Schoenfisch, M. H. Local delivery of nitric oxide: Targeted delivery of therapeutics to bone and connective tissues. *Adv. Drug Deliv. Rev.* **2012**, *64*, 1177-1188.

5. Carpenter, A. W.; Schoenfisch, M. H. Nitric oxide release: part II. Therapeutic applications. *Chem. Soc. Rev.* **2012**, *41*, 3742-3752.

6. Coneski, P. N.; Schoenfisch, M. H. Nitric oxide release: part III. Measurement and reporting. *Chem. Soc. Rev.* **2012**, *41*, 3753-3758.

7. Riccio, D. A.; Schoenfisch, M. H. Nitric oxide release: part I. Macromolecular scaffolds. *Chem. Soc. Rev.* **2012**, *41*, 3731-3741.

8. Hetrick, E. M.; Schoenfisch, M. H. Analytical chemistry of nitric oxide. *Annu. Rev. Anal. Chem. (Palo Alto Calif)* **2009,** *2*, 409-433.

9. Hetrick, E. M.; Schoenfisch, M. H. Reducing implant-related infections: active release strategies. *Chem. Soc. Rev.* **2006,** *35*, 780-789.

10. Ghaffari, A.; Miller, C. C.; McMullin, B.; Ghahary, A. Potential application of gaseous nitric oxide as a topical antimicrobial agent. *Nitric Oxide-Biol. Chem.* **2006,** *14*, 21-29.

11. Hetrick, E. M.; Shin, J. H.; Stasko, N. A.; Johnson, C. B.; Wespe, D. A.; Holmuhamedov, E.; Schoenfisch, M. H. Bactericidal efficacy of nitric oxide-releasing silica nanoparticles. *ACS Nano* **2008,** *2*, 235-246.

12. Privett, B. J.; Deupree, S. M.; Backlund, C. J.; Rao, K. S.; Johnson, C. B.; Coneski, P. N.; Schoenfisch, M. H. Synergy of Nitric Oxide and Silver Sulfadiazine against Gram-Negative, Gram-Positive, and Antibiotic-Resistant Pathogens. *Mol. Pharm.* **2010,** *7*, 2289-2296.

13. McMullin, B. B.; Chittock, D. R.; Roscoe, D. L.; Garcha, H.; Wang, L.; Miller, C. C. The antimicrobial effect of nitric oxide on the bacteria that cause nosocomial pneumonia in mechanically ventilated patients in the intensive care unit. *Respir. Care* **2005,** *50*, 1451-1456.

14. Shin, J. H.; Metzger, S. K.; Schoenfisch, M. H. Synthesis of nitric oxide-releasing silica nanoparticles. *J. Am. Chem. Soc.* **2007,** *129*, 4612-4619.

15. Lu, Y.; Sun, B.; Li, C. H.; Schoenfisch, M. H. Structurally Diverse Nitric Oxide-Releasing Poly(propylene imine) Dendrimers. *Chem. Mater.* **2011,** *23*, 4227-4233.

16. Carpenter, A. W.; Slomberg, D. L.; Rao, K. S.; Schoenfisch, M. H. Influence of Scaffold Size on Bactericidal Activity of Nitric Oxide-Releasing Silica Nanoparticles. *ACS Nano* **2011,** *5*, 7235-7244.

17. Decuzzi, P.; Pasqualini, R.; Arap, W.; Ferrari, M. Intravascular Delivery of Particulate Systems: Does Geometry Really Matter? *Pharm. Res.* **2009,** *26*, 235-243.

18. Champion, J. A.; Katare, Y. K.; Mitragotri, S. Making polymeric micro- and nanoparticles of complex shapes. *Proc. Natl. Acad. Sci. U. S. A.* **2007,** *104*, 11901-11904.

19. Petros, R. A.; DeSimone, J. M. Strategies in the design of nanoparticles for therapeutic applications. *Nat. Rev. Drug Discovery* **2010,** *9*, 615-627.

20. Wong, J.; Brugger, A.; Khare, A.; Chaubal, M.; Papadopoulos, P.; Rabinow, B.; Kipp, J.; Ning, J. Suspensions for intravenous (IV) injection: A review of development, preclinical and clinical aspects. *Adv. Drug Delivery Rev.* **2008,** *60*, 939-954.

21. Huang, X. L.; Li, L. L.; Liu, T. L.; Hao, N. J.; Liu, H. Y.; Chen, D.; Tang, F. Q. The Shape Effect of Mesoporous Silica Nanoparticles on Biodistribution, Clearance, and Biocompatibility in Vivo. *ACS Nano* **2011,** *5*, 5390-5399.

22. Yu, T.; Malugin, A.; Ghandehari, H. Impact of Silica Nanoparticle Design on Cellular Toxicity and Hemolytic Activity. *ACS Nano* **2011,** *5*, 5717-5728.

23. Gratton, S. E. A.; Ropp, P. A.; Pohlhaus, P. D.; Luft, J. C.; Madden, V. J.; Napier, M. E.; DeSimone, J. M. The effect of particle design on cellular internalization pathways. *Proc. Natl. Acad. Sci. U. S. A.* **2008,** *105*, 11613-11618.

24. Huang, X. L.; Teng, X.; Chen, D.; Tang, F. Q.; He, J. Q. The effect of the shape of mesoporous silica nanoparticles on cellular uptake and cell function. *Biomaterials* **2010,** *31*, 438-448.

25. Meng, H.; Yang, S.; Li, Z. X.; Xia, T.; Chen, J.; Ji, Z. X.; Zhang, H. Y.; Wang, X.; Lin, S. J.; Huang, C.; Zhou, Z. H.; Zink, J. I.; Nel, A. E. Aspect Ratio Determines the Quantity of Mesoporous Silica Nanoparticle Uptake by a Small GTPase-Dependent Macropinocytosis Mechanism. *ACS Nano* **2011,** *5*, 4434-4447.

26. Kolhar, P.; Doshi, N.; Mitragotri, S. Polymer Nanoneedle-Mediated Intracellular Drug Delivery. *Small* **2011,** *7*, 2094-2100.

27. Yoo, J. W.; Doshi, N.; Mitragotri, S. Endocytosis and Intracellular Distribution of PLGA Particles in Endothelial Cells: Effect of Particle Geometry. *Macromol. Rapid Commun.* **2010,** *31*, 142-148.

28. Qiu, Y.; Liu, Y.; Wang, L. M.; Xu, L. G.; Bai, R.; Ji, Y. L.; Wu, X. C.; Zhao, Y. L.; Li, Y. F.; Chen, C. Y. Surface chemistry and aspect ratio mediated cellular uptake of Au nanorods. *Biomaterials* **2010,** *31*, 7606-7619.

29. Champion, J. A.; Katare, Y. K.; Mitragotri, S. Particle shape: A new design parameter for micro- and nanoscale drug delivery carriers. *J. Controlled Release* **2007,** *121*, 3-9.

30. Geng, Y.; Dalhaimer, P.; Cai, S. S.; Tsai, R.; Tewari, M.; Minko, T.; Discher, D. E. Shape effects of filaments versus spherical particles in flow and drug delivery. *Nat. Nanotechnol.* **2007,** *2*, 249-255.

31. Yu, T.; Greish, K.; McGill, L. D.; Ray, A.; Ghandehari, H. Influence of Geometry, Porosity, and Surface Characteristics of Silica Nanoparticles on Acute Toxicity: Their Vasculature Effect and Tolerance Threshold. *ACS Nano* **2012,** *6*, 2289-2301.

32. Kresge, C. T.; Leonowicz, M. E.; Roth, W. J.; Vartuli, J. C.; Beck, J. S. Ordered Mesoporous Molecular-Sieves Synthesized by a Liquid-Crystal Template Mechanism. *Nature* **1992,** *359*, 710-712.

33. Huo, Q. S.; Margolese, D. I.; Ciesla, U.; Demuth, D. G.; Feng, P. Y.; Gier, T. E.; Sieger, P.; Firouzi, A.; Chmelka, B. F.; Schuth, F.; Stucky, G. D. Organization of Organic-Molecules with Inorganic Molecular-Species into Nanocomposite Biphase Arrays. *Chem. Mater.* **1994,** *6*, 1176-1191.

34. Huo, Q. S.; Margolese, D. I.; Ciesla, U.; Feng, P. Y.; Gier, T. E.; Sieger, P.; Leon, R.; Petroff, P. M.; Schuth, F.; Stucky, G. D. Generalized Synthesis of Periodic Surfactant Inorganic Composite-Materials. *Nature* **1994,** *368*, 317-321.

35. Yanagisawa, T.; Shimizu, T.; Kuroda, K.; Kato, C. The Preparation of Alkyltrimethylammonium-Kanemite Complexes and Their Conversion to Microporous Materials. *Bull. Chem. Soc. Jpn.* **1990,** *63*, 988-992.

36. Beck, J. S.; Vartuli, J. C.; Roth, W. J.; Leonowicz, M. E.; Kresge, C. T.; Schmitt, K. D.; Chu, C. T. W.; Olson, D. H.; Sheppard, E. W.; Mccullen, S. B.; Higgins, J. B.; Schlenker, J. L. A New Family of Mesoporous Molecular-Sieves Prepared with Liquid-Crystal Templates. *J. Am. Chem. Soc.* **1992,** *114* (27), 10834-10843.

37. Yang, H.; Coombs, N.; Ozin, G. A. Morphogenesis of shapes and surface patterns in mesoporous silica. *Nature* **1997,** *386*, 692-695.

38. Ozin, G. A.; Yang, H.; Sokolov, I.; Coombs, N. Shell mimetics. *Adv. Mater.* **1997,** *9*, 662-667.

39. Israelachvili, J. N.; Mitchell, D. J.; Ninham, B. W. Theory of Self-Assembly of Hydrocarbon Amphiphiles into Micelles and Bilayers. *J. Chem. Soc., Faraday Trans.* **1976,** *72*, 1525-1568.

40. Chan, H. B. S.; Budd, P. M.; Naylor, T. D. Control of mesostructured silica particle morphology. *J. Mater. Chem.* **2001,** *11*, 951-957.

41. Mou, C. Y.; Lin, H. P. Control of morphology in synthesizing mesoporous silica. *Pure and Appl. Chem.* **2000,** *72*, 137-146.

42. Firouzi, A.; Kumar, D.; Bull, L. M.; Besier, T.; Sieger, P.; Huo, Q.; Walker, S. A.; Zasadzinski, J. A.; Glinka, C.; Nicol, J.; Margolese, D.; Stucky, G. D.; Chmelka, B. F. Cooperative Organization of Inorganic-Surfactant and Biomimetic Assemblies. *Science* **1995,** *267*, 1138-1143.

43. Naik, S. P.; Elangovan, S. P.; Okubo, T.; Sokolov, I. Morphology control of mesoporous silica particles. *J. Phys. Chem. C* **2007,** *111*, 11168-11173.

44. Yang, H.; Ozin, G. A.; Kresge, C. T. The role of defects in the formation of mesoporous silica fibers, films, and curved shapes. *Adv. Mater.* **1998,** *10*, 883-887.

45. Hayakawa, K.; Kwak, J. C. T. in *Cationic Surfactants. In: Surfactant Science Series*, (Eds: E. D. Gorddard, K. P. Ananthapadmanabham), Marcel Dekker, New York, USA **1991**, pp. 189-248.

46. Li, C.; Han, J.; Ryu, C. Y.; Benicewicz, B. C. A versatile method to prepare RAFT agent anchored substrates and the preparation of PMMA grafted nanoparticles. *Macromolecules* **2006,** *39*, 3175-3183.

47. Pruitt, B. A.; McManus, A. T.; Kim, S. H.; Goodwin, C. W. Burn wound infections: Current status. *World J. Surg.* **1998,** *22*, 135-145.

48. Lyczak, J. B.; Cannon, C. L.; Pier, G. B. Establishment of Pseudomonas aeruginosa infection: lessons from a versatile opportunist. *Microbes Infect.* **2000,** *2*, 1051-1060.

49. Howell-Jones, R. S.; Wilson, M. J.; Hill, K. E.; Howard, A. J.; Price, P. E.; Thomas, D. W. A review of the microbiology, antibiotic usage and resistance in chronic skin wounds. *J. Antimicrob. Chemother.* **2005,** *55*, 143-149.

50. Bergey, D. H.; Holt, J. G.; Krieg, N. R.; Sneath, P. H. A. *Bergey's Manual of Determinative Bacteriology (9th ed.).* Lippincott Williams & Wilkins.: 1994.

51. Jackson, D. W.; Suzuki, K.; Oakford, L.; Simecka, J. W.; Hart, M. E.; Romeo, T. Biofilm formation and dispersal under the influence of the global regulator CsrA of Escherichia coli *J. Bacteriol.* **2002**, *184*, 290-301.

52. Smith, A. W. Biofilms and antibiotic therapy: Is there a role for combating bacterial resistance by the use of novel drug delivery systems? *Adv. Drug Delivery Rev.* **2005,** *57*, 1539-1550.

Chapter 5

Nitric Oxide-Releasing Chitosan Oligosaccharides as Anti-biofilm Agents

5.1 Introduction

Bacteria in nature exist in two states – free-floating planktonic bacteria and bacterial biofilms.[1] While many antimicrobial agents have proved effective against planktonic bacteria, medically relevant infections including the infections associated with medical implants, non-healing wounds, diabetic mellitus, and cystic fibrosis are often caused by bacterial biofilms.[2-5] Biofilms are communities of microorganisms adhered to a surface and surrounded by a self-produced extracellular polysaccharide (EPS) matrix that impedes immune response.[6-7] Compared to planktonic bacteria, biofilm-based bacteria are more resistant to antibiotics due to several specific defense mechanisms including inefficient penetration of antimicrobial agents cross EPS.[8-9] For example, the antibiotic dose to kill bacteria in biofilms may be 1000 times the dose required to kill planktonic bacteria.[10] As such, new antimicrobial agents capable of eradicating mature biofilms are urgently needed.

Nitric oxide (NO), a diatomic free radical produced endogenously, plays a key role in the mammalian immune response to pathogens.[11-13] The bactericidal properties of NO are attributed to the nitrosative and oxidative stress exerted by its reactive byproducts such as dinitrogen trioxide and peroxynitrite, ultimately leading to the disruption of bacteria membrane.[13] Nitric oxide-releasing materials have been widely developed for the use in a

number of different biomedical applications, many related to pathogen killing.[14-17] Recent research has demonstrated the antimicrobial efficacy of small molecule (e.g., 1-[2-(carboxylato)pyrrolidin-1-yl]diazen-1-ium-1,2-diolate (PROLI/NO)) and macromolecular (e.g., silica nanoparticles and dendrimers) NO-releasing vehicles against both Gram–positive and Gram–negative bacteria, including methicillin-resistant *Staphylococcus aureus* (MRSA).[18-23] Nitric oxide-releasing macromolecular scaffolds (e.g., silica nanoparticles and dendrimers) are particularly attractive due to enhanced bactericidal activity against planktonic bacteria and biofilms compared to small molecule NO donors (e.g., PROLI/NO).[20-23] Although NO-releasing silica particles proved effective at eradicating established biofilms, the lack of biodegradability greatly hinders the clinical utility of silica-based NO-releasing vehicles as antimicrobial agents.

Biodegradable NO-releasing materials have been developed as implant coatings (e.g., poly(diol citrate) elastomers[24] and polyesters[25-27]) to inhibit biofilm formation rather than eradicate established biofilms. To enable more efficient killing of biofilms, the design of new scaffolds is necessary to allow efficient EPS penetration and NO delivery to the bacteria embedded in the biofilms. Chitosan, the second most abundant natural biopolymer, has been widely used for biomedical applications including tissue engineering, drug delivery, and antimicrobial agents due to its biocompatibility, biodegradability and cationic composition.[28-31] The use of chitosan derivatives as NO-releasing scaffolds has also been investigated since these materials contain large concentrations of primary amines, necessary for *N*-diazeniumdiolate NO donor formation.[32-34] Unfortunately, previously reported *N*-diazeniumdiolate-functionalized chitosan polysaccharides have been characterized by low *N*-diazeniumdiolate conversion

efficiency and NO storage (~0.2 μmol/mg), likely the result of chitosan insolubility under the basic conditions required for *N*-diazeniumdiolate formation.[32-34] Additionally, the effectiveness of chitosan polysaccharides is a concern due to insolubility under physiological conditions.[35,36] To obtain *N*-diazeniumdiolate-functionalized chitosan derivatives with greater NO storage, we synthesized chitosan oligosaccharides that are soluble under both neutral and basic conditions and highly effective against *Pseudomonas aeruginosa* biofilms.

5.2 EXPERIMENTAL

5.2.1 Materials and Methods.

Medium molecular weight chitosan, 2-methyl aziridine (MAz), rhodamine B isothiocyanate (RITC), poly(ethylene glycol) methyl ether acrylate (average Mn = 480) (PEG), fetal bovine serum (FBS), Dulbecco's Modified Eagle's Medium (DMEM), phenazine methosulfate (PMS), 3-(4,5-dimethylthiazol-2-yl)-5-(3-carboxymethoxyphenyl)-2-(4-sulfophenyl)-2H-tetrazolium inner salt (MTS), trypsin, phosphate buffered saline (PBS), and penicillin streptomycin (PS) were purchased from the Aldrich Chemical Company (Milwaukee, WI). *Pseudomonas aeruginosa* (ATCC #19143) was obtained from the American Type Culture Collection (Manassas, VA). Trypic soy broth (TSB) and Tryptic soy agar (TSA) are purchased from Becton, Dickinson, and Company (Franklin Lakes, NJ). L929 mouse fibroblasts (ATCC #CCL-1) were obtained from the University of North Carolina Tissue Culture Facility (Chapel Hill, NC). Distilled water was purified with a Millipore Milli-Q Gradient A-10 water purification system (Bedford, MA). Syto 9 green fluorescent nucleic acid stain was purchased from Life Technologies (Grand Island, NY). Common laboratory salts and

solvents were purchased from Fisher Scientific (Pittsburgh, PA). All materials were used as received without further purification unless noted otherwise. Nuclear magnetic resonance (NMR) spectra were recorded on a 400 MHz Bruker instrument. Elemental (carbon, hydrogen, and nitrogen or CHN) analysis was performed using a PerkinElmer Elemental Analyzer Series 2400 instrument (Waltham, MA).

5.2.2 Synthesis of Chitosan Oligosaccharides.

Chitosan oligosaccharides were prepared by oxidative degradation using hydrogen peroxide. Medium molecular weight chitosan (2.5 g) was suspended in a hydrogen peroxide solution (15 or 30 wt%) under stirring for 1 h at 65–85 ^{o}C. Following the removal of undissolved chitosan by filtration, chitosan oligosaccharides were precipitated from solution by adding acetone to the filtrate. The precipitate was collected by centrifugation, washed twice with ethanol, and dried under vacuum at room temperature. The viscosity of the chitosan oligosaccharides was measured in a solution of NaCl (0.20 M) and CH_3COOH (0.10 M) at 25 ^{o}C using an Ubbleohde capillary viscometer. Oligosaccharide molecular weight was determined using the classic Mark-Houwink equation (i.e., $[\eta]=1.81\times10^{-3}\ M^{0.93}$).[39]

5.2.3 Synthesis of Secondary Amine-Functionalized Chitosan Oligosaccharides.

2-methyl aziridine (MAz) grafted chitosan oligosaccharides were synthesized following a previously reported procedure.[40] Briefly, a mixture of concentrated HCl (11 μL), water (100 μL) and MAz with a 1:1 (**Chitosan 1**) or 2:1 (**Chitosan 2**) molar ratio to primary amines on the chitosan oligosaccharides was added dropwise to a solution of chitosan oligosaccharides (100 mg) in deionized water (5 mL). The resulting solution was stirred at room temperature for 5 d, and then at 75 ^{o}C for 24 h. The product was purified

by dialysis and collected by lyophilization. Any high molecular weight poly(2-methyl aziridine) in the product was removed by washing with methanol, and the resulting material was dried under vaccum at room temperature. **Chitosan 2** was then dissolved in water at pH 10.0. The primary amine on the chitosan oligosaccharides was functionalized by adding poly(ethylene glycol) methyl ether acrylate to generate **Chitosan 3**. The resulting PEG-functionalized chitosan oligosaccharide derivative was purified by dialysis and collected by lyophilization.

^{1}H NMR data of **Chitosan 1** and **Chitosan 2** (400 MHz, CD_3OD, δ): 0.8–1.1 ($NH_2CH(CH_3)CH_2NH$), 1.9 (C7: $CHNHCOCH_3$), 2.3–2.7 ($NH_2CH(CH_3)CH_2NHCH$, C2: $NH_2CH(CH_3)CH_2NHCH$), 3.3–4.0 (C3, C4, C5, C6: $OHCH$, $OCHCH(OH)CH(NH_2)CH$, $OHCH_2CH$, $OHCH_2CH$), 4.4 (C1: $OCH(CHNH_2)O$). ^{1}H NMR data of **Chitosan 3** (400 MHz, CD_3OD, δ): 0.8–1.1 ($NH_2CH(CH_3)CH_2NH$), 1.9 (C7: $CHNHCOCH_3$), 2.3–2.7 ($NH_2CH(CH_3)CH_2NHCH$, C2: $NH_2CH(CH_3)CH_2NHCH$), 3.2 ($OCH_2CH_2OCH_3$), 3.3–4.0 (OCH_2CH_2O and C3, C4, C5, C6: $OHCH$, $OCHCH(OH)CH(NH_2)CH$, $OHCH_2CH$, $OHCH_2CH$), 4.4 (C1: $OCH(CHNH_2)O$).

5.2.4 Synthesis of N-Diazeniumdiolate-Functionalized Chitosan Oligosaccharides.

Secondary amine-functionalized chitosan oligosaccharides (**Chitosan 1**, **Chitosan 2**, and **Chitosan 3**) and 5.4 mM sodium methoxide (75 μL) were added to a methanol/water mixture (2 mL) of different v/v ratios (e.g., 10:0, 9:1, 8:2, 7:3, 6:4). The suspension was added to vials in a Parr hydrogenation vessel, which was purged rapidly (5–10 s) with argon three times followed by three longer argon purge cycles (10 min) to remove residual oxygen from the solution. The Parr hydrogenation vessel was then pressurized to 10 atm with NO gas purified over KOH pellets (to remove NO degradation products) and

maintained at 10 atm for 3 d. The same argon purging protocol was performed to remove unreacted NO and degradation products from the solution prior to removing the vials from the vessel.

5.2.5 Characterization of NO Storage and Release.

N-diazeniumdiolate-functionalized chitosan oligosaccharides (1 mg) (**Chitosan 1/NO**, **Chitosan 2/NO**, **Chitosan 3/NO**) in the water/methanol mixture were added into a sample vessel containing 30 mL deoxygenated phosphate buffered saline (PBS) (10 mM, pH = 7.4) at 37 °C, which initiated NO release. To quantify the NO released, the solution was purged with nitrogen at a flow rate of 70 mL/min to carry the liberated NO to the analyzer. Additional nitrogen flow was supplied to the vessel to match the collection rate of the instrument (200 mL/min). The analysis of NO was terminated when the NO release levels fell to below 10 ppb NO/mg chitosan oligosaccharides. Chemiluminescence data for the NO-releasing chitosan oligosaccharides were represented as: 1) total amount of NO release (t[NO], μmol NO/mg of secondary amine-functionalized chitosan oligosaccharides); 2) the maximum flux of NO release ($[NO]_{max}$, ppb/mg of secondary amine-functionalized chitosan oligosaccharides); and 3) the half-life of NO release ($t_{1/2}$).

5.2.6 Synthesis of Fluorescently-Labeled Chitosan Oligosaccharides.

Fluorescently-labeled chitosan oligosaccharides were prepared following a previously reported procedure.[41] Briefly, chitosan oligosaccharides (50 mg) were dissolved in water (2 mL) at pH 9.0. Rhodamine B isothiocyanate (RITC) was added to the solution in a 1:100 molar ratio to the primary amine of the chitosan oligosaccharides prior to the grafting of 2-methyl aziridine. The solution was stirred at room temperature for 3 d in the

dark. Subsequent dialysis and lyophilization yielded the RITC-labeled chitosan oligosaccharides.

5.2.7 Bactericidal Assays Under Static Conditions.

P. aeruginosa bacterial cultures were grown from a frozen (-80 ^{o}C) stock overnight in TSB at 37 ^{o}C. A 500 μL aliquot of the resulting suspension was added into 50 mL fresh TSB and incubated at 37 ^{o}C for ~2 h until the concentration reached ~1×10^{8} colony forming units (CFU)/mL, as confirmed by the OD_{600}, replicate plating and enumeration on nutrient agar. A working bacterial stock was generated by plating the bacterial suspension on TSA and incubating at 37 ^{o}C overnight. The TSA bacterial stocks were prepared weekly and stored at 4 ^{o}C. For bactericidal assays, colonies of *P. aeruginosa* were taken from the TSA plate, dispersed in 3 mL TSB, and incubated at 37 ^{o}C overnight. A 500 μL aliquot of culture was added to 50 mL fresh TSB and incubated to a concentration of ~1×10^{8} CFU/mL. The bacteria was collected by centrifugation, resuspended in PBS, and diluted to ~1×10^{6} CFU/mL. The bactericidal efficacy of NO-releasing chitosan oligosaccharides against *P. aeruginosa* was evaluated by incubating the bacteria suspension with NO-releasing chitosan oligosaccharides at 37 ^{o}C. At 4 h, 100 μL aliquots of the bacterial suspensions were removed, diluted 10-fold in PBS, plated on TSA, and incubated overnight at 37 ^{o}C. The minimum concentration of NO-releasing chitosan oligosaccharides that resulted in a 3-log reduction of bacterial viability was defined as the minimum bactericidal concentration (MBC) for planktonic studies.

5.2.8 Growth of P. aeruginosa Biofilms.

A CDC bioreactor (Biosurface Technologies, Bozeman, MT) was used to grow *P. aeruginosa* biofilms over a 48 h period. Briefly, medical grade silicone rubber substrates

were mounted in coupon holders prior to assembling the reactor. The assembled reactor was then autoclaved. The reactor effluent line was clamped, and 1% (v/v) sterile TSB (500 mL) was added aseptically. *P. aeruginosa* was then cultured in TSB to 10^8 CFU/mL. The reactor was inoculated with an aliquot (1 mL) of this bacterial suspension at a final concentration ~2×10^5 CFU/mL. The reactor was incubated at 37 °C for 24 h with slow stirring (150 rpm). Following this "batch phase" growth, the reactor media was refreshed continuously with 0.33% (v/v) TSB at 6 mL/min for another 24 h through the effluent line.

5.2.9 Treatment of P. aeruginosa Biofilms with NO-releasing Chitosan Oligosaccharides.

P. aeruginosa biofilms grown on silicone rubber substrates were exposed to chitosan oligosaccharide in PBS with slight agitation (37 °C, 24 h) to determine the minimum bactericidal concentration (MBC) necessary to elicit a 5-log reduction in viability. At 24 h, samples were then sonicated and vortexed to disrupt the biofilm. Aliquots (100 μL) of the bacteria/chitosan suspensions were diluted and plated on TSA. After incubating the TSA plates overnight at 37 ^{o}C, bacteria viability was determined by counting observed colonies. Of note, the limit of detection for this selected plate counting method is 2.5×10^3 CFU/mL. As such, biofilm growth conditions were selected to accurately represent a 5-log reduction in viability for biofilms.

5.2.10 Confocal Microscopy.

P. aeruginosa was cultured in TSB to a concentration of ~1×10^8 CFU/mL, collected *via* centrifugation (3645 × *g* for 10 min), resuspended in sterile PBS, and adjusted to ~1×10^6 CFU/mL. Aliquots of the bacteria solution were incubated in a glass bottom confocal

dish for 1.5 h at 37 °C. A Zeiss 510 Meta inverted laser scanning confocal microscope with a 543 nm HeNe excitation laser and a LP 585 nm filter was used to obtain fluorescence images of the rhodamine B isothiocyanate (RITC)-modified chitosan oligosaccharides. The bright field and fluorescence images were collected by a N.A. 1.2 C-apochromat water immersion lens with a 40x objective. Solutions of RITC-labeled NO-releasing chitosan oligosaccharides in PBS (1.5 mL) were added to the bacteria solution (1.5 mL) in the glass confocal dish to achieve a final concentration of 150 μg/mL. Images were collected every 2 min to characterize the association, if any, of the chitosan oligosaccharides with *P. aeruginosa* temporally. To observe the association of chitosan oligosaccharides with bacteria within biofilms, Established biofilms stained with syto 9 (10 μM) were incubated with RITC-labeled chitosan oligosaccharides (150 μg/mL in PBS) for 2.5 h. Prior to imaging, samples were rinsed with PBS (3x). A Zeiss 510 Meta inverted laser scanning confocal microscope with 488 nm Ar and 543 nm HeNe excitation lasers, and a BP 505–530 nm and LP 585 nm filters, respectively, was used to obtain all confocal images. Fluorescence images were collected with a 20x objective.

5.2.11 In Vitro Cytotoxicity Testing of NO-releasing Chitosan Oligosaccharides.

L929 mouse fibroblasts were grown in DMEM supplemented with 10% v/v fetal bovine serum (FBS) and 1 wt% penicillin/streptomycin, and incubated in 5% v/v CO_2 under humidified conditions at 37 ^{o}C. After reaching confluency (80%), the cells were trypsinized, seeded onto tissue-culture treated polystyrene 96-well plates at a density of 3×10^4 cells/mL, and incubated at 37 ^{o}C for 48 h. The supernatant was then aspirated prior to adding fresh DMEM (200 μL) and the NO-releasing chitosan oligosaccharides solution in PBS (50 μL) to each well. After incubation at 37 ^{o}C for 24 h, the supernatant was

aspirated and a mixture of DMEM/MTS/PMS (105/20/1, v/v/v) (120 μL) was added to each well. The absorbance of the resulting colored solution after 1.5 h incubation at 37 ^{o}C was quantified using a Thermoscientific Multiskan EX plate reader at 490 nm. The mixture of DMEM/MTS/PMS and untreated cells were used as a blank and control, respectively. Cell viability was calculated as follows (Eq. 5.1).

$$\text{Cell Viability} = \frac{(\text{Absorbance}_{\text{treated cell}} - \text{Absorbance}_{\text{blank}})}{(\text{Absorbance}_{\text{untreated cell}} - \text{Absorbance}_{\text{blank}})} \qquad \text{Eq. 5.1}$$

5.3 Results and Discussion

Chitosan has been widely used in antitumor, antimicrobial, and wound healing applications due to favorable biocompatibility and the ability to slowly degrade into nontoxic byproducts.[40-43] This polymer has also been modified to store and release NO by functionalizing the primary amines with NO to form *N*-diazeniumdiolates. [32-34] Unfortunately, the NO storage is rather modest (~0.2 μmol/mg) due to poor solubility of polysaccharides in basic solutions necessary for NO donor formation.[32-34] To synthesize *N*-diazeniumdiolate-functionalized chitosan derivatives with improved NO storage, we prepared water-soluble chitosan oligosaccharides by the degradation of chitosan polysaccharides in hydrogen peroxide. An additional benefit of the low-molecular weight (MW < 8000) chitosan oligosaccharides involves their ability to more easily penetrate biofilms.[39, 44] In this regard, we predict that low-molecular weight *N*-diazeniumdiolate-modified chitosan oligosaccharides would have even greater bactericidal activity compared to the polysaccharides.

5.3.1 Synthesis of Secondary Amine-Functionalized Chitosan Oligosaccharides.

A number of strategies have been reported for degrading chitosan into oligomer derivatives.[38, 45] Rather than use enzymatic degradation requiring costly enzymes (e.g., chitosanase), we adapted an oxidative degradation strategy using hydrogen peroxide to synthesize chitosan oligosaccharides.[38] Control of the molecular weight (M_w) was achieved by varying the concentration of hydrogen peroxide and degradation temperature. The viscosity of the chitosan oligosaccharides was determined in a solution of sodium chloride (0.20 M) and acetic acid (0.10 M) using an Ubbleohde capillary viscometer.[37] In combination with the Mark-Houwink equation (i.e., $[\eta] = 1.81\times10^{-3}\ M^{0.93}$), molecular weights were determined as a function of processing conditions. Collectively, larger concentrations of hydrogen peroxide and elevated degradation temperatures led to lower molecular weight chitosan. As shown in Table 5.1, chitosan oligosaccharides of ~10 kD molecular weight were prepared in 15 wt% hydrogen peroxide at 65 ^{o}C for 1 h. Increasing the degradation temperature to 85 ^{o}C resulted in significantly smaller size (MW ~5 kD). When both a larger concentration of hydrogen peroxide (i.e., 30 wt%) and elevated temperature (i.e., 85 ^{o}C) were adopted, the molecular weight of chitosan oligosaccharides decreased further (~ 2.5 kD) were achieved. As shown in Table 5.2, the CHN elemental analysis of the oligosaccharides indicated an overall nitrogen content of 6.3 wt%.

To enhance NO storage (secondary amines are more readily converted to NO form due to their increased basicity[22, 46-47]), the primary amines on the synthesized chitosan oligosaccharides were thus modified by a cationic ring opening of MAz to produce secondary amine functionalities (Scheme 5.1A).

Table 5.1 Degradation conditions and elemental analysis of chitosan oligosaccharides of different molecular weights.

Chitosan oligosaccharides	M_v[a]	T (^oC)	[H_2O_2] (wt%)
2.5 k	2657	85	30
5 k	5370	85	15
10 k	10142	65	15

[a] viscosity average molecular weight as determined by classic Mark-Houwink equation (i.e., $[\eta] = 1.81\times10^{-3} M^{0.93}$).

Table 5.2 Elemental (CHN) analysis of chitosan oligosaccharides and secondary amine-functionalized derivatives.

Materials	C (%)	H (%)	N (%)
Chitosan oligosaccharides[a]	42.2 ± 1.6	6.8 ± 0.1	6.3 ± 0.2
Chitosan 1-5k	43.5 ± 1.2	7.7 ± 0.3	8.9 ± 0.1
Chitosan 2-5k	44.7 ± 1.8	8.4 ± 0.2	10.8 ± 0.8
Chitosan 3-5k	51.0 ± 0.2	9.0 ± 0.2	3.1 ± 0.1
Chitosan 2-2.5k	43.7 ± 0.7	8.5 ± 0.2	10.9 ± 0.1
Chitosan 2-10k	44.7 ± 1.8	8.4 ± 0.2	10.8 ± 0.8

[a] chitosan oligosaccharides before the grafting of 2-methyl aziridine.
Each parameter was analyzed with multiple replicates (n=3).

By tuning the ratio of MAz and primary amine (e.g., 1:1 **Chitosan 1**, 2:1 **Chitosan 2**), the number of MAz repeating units grafted onto the chitosan oligosaccharides proved tunable (as verified by NMR), leading to a range of secondary amine concentrations and NO storage. To investigate how the local environment surrounding the *N*-diazeniumdiolate NO donors affected the NO-release kinetics,[22] acrylate-functionalized PEG chains were conjugated to the primary amines on **Chitosan 2** by the Michael addition reaction to yield PEG-modified scaffolds (e.g., **Chitosan 3**, Scheme 5.1B). Grafting of 2-methyl aziridine to the oligosaccharides increased the corresponding nitrogen content from 6.3 to 8.9 and 10.8 wt% for **Chitosan 1** and **Chitosan 2**, respectively. As expected, the PEGylation of **Chitosan 2** led to a corresponding decrease in nitrogen content (3.1 wt%) (**Chitosan 3**).

5.3.2 Synthesis of NO-releasing Chitosan Oligosaccharides.

Reaction of the secondary amine-functionalized chitosan oligosaccharides (**Chitosan 1**, **Chitosan 2**, and **Chitosan 3**) with NO (10 atm under basic conditions) yielded *N*-diazeniumdiolate NO donor-functionalized chitosan oligosaccharides (**Chitosan 1/NO**, **Chitosan 2/NO**, and **Chitosan 3/NO**). The NO conjugation ("charging") solvent dictates the charging efficiency and thus total NO storage.[22] Aqueous solutions were necessary in order to adequately dissolve the chitosan oligosaccharides. Despite the high pH that should inhibit NO donor breakdown,[47] NO donor formation due to the presence of water was a concern. To examine the influence of water concentration on *N*-diazeniumdiolate conversion efficiency, mixtures of methanol (a common charging solvent)[22, 48] and water were prepared (10:0, 9:1, 8:2, 7:3, and 6:4 v/v) and the pH was adjusted to above 10 by adding sodium methoxide.

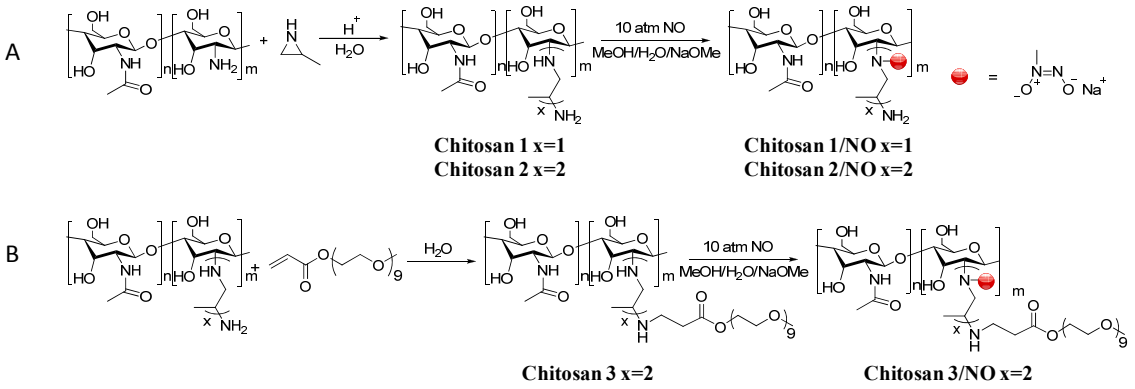

Scheme 5.1 Synthesis of secondary amine- and *N*-diazeniumdiolate-functionalized chitosan oligosaccharide derivatives. (A) grafting of 2-methyl aziridine onto primary amines of chitosan oligosaccharides (**Chitosan 1** and **2**) and *N*-diazeniumdiolation of the resulting materials (**Chitosan 1** and **2-NO**); (B) PEGylation of 2-methyl aziridine-grafted-chitosan oligosaccharide (**Chitosan 3**) and the *N*-diazeniumdiolation of the resulting material (**Chitosan 3-NO**).

Chitosan 2/NO-5k was used as a representative oligosaccharide for these studies with the assumption that lower and greater MW chitosan oligosaccharides would behave similarly. The NO release profile for **Chitosan 2/NO-5k** as a function of the charging solvent are shown in Figure 5.1. Specific NO-release parameters (e.g., total NO release, maximum flux, and half-life) were extracted from these profiles and are provided in Table 5.3. The NO storage increased with increasing water/methanol ratios up to 7:3. The maximum NO storage (using the 7:3 methanol/water charging solvent ratio) was 0.87 μmol/mg, roughly 4x larger than that for previously reported chitosan polysaccharides (~0.2 μmol/mg).[37-39] The improved NO storage may be attributed to the enhanced solubility of **Chitosan 2-5k** in the charging solvents (e.g., methanol/water 9:1, 8:2, 7:3) relative to methanol. In charging solvent where **Chitosan 2-5k** was essentially insoluble (e.g., methanol), only secondary amines on the exterior of the **Chitosan 2-5k** precipitate were accessible to NO, leading to a lower NO donor formation efficiency. In contrast, complete dissolution exposes a significantly greater proportion of secondary amines to the base and NO. At larger water concentrations (i.e., methanol/water 6:4 v/v or 40% water), the NO storage decreased slightly (~0.76 μmol/mg), suggesting destabilization of the *N*-diazeniumdiolate NO donor by water. **Chitosan 2/NO-5k** exhibited similar NO-release kinetics (e.g., half-life of ~2 h) regardless of the charging solvent, indicating that while the chemical structure (e.g., the local environment surrounding *N*-diazeniumdiolates) of the NO-releasing scaffolds dictates NO-release kinetics, variation in charging solvent only affects the total NO storage. Overall, the NO-release data revealed that the optimal charging solvent was methanol/water 7:3 (v/v).

Table 5.3 Influence of charging solvent on nitric oxide-release properties for secondary amine-functionalized chitosan oligosaccharides (**Chitosan 2/NO-5k**) in PBS (pH = 7.4, 37 °C) as measured using a chemiluminescence NO analyzer.

$MeOH/H_2O$	10:0	9:1	8:2	7:3	6:4
t[NO][a] (μmol/mg)	0.58 ± 0.09	0.74 ± 0.12	0.81 ± 0.14	0.87 ± 0.16	0.75 ± 0.18
$[NO]_{max}$ (ppb/mg)	2648 ± 120	4150 ± 70	4350 ± 484	5500 ± 414	5000 ± 572
Half-life (h)	2.40 ± 0.13	2.25 ± 0.02	2.05 ± 0.07	2.20 ± 0.14	2.05 ± 0.25

[a] total NO storage per mg chitosan. Each parameter was analyzed with multiple replicates (n=3).

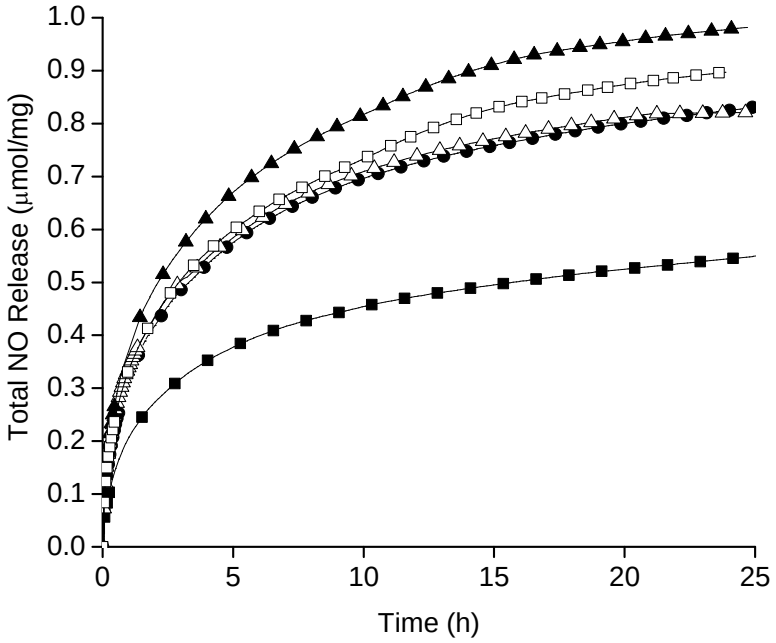

Figure 5.1 Nitric oxide release profiles of **Chitosan 2/NO-5k** in methanol (solid square), methanol/water 9:1 (solid circle), 8:2 (open triangle), 7:3 (solid triangle), and 6:4 v/v (open square).

This solvent composition was used for the functionalization of the other secondary amine-functionalized chitosan oligosaccharides (**Chitosan 1-5k** and **Chitosan 3-5k**).

The antibacterial efficacy of NO-releasing materials has been reported to be dependent on both NO storage (i.e., payload) and release kinetics.[49] 2-methyl aziridine (MAz) was grafted onto the chitosan oligosaccharides at different feed ratios (i.e., 2:1 and 1:1) to alter the secondary amine functionalization and NO storage. As expected, increasing the feed ratio of 2-methyl aziridine to primary amines from 1:1 (**Chitosan 1-5k**) to 2:1 (**Chitosan 2-5k**) resulted in greater NO storage (e.g., ~0.30 to 0.87 μmol/mg, respectively). As shown in Figure 5.2, the NO flux and storage of **Chitosan 1/NO-5k** were lower than **Chitosan 2/NO-5k**, a result that is attributable to the smaller amine concentration of **Chitosan 1-5k** (~8.9 wt%) compared to **Chitosan 2-5k** (~10.8 wt%).

To tune the NO-release kinetics of chitosan oligosaccharides further, **Chitosan 2-5k** was modified with acrylate-functionalized PEG chains (**Chitosan 3-5k**). As expected, hydrophilic functionalization of the oligosaccharides with PEG facilitated a more aqueous local environment and result in both larger initial NO flux (~12600 ppb/mg) and faster overall NO release (half-life ~0.15 h) relative to **Chitosan 2-5k** (Figure 5.2).[22] The PEGylation of primary amines on **Chitosan 2-5k** also affected its ionic characteristics by shielding the amine moieties, a key factor influencing the association of chitosan-based materials with bacteria.[36] The distinct NO-release kinetics and ionic characteristics of the resulting NO-releasing chitosan oligosaccharides allowed for the study of how surface charge and NO release affect anti-biofilm activity.

Table 5.4 Nitric oxide-release properties of different *N*-diazeniumdiolate NO donor-functionalized chitosan oligosaccharides in PBS (pH = 7.4, 37 °C) as measured using a chemiluminescence NO analyzer.

Material	t[NO][a] (μmol/mg)	t[NO][b] (μmol/mg)	$[NO]_{max}$ (ppb/mg)	$t_{1/2}$ (h)
Chitosan 1/NO-5 k	0.30 ± 0.04	0.16 ± 0.03	1600 ± 215	3.60 ± 0.13
Chitosan 2/NO-5 k	0.87 ± 0.16	0.52 ± 0.15	5500 ± 414	2.20 ± 0.14
Chitosan 3/NO-5 k	0.35 ± 0.02	0.29 ± 0.01	12600 ± 2121	0.15 ± 0.01
Chitosan 2/NO-2.5 k	0.84 ± 0.04	0.49 ± 0.02	7500 ± 550	2.06 ± 0.10
Chitosan 2/NO-10 k	0.81 ± 0.05	0.47 ± 0.03	7350 ± 672	2.04 ± 0.05

[a] total NO released and [b] NO released over 24 and 4 h (μmol) per milligram of secondary amine-functionalized PPI. Each parameter was analyzed with multiple replicates (n=3).

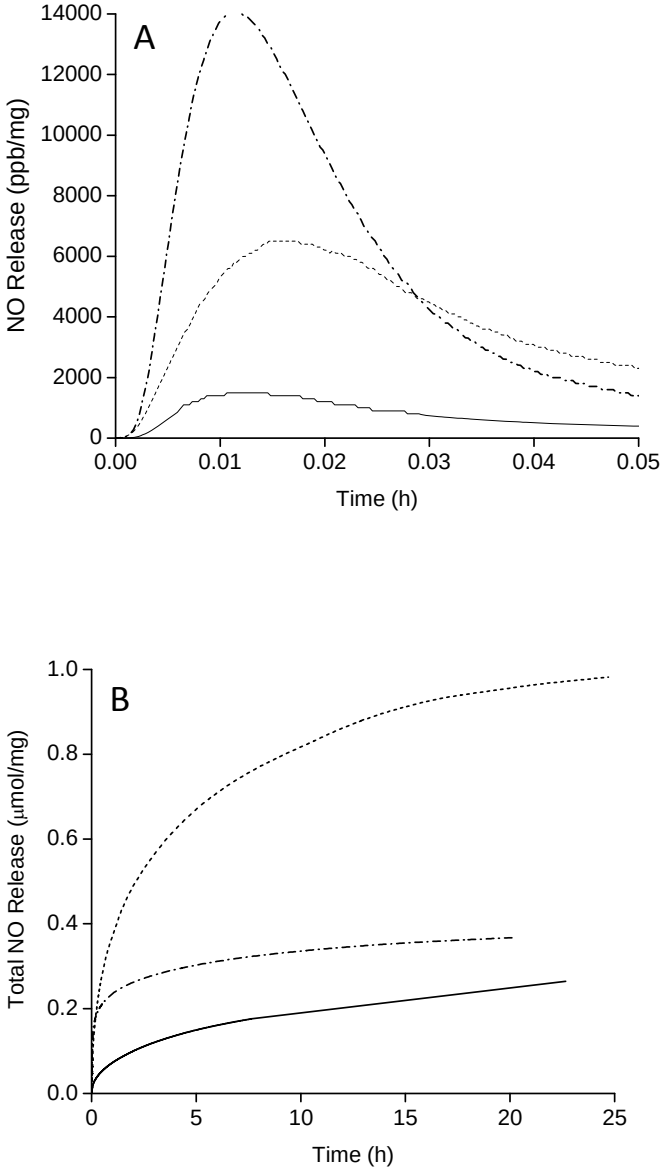

Figure 5.2 Real-time NO release profiles (A) and plot of t[NO] vs time (B) for NO-releasing chitosan oligosaccharides (e.g., **Chitosan 1-5k** (solid line), **Chitosan 2-5k** (dot line), and **Chitosan 3-5k** (dash dot line)).

5.3.3 Bactericidal Studies: Planktonic Bacteria.

Control and NO-releasing chitosan oligosaccharides (e.g., **Chitosan 1/NO -5k**, **Chitosan 2/NO-5k**, **Chitosan 3/NO -5k**) were exposed to Gram–negative *P. aeruginosa*, a pathogen involved in infections associated with burn wounds and cystic fibrosis, to evaluate their ability to kill bacteria.[5, 50] Bacterial viability assays were performed under static conditions to determine the concentration of chitosan required to reduce bacteria viability by 3 logs (i.e., 99.9% killing), which hereafter will be referred to as the minimum bactericidal concentration or MBC. The amount of NO delivered from NO-releasing chitosan oligosaccharides (Table 5.4) over the time of the assay (4 h) was also examined to quantitatively assess the NO dose necessary for 99.9% bacterial killing. Both MBCs and the bactericidal NO doses required for the chitosan oligosaccharides are provided in Table 5.5. Each of the NO-releasing chitosan oligosaccharides studied (**Chitosan 1/NO-5k**, **Chitosan 2/NO-5k** and **Chitosan 3/NO-5k**) resulted in ≥99.9% killing of *P. aeruginosa*. At equivalent concentrations, the control (non-NO-releasing) chitosan did not lead to a significant reduction in bacterial viability, indicating NO as the bactericidal agent (data not shown). Further inspection of the bactericidal NO doses in Table 5.5 reveals that greater NO levels were required from **Chitosan 3/NO-5k** compared to **Chitosan 1/NO-5k** and **Chitosan 2/NO-5k** to kill *P. aeruginosa*. This behavior may be attributed to decreased interaction between the chitosan oligosaccharides and bacteria membrane. Sun et al. previously reported that positively charged dendrimers associated more readily with bacteria than neutral dendrimers. enhanced bactericidal action was the result of such interactions.[23] The less effective bacteria killing observed for **Chitosan 3/NO-5k** could stem from the ability of the neutral

PEG chains to shield the amine moieties. In contrast, **Chitosan 1/NO-5k** and **Chitosan 2/NO-5k** have positively charged primary amines at pH 7.4 on their exterior that enhance their association with the bacteria and facilitate more localized NO delivery.

To further confirm that the lessened antibacterial activity of **Chitosan 3/NO-5k** was the result of decreased interactions with the bacteria membrane, confocal microscopy was utilized to compare the association kinetics of **Chitosan 3/NO-5k** and **Chitosan 2/NO-5k** with bacteria. Rhodamine B isothiocyanate (RITC)-labeled **Chitosan 2/NO-5k** and **Chitosan 3/NO-5k** were synthesized as previously reported.[39] The potential impact of RITC on chitosan-bacteria association was minimized by using small concentration of RITC (i.e., in 1:100 molar ratio to total primary amines). The degree of association of the NO-releasing chitosan oligosaccharides with bacteria was then followed by measuring red fluorescence surrounding the bacteria. As expected, **Chitosan 2/NO-5k** associated with the bacteria more rapidly (within 24 min) than **Chitosan 3/NO-5k** (86 min) (Figure 5.3). The fluorescence from **Chitosan 2/NO-5k** at 42 min was significantly greater than that of **Chitosan 3/NO-5k** at 110 min, further demonstrating that **Chitosan 3/NO-5k** associated with the bacteria at a much slower rate due to the PEG (neutral) modification. Further inspection of **Chitosan 2/NO-5k** and **Chitosan 3/NO-5k** association with *P. aeruginosa* revealed enhanced bacteria association for **Chitosan 2/NO-5k** (Figure 5.3-G, H), confirming the benefits of the cationic/positive properties of **Chitosan 2/NO-5k** over **Chitosan 3/NO-5k**.

Table 5.5 Minimum bactericidal concentration (MBC) and NO doses of NO-releasing chitosan oligosaccharides for 3-log reduction in planktonic *P. aeruginosa* viability.

Chitosans	MBC (μg/mL)	NO dose (μmol/mL)
Chitosan 1/NO-5k	2000	0.32
Chitosan 2/NO-5k	200	0.10
Chitosan 3/NO-5k	1500	0.45
Chitosan 2/NO-2.5k	250	0.12
Chitosan 2/NO-10k	250	0.12

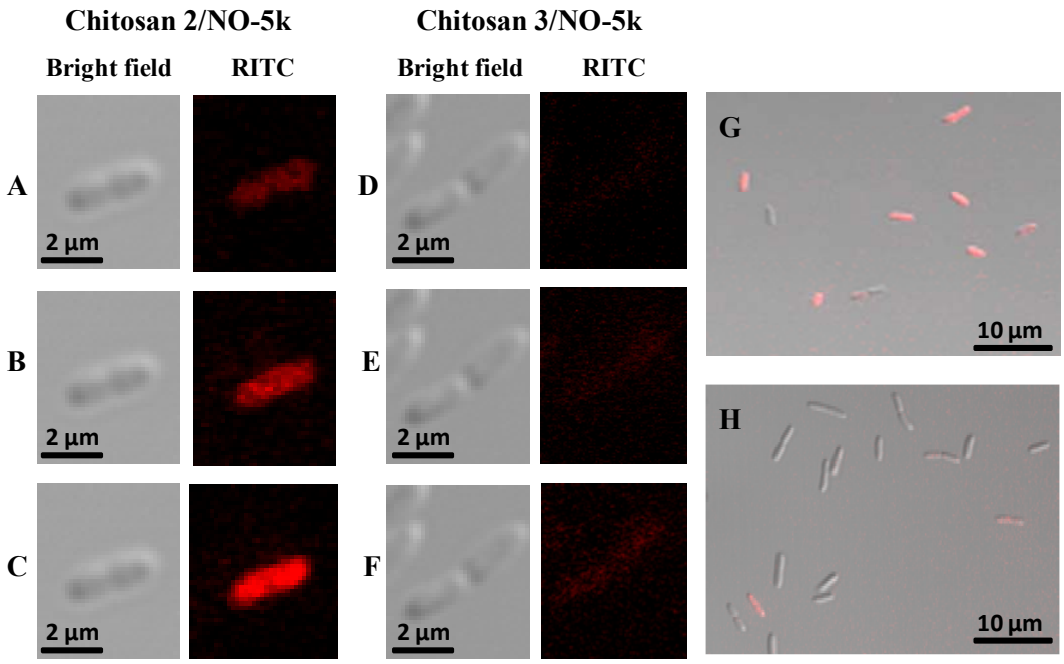

Figure 5.3 Bright field and fluorescent images of RITC-modified **Chitosan 2/NO-5k** at A) 24, B) 28, C) 42 min and **Chitosan 3/NO-5k** at D) 82, E) 86, F) 110, H) 120 min (150 µg mL^{-1}) association with *P. aeruginosa*. Overlay images of *P. aeruginosa* incubated with G) **Chitosan 2/NO-5k** at 44 min and H) **Chitosan 2/NO-5k** at 120 min.

In addition to charge effect, we sought to study the role of molecular weight in *P. aeruginosa* killing. Chitosan oligosaccharides of ~2.5, 5, and 10 kD were synthesized and functionalized with NO (**Chitosan 2/NO-2.5 k**, **Chitosan 2/NO-5 k**, **Chitosan 2/NO-10 k**). As expected, these materials exhibited similar NO-release kinetics (Table 5.4) due to the similar nitrogen content, allowing for the study of how molecular weight impacts bactericidal efficacy. Regardless of size (i.e., molecular weight), each of the NO-releasing chitosan oligosaccharides (**Chitosan 2/NO-2.5 k**, **Chitosan 2/NO-5 k**, **Chitosan 2/NO-10 k**) exhibited similar bactericidal NO concentrations (i.e., ~10 μmol NO/mL) for 3-log killing (Table 5.5).

5.3.4 Bactericidal Studies: Biofilms Eradication.

As previously reported, NO-releasing scaffolds have proven effective against both planktonic and biofilm bacteria.[20, 23, 51-52] For example, Barraud et al. reported that exposing established biofilms to NO (from small molecule NO donors) greatly enhanced the anti-biofilm efficacy of antimicrobial compounds including tobramycin, hydrogen peroxide, and sodium dodecyl sulfate.[52] Hetrick et al. demonstrated the use of macromolecular NO-releasing scaffolds (e.g., *N*-diazeniumdiolate-modified silica particles) to eradicate a broad-spectrum of biofilms with comparable or reduced toxicity (~80% viability reduction) against mammalian cells versus currently administered antiseptics (e.g., povidone iodine or chlorhexidine).[51] Based on these prior studies, we expected the NO-releasing chitosan oligosaccharides to also be effective against biofilms with perhaps less toxicity against mammalian cells than other scaffolds (e.g., silica, dendrimers).[53].

To evaluate the anti-biofilm activity of NO-releasing chitosan oligosaccharides (e.g., **Chitosan 1/NO-5k**, **Chitosan 2/NO-5k**, **Chitosan 3/NO-5k**), *P. aeruginosa* biofilms were exposed to 0.2–1.3 mg/mL NO-releasing chitosan oligosaccharides for 24 h (corresponding to ~0.17–0.46 μmol NO/mL). After treatment, the biofilms were removed from the silicone rubber substrates by vortexing and sonication to enable viability quantification.[52] Control experiments were performed to confirm the growth of *P. aeruginosa* biofilms using the selected protocol. As shown in Figure 5.4, the viability of *P. aeruginosa* in the biofilm was ~2×10^8 CFU when exposed only to PBS. The chitosan concentrations for 5-log reduction of biofilm bacteria viability (MBC) were 400, 700, and 1000 μg/mL for **Chitosan 2/NO-5k**, **Chitosan 1/NO-5k**, and **Chitosan 3/NO-5k**, respectively. **Chitosan 2/NO-5k** exhibited the greatest anti-biofilm efficacy, a likely result due to both increased NO storage/release and rapid association with the negatively charged bacteria. Although **Chitosan 1/NO-5k** and **Chitosan 3/NO-5k** stored similar levels of NO (~0.3 μmol/mg), **Chitosan 1/NO-5k** was more effective at eradicating the biofilm bacteria (MBC 700 μg/mL) compared to **Chitosan 3/NO-5k** (MBC 1000 μg/mL). The decreased antibiofilm efficacy for **Chitosan 3/NO-5k** may result from the shielding of the amine moieties by the neutral PEG chains, thus impeding association with the negatively charged exterior of the bacteria. To confirm this hypothesis, the association of **Chitosan 2/NO-5k** and **Chitosan 3/NO-5k** with *P. aeruginosa* biofilm was evaluated using confocal microscope. As shown in Figure 5.5, biofilms exposed to **Chitosan 2/NO-5k** exhibited more intense red fluorescence compared to **Chitosan 3/NO-5k**, again confirming the enhanced association of the positively charged **Chitosan 2/NO-5k** with the bacteria.

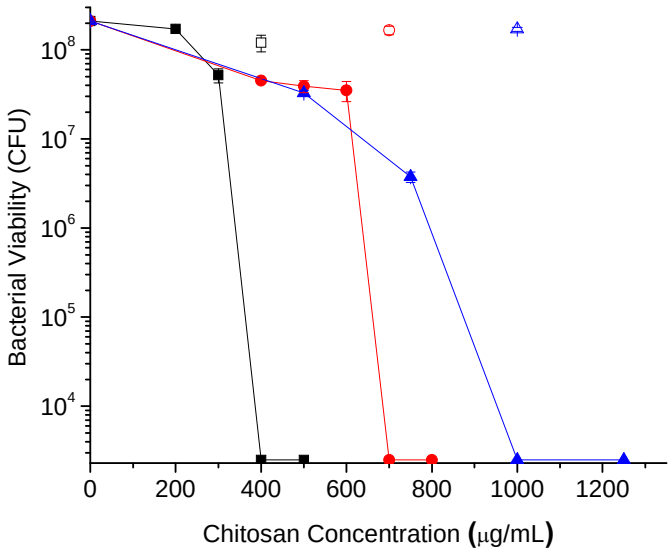

Figure 5.4 Anti-biofilm efficacy of NO-releasing (solid symbols) and control (open symbols) chitosan oligosaccharides (**Chitosan 1-5k** (sphere), **Chitosan 2-5k** (square), and **Chitosan 3-5k** (triangle)) against established *P. aeruginosa* biofilms. Control chitosan oligosaccharides resulted in no significant reduction in bacteria viability.

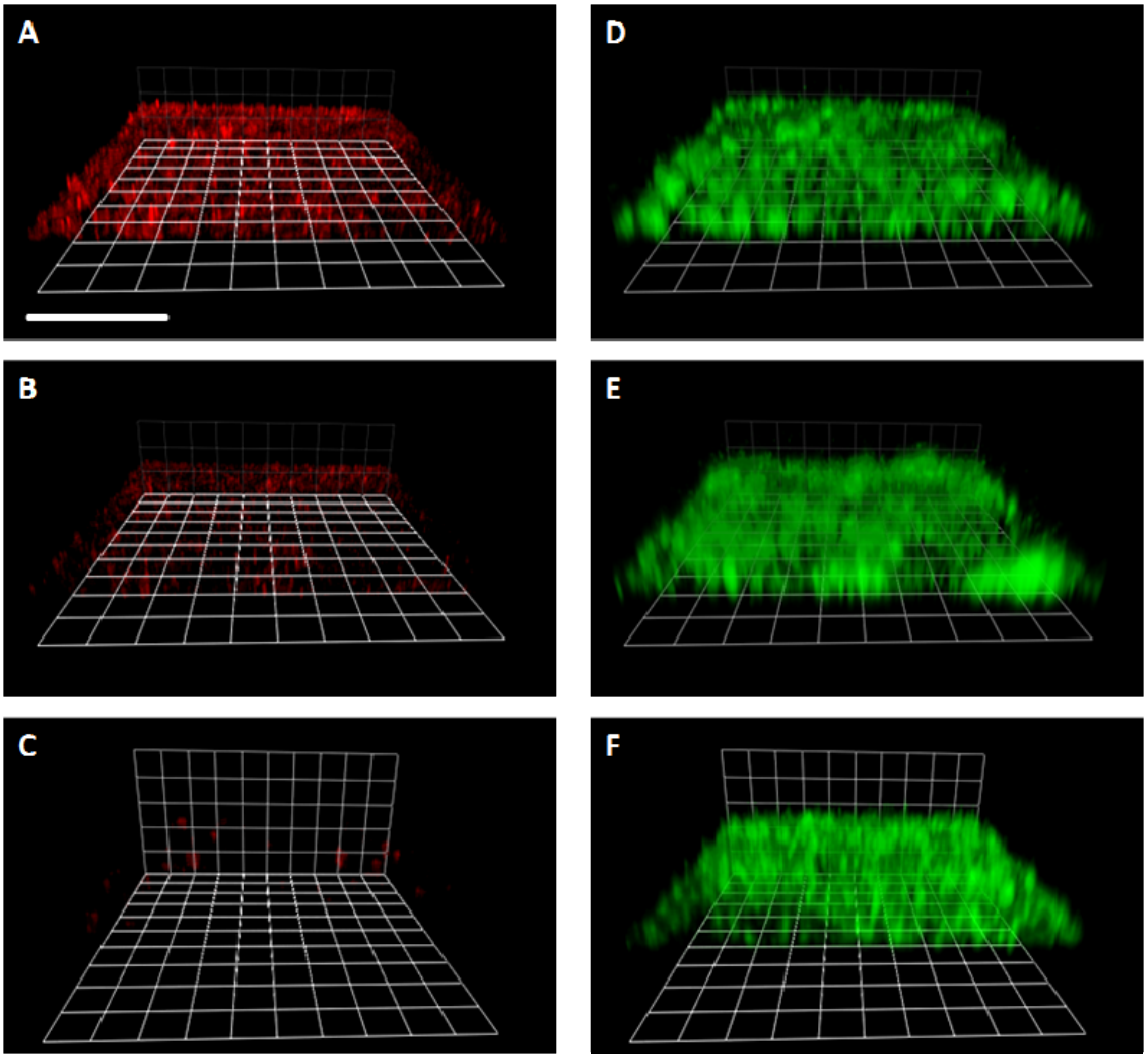

Figure 5.5 Confocal fluorescence images of RITC-labeled chitosan oligosaccharide association with *P. aeruginosa* in biofilms (A. **Chitosan 2/NO-5k**, B. **Chitosan 3/NO-5k**, C. **Chitosan 2-10k**) and images of syto 9 labeled biofilms incubated with D) **Chitosan 2/NO-5k**, E) **Chitosan 3/NO-5k** and F) **Chitosan 2/NO-10k**. Green fluorescence of syto 9 indicates the *P. aeruginosa* bacteria embedded in the biofilms. Red fluorescence of RITC indicates the association of RITC-labeled chitosan oligosaccharides with *P. aeruginosa* in biofilms. Scale bar: 40 μm.

The efficient association of chitosan oligosaccharides with bacteria in biofilms is a great advantage over previously reported NO-releasing polysaccharides which are not expected to penetrate the exopolysaccharides matrix due to their insolubility under physiological conditions.

Although chitosan molecular weight was not observed to play a significant role in planktonic killing, less effective bacteria killing was observed when using **Chitosan 2/NO-10k**, the largest chitosan oligosaccharides (600 μg/mL vs. 400 μg/mL for **Chitosan 2/NO-10k** and **Chitosan 2/NO-2.5k**) against biofilms. The exopolysaccharides matrix is likely slowing the diffusion of the largest chitosan structure. Takenaka et al., previously reported less efficient EPS penetration of high (vs low)-molecular weight dextran,[53] further supporting this hypothesis that the impeded diffusion of **Chitosan 2/NO-10k** led to slow association with bacteria within the biofilms (Figure 5.5). Control chitosan oligosaccharides (e.g., **Chitosan 1**, **Chitosan 2**, and **Chitosan 3**) did not lead to a significant reduction in bacterial viability at the same concentrations as their NO-releasing counterparts, indicating that the observed bacterial killing was due to NO from the *N*-diazeniumdiolate-functionalized chitosan oligosaccharides rather than the chitosan scaffolds themselves.

5.3.5 Cytotoxicity of NO-releasing Chitosan Oligosaccharides to Mammalian Fibroblasts.

The benefit of utilizing chitosan as NO-releasing vehicles includes its non-toxic nature to mammalian cells. The cytotoxicity of control and NO-releasing chitosan oligosaccharides were compared by exposing mouse fibroblast cells to the oligosaccharides at the MBCs against *P. aerugionsa* biofilms noted above. The normalized cell viabilities of control and NO-releasing chitosan oligosaccharides after 24

h incubation are shown in Figure 5.6. Regardless of size (i.e., molecular weight), the control and NO-releasing chitosan oligosaccharides were non-toxic against mouse fibroblast cells at the MBCs for the NO-releasing scaffolds, indicating an advantage of these materials as anti-biofilm agents compared to other antibacterial agents.[51] Of note, the NO-releasing chitosan oligosaccharides exhibited lower cytotoxicity than the chitosan controls, corroborating previous reports that certain levels of NO may promote cell proliferation.[54-55] Indeed, treatment of mouse lung endothelial cells and human aortic endothelial cells with small molecule NO donors such as *S*-nitroso-L-glutathione (GSNO), *S*-nitroso-N-acetylpenicillamine (SNAP), *N*-diazeniumdiolated-diethyltriamine (DETA/NO) has been shown to promote proliferation.[56-57] Collectively, the antimicrobial activity against planktonic and biofilm bacterial and the lack of toxicity of NO-releasing chitosan oligosaccharides suggests that NO-releasing chitosan oligosaccharides may serve as ideal antimicrobial agents for applications including wound healing and cystic fibrosis.

5.4 Conclusions

Chronic infections associated with diabetic mellitus and cystic fibrosis pose great medical challenges and cost billions of dollars annually.[58] Nitric oxide-releasing materials hold great potential as antimicrobial therapeutics due to their biocidal efficacy against medically relevant and antibiotic-resistant bacteria and non-systemic risk.[23, 48] This chapter focused on the synthesis of *N*-diazeniumdiolate-modified chitosan oligosaccharides with controlled NO storage (e.g., four times greater than prior NO-releasing chitosan polysaccharides) and tunable NO-release kinetics by tailoring the number of secondary amines and the hydrophobicity of the local environment

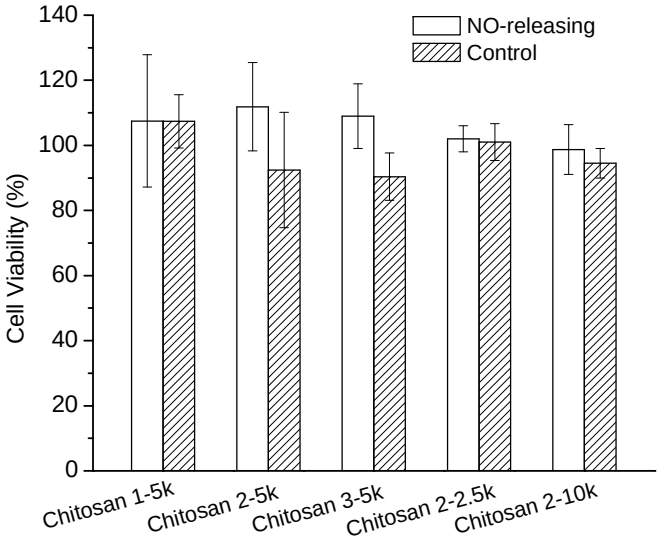

Figure 5.6 Viability of L929 mouse fibroblasts exposed to control and NO-releasing chitosan oligosaccharides at concentration for 5-log bacteria viability reduction (MBC) against *P. aeruginosa* biofilms. Each parameter was analyzed with multiple replicates (n=3).

surrounding the *N*-diazeniumdiolates, respectively.The water solubility of chitosan oligosaccharides allows for both beneficial diffusion into biofilms and subsequent association with bacteria, resulting in efficient eradication of biofilm bacteria at concentrations eliciting minimal toxicity against L929 mouse fibroblast cells. This study demonstrates the potential of NO-releasing chitosan oligosaccharides as antimicrobial agents. Experiments are underway to evaluate the biocidal efficacy of these materials against a broad spectrum of bacteria strains including methicillin-resistant *Staphylococcus aureus* and cystic fibrosis-related *P. aeruginosa* strains (e.g., mucoid/alginate-producing strains). Future work should also focus on evaluating their anti-biofilm efficacy in vivo and more detailed pharmacological toxicity testing of the NO-releasing chitosan oligosaccharides with human cells.

5.5 References

1. DeQueiroz, G. A.; Day, D. F. Antimicrobial activity and effectiveness of a combination of sodium hypochlorite and hydrogen peroxide in killing and removing Pseudomonas aeruginosa biofilms from surfaces. *J. Appl. Microbiol.* **2007,** *103*, 794-802.

2. Nikitkova, A. E.; Haase, E. M.; Scannapieco, F. A., Taking the starch out of oral biofilm formation: molecular basis and functional significance of salivary alpha-amylase binding to oral streptococci. *Appl. Environ. Microbiol.* **2013,** *79*, 416-423.

3. Costerton, J. W.; Stewart, P. S.; Greenberg, E. P. Bacterial biofilms: A common cause of persistent infections. *Science* **1999,** *284*, 1318-1322.

4. Dowd, S. E.; Wolcott, R. D.; Sun, Y.; McKeehan, T.; Smith, E.; Rhoads, D. Polymicrobial nature of chronic diabetic foot ulcer biofilm infections determined using bacterial tag encoded FLX amplicon pyrosequencing (bTEFAP). *PLOS One* **2008,** *3*, e3326.

5. Lyczak, J. B.; Cannon, C. L.; Pier, G. B. Lung infections associated with cystic fibrosis. *Clin. Microbiol. Rev.* **2002,** *15*, 194-222.

6. Sauer, K.; Camper, A. K.; Ehrlich, G. D.; Costerton, J. W.; Davies, D. G. Pseudomonas aeruginosa displays multiple phenotypes during development as a biofilm. *J.Bacteriol.* **2002,** *184*, 1140-1154.

7. Wolcott, R. D.; Rhoads, D. D.; Dowd, S. E., Biofilms and chronic wound inflammation. *J. Wound Care* **2008,** *17*, 333-341.

8. Fux, C. A.; Costerton, J. W.; Stewart, P. S.; Stoodley, P. Survival strategies of infectious biofilms. *Trends Microbiol.* **2005,** *13*, 34-40.

9. Keren, I.; Kaldalu, N.; Spoering, A.; Wang, Y.; Lewis, K. Persister cells and tolerance to antimicrobials. *FEMS Microbiol. Lett.* **2004,** *230*, 13-18.

10. Smith, A. W. Biofilms and antibiotic therapy: Is there a role for combating bacterial resistance by the use of novel drug delivery systems? *Adv. Drug Deliver. Rev.* **2005,** *57*, 1539-1550.

11. Pyo, H. C.; Kim, Y. K.; Whang, K. U.; Park, Y. L.; Eun, H. C. A comparative study of cytotoxicity of topical antimicrobials to cultured human keratinocytes and fibroblasts. *Korean J. Dermatol.* **1995,** *33*, 895-906.

12. Marletta, M. A.; Tayeh, M. A.; Hevel, J. M. Unraveling the biological significance of nitric oxide. *Biofactors* **1990,** *2*, 219-225.

13. MacMicking, J.; Xie, Q. W.; Nathan, C. Nitric oxide and macrophage function. *Annu. Rev. Immunol.* **1997,** *15*, 323-350.

14. Fang, F. C. Perspectives series: host/pathogen interactions. Mechanisms of nitric oxide-related antimicrobial activity. *J. Clin. Invest.* **1997,** *99*, 2818-2825.

15. Riccio, D. A.; Schoenfisch, M. H. Nitric oxide release: part I. Macromolecular scaffolds. *Chem. Soc. Rev.* **2012,** *41*, 3731-3741.

16. Carpenter, A. W.; Schoenfisch, M. H. Nitric oxide release: part II. Therapeutic applications. *Chem. Soc. Rev.* **2012,** *41*, 3742-3752.

17. Coneski, P. N.; Schoenfisch, M. H. Nitric oxide release: part III. Measurement and reporting. *Chem. Soc. Rev.* **2012,** *41*, 3753-3758.

18. Nichols, S. P.; Storm, W. L.; Koh, A.; Schoenfisch, M. H. Local delivery of nitric oxide: targeted delivery of therapeutics to bone and connective tissues. *Adv. Drug Deliv. Rev.* **2012,** *64*, 1177-1188.

19. Fang, F. C. Antimicrobial reactive oxygen and nitrogen species: Concepts and controversies. *Nat. Rev. Microbiol.* **2004,** *2*, 820-832.

20. Ghaffari, A.; Miller, C. C.; McMullin, B.; Ghahary, A. Potential application of gaseous nitric oxide as a topical antimicrobial agent. *Nitric Oxide-Biol. Chem.* **2006,** *14*, 21-29.

21. Hetrick, E. M.; Shin, J. H.; Stasko, N. A.; Johnson, C. B.; Wespe, D. A.; Holmuhamedov, E.; Schoenfisch, M. H. Bactericidal efficacy of nitric oxide-releasing silica nanoparticles. *ACS Nano* **2008,** *2*, 235-246.

22. Carpenter, A. W.; Slomberg, D. L.; Rao, K. S.; Schoenfisch, M. H., Influence of scaffold size on bactericidal activity of nitric oxide-releasing silica nanoparticles. *ACS Nano* **2012,** *5*, 7235-7244.

23. Lu, Y.; Sun, B.; Li, C.; Schoenfisch, M. H. Structurally Diverse Nitric Oxide-Releasing Poly(propylene Imine) Dendrimers. *Chem. Mater.* **2011,** *23*, 4227-4233.

24. Sun, B.; Slomberg, D. L.; Chudasama, S. L.; Lu, Y.; Schoenfisch, M. H. Nitric oxide-releasing dendrimers as antibacterial agents. *Biomacromolecules* **2012,** *13*, 3343-3354.

25. Hetrick, E. M.; Shin, J. H.; Paul, H. S.; Schoenfisch, M. H. Anti-biofilm efficacy of nitric oxide-releasing silica nanoparticles. *Biomaterials* **2009,** *30*, 2782-2789.

26. Zhao, H.; Serrano, M. C.; Popowich, D. A.; Kibbe, M. R.; Ameer, G. A. Biodegradable nitric oxide-releasing poly(diol citrate) elastomers. *J. Biomed. Mater. Res. A* **2010,** *93*, 356-363.

27. Coneski, P. N.; Rao, K. S.; Schoenfisch, M. H. Degradable nitric oxide-releasing biomaterials via post-polymerization functionalization of cross-linked polyesters. *Biomacromolecules* **2010**, *11*, 3208–3215

28. Wold, K. A.; Damodaran, V. B.; Suazo, L. A.; Bowen, R. A.; Reynolds, M. M. Fabrication of biodegradable polymeric nanofibers with covalently attached NO donors. *ACS Appl. Mater. Interfaces* **2012**, 4, 3022–3030.

29. Damodaran, V. B.; Reynolds, M. M., Biodegradable S-nitrosothiol tethered multiblock polymer for nitric oxide delivery. *J. Mater. Chem.* **2011,** *21*, 5870-5872.

30. Dash, M.; Chiellini, F.; Ottenbrite, R. M.; Chiellini, E. Chitosan-A versatile semi-synthetic polymer in biomedical applications. *Prog. Polym. Sci.* **2011,** *36*, 981-1014.

31. Jayakumar, R.; Prabaharan, M.; Nair, S. V.; Tamura, H. Novel chitin and chitosan nanofibers in biomedical applications. *Biotechnol. Adv.* **2010,** *28*, 142-150.

32. Valmikinathan, C. M.; Mukhatyar, V. J.; Jain, A.; Karumbaiah, L.; Dasari, M.; Bellamkonda, R. V. Photocrosslinkable chitosan based hydrogels for neural tissue engineering. *Soft Matter* **2012,** *8*, 1964-1976.

33. Zhang, J. L.; Xia, W. S.; Liu, P.; Cheng, Q. Y.; Tahirou, T.; Gu, W. X.; Li, B. Chitosan Modification and Pharmaceutical/Biomedical Applications. *Mar. Drugs* **2010,** *8*, 1962-1987.

34. Wan, A.; Gao, Q.; Li, H. L. Effects of molecular weight and degree of acetylation on the release of nitric oxide from chitosan-nitric oxide adducts. *J. Appl. Polym. Sci.* **2010,** *117*, 2183-2188.

35. Wan, A.; Sun, Y.; Li, H. L. Characterization of folate-graft-chitosan as a scaffold for nitric oxide release. *Int. J. Biol. Macromol.* **2008,** *43*, 415-421.

36. Smith, D. J.; Serhatkulu, S. Chitosan-based nitric oxide donor compositions. (Akron, OH) US Patent 6,261,594, July 17, 2001.

37. Du, J.; Hsieh, Y. L. Nanofibrous membranes from aqueous electrospinning of carboxymethyl chitosan. *Nanotechnology* **2008,** *19*, 125707.

38. Kim, S. K.; Rajapakse, N. Enzymatic production and biological activities of chitosan oligosaccharides (COS): A review. *Carbohydr. Polym.* **2005,** *62*, 357-368.

39. Maghami, G. G.; Roberts, G. A. F. Evaluation of the viscometric constants for chitosan. *Makromol. Chem.* **1988,** *189*, 195-200.

40. Wong, K.; Sun, G. B.; Zhang, X. Q.; Dai, H.; Liu, Y.; He, C. B.; Leong, K. W. PEI-g-chitosan, a novel gene delivery system with transfection efficiency comparable to polyethylenimine in vitro and after liver administration in vivo. *Bioconj. Chem.* **2006,** *17*, 152-158.

41. Tokura, S.; Ueno, K.; Miyazaki, S.; Nishi, N., Molecular weight dependent antimicrobial activity by chitosan. *Macromol. Symp.* **1997,** *120*, 1-9.

42. Tokoro, A.; Tatewaki, N.; Suzuki, K.; Mikami, T.; Suzuki, S.; Suzuki, M. Growth-inhibitory effect of hexa-N-Acetylchitohexaose and chitohexaose against meth-a solid tumor. *Chem. Pharm. Bull.* **1988,** *36*, 784-790.

43. Pae, H. O.; Seo, W. G.; Kim, N. Y.; Oh, G. S.; Kim, G. E.; Kim, Y. H.; Kwak, H. J.; Yun, Y. G.; Jun, C. D.; Chung, H. T. Induction of granulocytic differentiation in acute promyelocytic leukemia cells (HL-60) by water-soluble chitosan oligomer. *Leukemia Res.* **2001,** *25*, 339-346.

44. Porporatto, C.; Bianco, I. D.; Riera, C. M.; Correa, S. G., Chitosan induces different L-arginine metabolic pathways in resting and inflammatory macrophages. *Biochem. Biophy. Res. Comm.* **2003,** *304*, 266-272.

45. Hirano, S. Chitin biotechnology applications. *Biotechnol. Annu. Rev.* **1996,** *2*, 237-58.

46. Xu, J. G.; Zhao, X. M.; Wang, X. L.; Zhao, Z. B.; Du, Y. G. Oligochitosan inhibits Phytophthora capsici by penetrating the cell membrane and putative binding to intracellular targets. *Pestic. Biochem. Physiol.* **2007,** *88*, 167-175.

47. Hu, F. Q.; Liu, L. N.; Du, Y. Z.; Yuan, H. Synthesis and antitumor activity of doxorubicin conjugated stearic acid-g-chitosan oligosaccharide polymeric micelles. *Biomaterials* **2009,** *30*, 6955-6963.

48. Stasko, N. A.; Schoenfisch, M. H. Dendrimers as a scaffold for nitric oxide release. *J. Am. Chem. Soc.* **2006,** *128*, 8265-8271.

49. Davies, K. M.; Wink, D. A.; Saavedra, J. E.; Keefer, L. K., Chemistry of the diazeniumdiolates. 2. Kinetics and mechanism of dissociation to nitric oxide in aqueous solution. *J. Am. Chem. Soc.* **2001,** *123*, 5473-5481.

50. Hetrick, E. M.; Shin, J. H.; Stasko, N. A.; Johnson, C. B.; Wespe, D. A.; Holmuhamedov, E.; Schoenfisch, M. H. Bactericidal efficacy of nitric oxide-releasing silica nanoparticles. *ACS Nano* **2008,** *2*, 235-246.

51. Lu, Y., Shape- and NO flux dependent bactericidal efficacy. *Small* **2013**, in press.

52. Salmon, D. J.; Torres de Holding, C. L.; Thomas, L.; Peterson, K. V.; Goodman, G. P.; Saavedra, J. E.; Srinivasan, A.; Davies, K. M.; Keefer, L. K.; Miranda, K. M. HNO and NO release from a primary amine-based diazeniumdiolate as a function of pH. *Inorg. Chem. 50*, 3262-70.

53. Barraud, N.; Hassett, D. J.; Hwang, S. H.; Rice, S. A.; Kjelleberg, S.; Webb, J. S. Involvement of nitric oxide in biofilm dispersal of Pseudomonas aeruginosa. *J. Bacteriol.* **2006,** *188*, 7344-7353.

54. Takenaka, S.; Pitts, B.; Trivedi, H. M.; Stewart, P. S. Diffusion of macromolecules in model oral biofilms. *Appl. Environ. Microbiol.* **2009,** *75*, 1750-1753.

55. Al-Ani, B.; Hewett, P. W.; Ahmed, S.; Cudmore, M.; Fujisawa, T.; Ahmad, S.; Ahmed, A. The release of nitric oxide from S-nitrosothiols promotes angiogenesis. *PlOS One* **2006,** *1*, e25.

56. Cooke, J. P.; Losordo, D. W. Nitric oxide and angiogenesis. *Circulation* **2002,** *105*, 2133-2135.

57. Kawasaki, K.; Smith, R. S., Jr.; Hsieh, C. M.; Sun, J.; Chao, J.; Liao, J. K. Activation of the phosphatidylinositol 3-kinase/protein kinase Akt pathway mediates nitric oxide-induced endothelial cell migration and angiogenesis. *Mol. Cell. Biol.* **2003,** *23*, 5726-5737.

58. MacLauchlan, S.; Yu, J.; Parrish, M.; Asoulin, T. A.; Schleicher, M.; Krady, M. M.; Zeng, J.; Huang, P. L.; Sessa, W. C.; Kyriakides, T. R. Endothelial nitric oxide synthase controls the expression of the angiogenesis inhibitor thrombospondin 2. *Proc. Natl. Acad. Sci. U. S. A. 108*, E1137-1145.

59. James, G. A.; Swogger, E.; Wolcott, R.; Pulcini, E. D.; Secor, P.; Sestrich, J.; Costerton, J. W.; Stewart, P. S. Biofilms in chronic wounds. *Wound Repair Regen.* **2008,** *16*, 37-44.

Chaper 6

Summary and Future Directions

6.1 Summary

In recent years, nitric oxide-releasing scaffolds have been used as antimicrobial agents and have been proved effective at inhibiting bacterial growth and also bacteria killing.[1-3] *N*-diazeniumdiolate-modified silica particles and dendrimer exhibited enhanced bactericidal efficacy compared to small molecule NO donors due to the association of such (macromolecular) scaffolds with bacteria.[1, 4] Size- and NO release-dependent bacteria killing of NO-releasing silica particles and dendrimers have also been observed with smaller scaffolds and high NO flux more effective.[4-5] Clearly, the scaffold for NO delivery plays an important role in the delivery efficiency and the subsequent bactericidal efficacy. My research has focused on the development of NO-releasing silica particles, dendrimers, and chitosans for enhanced bactericidal efficacy and reduced toxicity to mammalian cells.

Chapter 2 presented the synthesis of structurally diverse secondary amine-functionalized poly(propylene imine) (PPI) dendrimers capable of tunable nitric oxide (NO) release using ring-opening or conjugate-addition reactions with propylene oxide (PO), styrene oxide (SO), acrylonitrile (ACN), poly(ethylene glycol) methyl ether acrylate (average Mn = 480) (PEG) or 1,2-epoxy-9-decene (ED). *N*-Diazeniumdiolate nitric oxide donors were formed on the resulting secondary amine-functionalized G2-G5

PPI dendrimers by reaction with NO gas in basic solution. The NO storage and release kinetics for the resulting dendritic scaffolds were diverse (0.9-3.8 μmol NO/mg totals and 0.3 to 4.9 h half lives), illustrating the importance of the exterior chemical modification (e.g., steric environments, hydrophobicity, etc.) on diazeniumdiolate stability/decomposition. Even more tunable NO release was demonstrated by combining two NO donor systems on the exterior of one macromolecular scaffold. The approaches described in this chapter extend the range and scope of NO-releasing macromolecular scaffolds by unlocking a series of materials for use as dopants in biomedical polymers or stand-alone therapeutics depending on the exterior modification.

In Chapter 3, a series of amphiphilic nitric oxide (NO)-releasing poly(amidoamine) (PAMAM) dendrimers with different exterior hydrophobicities were synthesized by a ring-opening reaction between primary amines of the dendrimers and propylene oxide (PO), 1,2-epoxy-9-decene (ED), or a ratio of the two, followed by reaction with NO at 10 atm to produce *N*-diazeniumdiolate-modified scaffolds with a total storage of ~1 μmol/mg to study how the hydrophobiciy affects their NO delivery efficiency, penetration of extracellular polysaccharides, and bactericidal efficacy. The hydrophobicity of the exterior functionality was tuned by varying the ratio of PO and ED grafted onto the dendrimers. The bactericidal efficacy of these NO-releasing vehicles was then evaluated as a function of dendrimer exterior hydrophobicity (i.e., ratio of PO/ED), size (i.e., generation), and NO release against established Gram-negative *Pseudomonas aeruginosa* biofilms. Both the size and the exterior functionalization of dendrimer proved important for dendrimer association with bacteria, the efficiency of NO delivery, bacteria membrane disruption, migration within the biofilm, and toxicity to mammalian cells.

Although enhanced bactericidal efficacy was observed for the hydrophobic chains (e.g., ED), toxicity to L929 mouse fibroblast cells was also noted at the concentrations necessary to reduce bacterial viability by 5-logs (99.999% killing). The optimal PO to ED ratios for biofilm eradication with minimal toxicity against L929 mouse fibroblast cells were 7:3 and 5:5. This study demonstrates the importance of both dendrimer size and exterior properties in determining ultimate therapeutic utility (i.e., efficacy against established biofilms without compromising biocompatibility to mammalian cells).

The synthesis of silica nanorods (SNRs) was decribed in Chapter 4 Aminoalkoxysilanes were used to modify the surface of the rods to prepare a new class of nitric oxide (NO)-releasing materials. Both the aspect ratio and size of the SNRs were tuned by varying the temperature, pH, and silane concentration used during the surfactant-templated synthesis. *N*-Diazeniumdiolates nitric oxide (NO) donors were formed on the secondary amine-functionalized SNRs by reaction with NO gas under basic conditions. Particle surface modification by hydrophilic poly(ethylene glycol) was employed to yield rapid NO-release kinetics. The diverse morphology (i.e., aspect ratio ~1–8), NO-release kinetics (2000–14000 ppb NO/mg particle) and similar size (i.e., particle volume ~0.02 μm^3) of the resulting NO-releasing SNRs facilitated further study of how particle shape and NO flux impacts bactericidal activity against Gram–positive *Staphylococcus aureus* (*S. aureus*) and Gram–negative *Pseudomonas aeruginosa* (*P. aeruginosa*) bacteria. The biocidal action of these materials improved with increasing particle aspect ratio and initial NO flux. Both chemical (i.e., NO-release kinetics) and physical (i.e., morphology) properties greatly influenced the bactericidal activity of these materials.

In Chapter 5, I described the synthesis of secondary amine-functionalized chitosan oligosaccharides of different molecular weights (i.e., ~2500, 5000, 10000) by grafting 2-methyl aziridine onto the primary amines on chitosan oligosaccharides. The amines were then reacted with nitric oxide (NO) gas under basic conditions to yield *N*-diazeniumdiolate NO donors. The total NO storage (e.g., 0.30–0.87 μmol/mg) and maximum NO flux (e.g., 1600–12600 ppb/mg) of the resulting NO-releasing chitosan oligosaccharides were controlled by the molar ratio of 2-methyl aziridine to primary amines (e.g., 1:1, 2:1) and the functional group surrounding the *N*-diazeniumdiolates (e.g., polyethylene glycol (PEG) chains), respectively. Compared to previous chitosan-based materials, significantly greater NO storage was achieved through increased solubility of the chitosan oligosaccharides in the basic conditions necessary for *N*-diazeniumdiolate formation. In addition, the water-solublibility of the chitosan oligosaccharides facilitated their diffusion into *Pseudomonas aeruginosa* biofilms and association with embedded bacteria. The resulting biofilm eradication of these chitosan oligosaccharides was shown to depend on both the molecular weight and ionic characteristics. Low molecular weight (i.e., ~2500 and 5000) and cationic chitosan oligosaccharides exhibited rapid diffusion into biofilms and association with bacteria, leading to enhanced biofilm killing. At concentrations resulting in 5-log killing (≥ 99.999%), the NO-releasing and control chitosan oligosaccharides elicited no cytotoxicity to mouse fibroblast L929 cells *in vitro*. Conversely, antiseptics such as povidone iodine and chlorhexidine reduce mouse fibroblast L929 cells viability by ~90%. The water soluble NO-releasing chitosan oligosaccharides presented in this chapter effectively eradicated bacterial biofilms with

no cytotoxicity to mammalian cells, thus demonstrating their potential as anti-biofilm agents.

6.2 Future Directions

The work presented in this thesis indicates the potential of NO-releasing amphiphilic dendrimers, silica nanorods, and chitosan oligosaccharides as antimicrobial agents. To fully explore their therapeutic effect, the bactericidal efficacy against a broader spectrum of bacteria should be undertaken, along with in animal models need to be evaluated. The development of materials with enhanced NO storage and NO delivery efficiency should also continue to further improve the therapeutic potential of NO release.

6.2.1 NO-Releasing Mesoporous Silica Nanorods with Enhanced NO Storage

The synthesis of NO-releasing mesoporous silica particles was presented in Chapter 3 by anchoring aminosilanes on the particle surface, followed by the reaction with NO gas to form *N*-diazeniudmiolate NO donors. The resulting particles were characterized by a NO storage of ~0.8 μmol/mg. To increase the NO storage, the synthesis of mesoporous silica particles consisting of aminosilanes throughout the particle should be investigated. Suteewong et al. reported the synthesis of mesoporous silica particles containing >50% 3-aminopropyltrimethoxysilane (APTES) via co-condensation of tetraethyoxysilane (TEOS) and APTES.[6] The highly aminated particles were prepared via base-catalyzed sol-gel silica reactions using hexadecyltrimethyl ammonium bromide (CTAB), TEOS, and large molar amounts of APTES in the presence of ethyl acetate. Significant amine content in these particles is reflected by a strongly positive zeta potential of the acid-extracted particles in water (i.e., 42 ± 5 mV). Following this procedure, hybrid particles via the co-condensation of TEOS and secondary amine-containing silanes (e.g., N-(6-

Aminohexyl)aminopropyltrimethoxysilane or AHAP) should be achievable and expected to have greater NO storage compared to aminosilane-grafted particles.

Another strategy of enhancing the total NO storage might be growing amine-containing polymer brushes from the surface of silica particles. As depicted in Scheme 6.1, an aminosilane is anchored onto the silica particle surface, following by the growth of the poly(2-methyl aziridine) "brushes" from the surface of the particles via the ring opening of 2-methyl aziridine.[7] Tunable NO storage could be yielded by controlling the molecular weight of the poly(2-methyl aziridine). The NO-release kinetics of the resulting particles may be adjusted by conjugating liphiphilic groups of varied hydrophobicity to the primary amines at the end of poly(2-methyl aziridine) brushes, as discussed in Chapter 5.

6.2.2 Nitric Oxide-Releasing Chitosan Oligosaccharides for Cystic Fibrosis

Cystic fibrosis (CF) is an inherited disease caused by mutations in the cystic fibrosis transmembrane conductance regulator (CFTR) gene,[8] resulting in the malfunction of CFTR gene and ultimately interfering with mucociliary clearance of inhaled microorganisms.[9] In healthy individuals, the cilia of epithelial cells in the upper airway efficiently remove microbes and particles that are trapped in the thin fluidic mucus (a process termed mucociliary clearance). In patients with CF, the cilia cannot clear the viscous and dehydrated mucus layer efficiently, which results in colonization by bacteria and chronic infection.[9] *P. aeruginosa* in the chronically infected lung leads to immune complex-mediated inflammation, dominated by polymorphonuclear leukocytes (PMNs), often resulting in lung tissue damage and decreased lung function, in addition to the damage that is actively caused by the bacteria.[10]

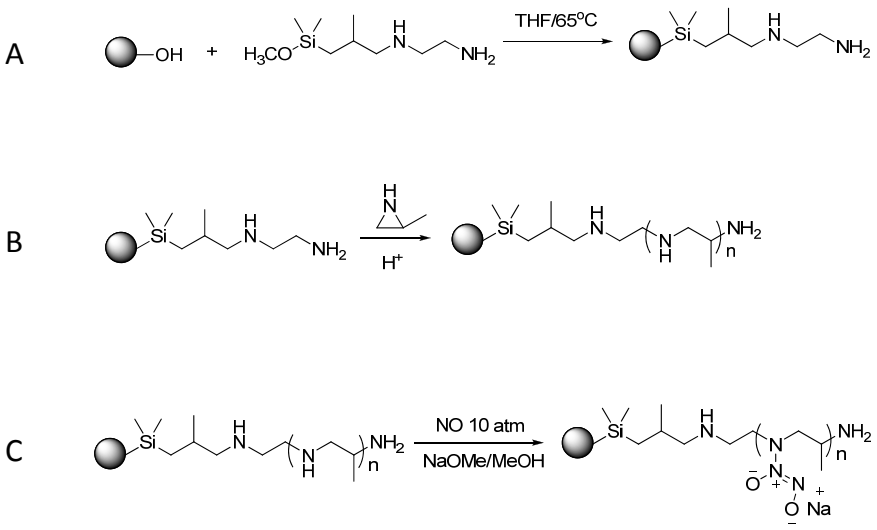

Scheme 6.1 Synthesis of NO-releasing silica particles with surface-grafted *N*-diazenimdiolate-modified polyamines. A) grafting of aminosilane on the particles surface; B) polymerization of 2-methyl aziridine on the particle surface; C) Diazeniumdiolation of secondary amines on the poly(2-methyl aziridine) chains.

Intensive treatment with antibiotics has extended the mean expected lifetime of CF patients dramatically,[11] but the heavy use of antibiotics in CF clinics has led to the development of antibiotic-resistant bacteria. For example, *P. aeruginosa* isolates from CF patients are commonly found to be resistant to all clinically relevant classes of antibiotics.[12] As such, the urgent need for a new class of antimicrobial agents for CF treatment is urgent.

Nebulization is one common method of pulmonary drug administration that has been used for many years to treat CF.[13] We hypothesize that water soluble NO-releasing chitosan oligosaccharides can be dissolved in water and nebulized for effective delivery of NO to the lungs. The diffusion of NO-releasing chitosan oliogsaccharides as a function of molecular weight in the mucus should be studied by monitoring the migration of fluorescently labeled chitosans using confocal microscopy. The bactericidal efficacy of these materials against CF bacterial strains should be evaluated in vitro and in vivo against clinically relevant planktonic and biofilm bacteria.

6.2.3 Nitric Oxide-Releasing Chitosan Nanoparticles for Cystic Fibrosis

Chitosan nanoparticles have been widely used as drug carriers due to their ability to pass through biological barriers in vivo (e.g., the blood/brain barrier) and deliver drugs to a lesion site to enhance efficacy.[14] In addition, chitosan nanoparticles also exhibit enhanced bactericidal activity against a wide range of bacterial strains.[15] One approach to prepare chitosan nanoparticles is ionic gelation of chitosan using a polyanionic molecule (e.g., sodium tripolyphosphate or TPP) under acidic condition. *S*-nitrosothiol NO donors can be encapsulated using this technique due to the stability of *S*-nitrosothiols under the same condition. In prior work, chitosan in diluted acetic acid has been added to the

solution of TPP dropwise under vigorous stirring and ionic cross-linking is generated by auto-aggregation between chitosan and TPP to form nanosized particles.[16] Of note, this method has been widely used to encapsulate proteins and gene drugs.[17] Similarly, NO-releasing chitosan nanoparticles could be synthesized by the encapsulation of *S*-nitrosothiol small molecules within chitosan/TPP particles. The NO payloads would be controlled by the concentration of *S*-nitrosothiol donors in the reaction solution. The gelation process would need to be conducted at low temperatures to avoid NO loss by thermal degradation. The performance of these particles as therapeutics for cystic fibrosis could be evaluated in terms of pulmonary delivery efficiency, diffusion within the mucus, and biofilm eradication in vivo.

6.3 Conclusions

A range of nitric oxide-releasing macromolecular scaffolds including silica nanorods, dendrimers, and chitosan oligosaccharides were synthesized and shown to possess enhanced bactericidal activity against problematic bacteria in vitro. The reduced toxicity of these scaffolds as presented in this thesis demonstrates their great potential as antimicrobial agents. The true ability to treat infections associated with different diseases (e.g., diabetic ulcers, cystic fibrosis) should now be evaluated in appropriate animal models to truly comprehend their therapeutic potential. The approaches described in the preceding chapters allow for the control of physical (e.g., size, shape, and molecular weight) and chemical (e.g., ionic characteristics, hydrophobicity) properties, thus greatly impacting the future development of NO-releasing materials.

6.4 References

1. Hetrick, E. M.; Shin, J. H.; Stasko, N. A.; Johnson, C. B.; Wespe, D. A.; Holmuhamedov, E.; Schoenfisch, M. H. Bactericidal efficacy of nitric oxide-releasing silica nanoparticles. *ACS Nano* **2008,** *2*, 235-46.

2. Hetrick, E. M.; Shin, J. H.; Paul, H. S.; Schoenfisch, M. H. Anti-biofilm efficacy of nitric oxide-releasing silica nanoparticles. *Biomaterials* **2009,** *30*, 2782-9.

3. Martinez, L. R.; Han, G.; Chacko, M.; Mihu, M. R.; Jacobson, M.; Gialanella, P.; Friedman, A. J.; Nosanchuk, J. D.; Friedman, J. M. Antimicrobial and Healing Efficacy of Sustained Release Nitric Oxide Nanoparticles Against Staphylococcus Aureus Skin Infection. *J. Invest. Dermatol.* **2009,** *129*, 2463-2469.

4. Sun, B.; Slomberg, D. L.; Chudasama, S. L.; Lu, Y.; Schoenfisch, M. H. Nitric oxide-releasing dendrimers as antibacterial agents. *Biomacromolecules 13*, 3343-3354.

5. Carpenter, A. W.; Slomberg, D. L.; Rao, K. S.; Schoenfisch, M. H. Influence of scaffold size on bactericidal activity of nitric oxide-releasing silica nanoparticles. *ACS Nano* **2012,** *5*, 7235-7244.

6. Suteewong, T.; Sai, H.; Cohen, R.; Wang, S. T.; Bradbury, M.; Baird, B.; Gruner, S. M.; Wiesner, U. Highly aminated mesoporous silica nanoparticles with cubic pore structure. *J. Am. Chem. Soc.* **2011,** *133*, 172-175.

7. Wong, K.; Sun, G. B.; Zhang, X. Q.; Dai, H.; Liu, Y.; He, C. B.; Leong, K. W. PEI-g-chitosan, a novel gene delivery system with transfection efficiency comparable to polyethylenimine in vitro and after liver administration in vivo. *Bioconj. Chem.* **2006,** *17*, 152-158.

8. Bye, M. R.; Ewig, J. M.; Quittell, L. M. Cystic fibrosis. *Lung* **1994**, *172*, 251–270.

9. Boucher, R. C. Relationship of airway epithelial ion transport to chronic bronchitis. *Proc. Am. Thorac. Soc.* **2004**, *1*, 66–70.

10. Nichols, D.; Chmiel, J.; Berger, M. Chronic inflammation in the cystic fibrosis lung: alterations in inter- and intracellular signaling. *Clin. Rev. Allergy Immunol.* **2008**, *34*, 146–162.

11. Cystic Fibrosis Foundation. Cystic Fibrosis Foundation patient registry 2010 annual data report (Cystic Fibrosis Foundation, 2011).

12. Lister, P. D.; Wolter, D. J.; Hanson, N. D. Antibacterial-resistant Pseudomonas aeruginosa: clinical impact and complex regulation of chromosomally encoded resistance mechanisms. *Clin. Microbiol. Rev.* **2009**, *22*, 582–610.

13. Labiris, N. R.; Dolovich, M. B. Pulmonary drug delivery. Part II: The role of inhalant delivery devices and drug formulations in therapeutic effectiveness of aerosolized medications. *J. Clin. Pharmacol.* **2003**, *56*, 600–612.

14. Pal, K.; Behera, B.; Roy, S.; Ray, S. S.; Thakur, G. Chitosan Based Delivery Systems on a Length Scale: Nano to Macro. *Soft Matter* **2013,** *11*, 125-142.

15. Du, W. L.; Xu, Y. L.; Xu, Z. R.; Fan, C. L. Preparation, characterization and antibacterial properties against E-coli K(88) of chitosan nanoparticle loaded copper ions. *Nanotechnology* **2008,** *19*, 153-160.

16. Amidi, M.; Mastrobattista, E.; Jiskoot, W.; Hennink, W. E. Chitosan-based delivery systems for protein therapeutics and antigens. *Adv. Drug Deliv. Rev.* **2010**, *62*, 59–82.

17. Avadi, M. R.; Sadeghi, A. M. M.; Mohammadpour, N.; Abedin, S.; Atyabi, F.; Dinarvand, R.; Rafiee-Tehrani, M. Preparation and characterization of insulin nanoparticles using chitosan and Arabic gum with ionic gelation method. *Nanomed. Nanotechnol. Biol. Med.* **2010**, *6*, 58–63.